

**Physical description
of transport processes inside an
Open Top Chamber in relation to
field conditions**

Ontvangen

25 MEI 1992

UB-CARDEX

CENTRALE LANDBOUWCATALOGUS



0000 0489 6409

BIBLIOTHEEK
LANDBOUWUNIVERSITEIT
WAGENINGEN

Promotor: Dr. ir. L. Wartena
hoogleraar in de Landbouw-
weerkunde en omgevings-
natuurkunde

Co-promotor: Dr. ir. A.F.G. Jacobs
universitair hoofddocent Meteorologie

T.H. Jetten

**Physical description
of transport processes inside an
Open Top Chamber in relation to
field conditions**

Proefschrift

ter verkrijging van de graad van doctor
in de landbouw- en milieuwetenschappen,
op gezag van de rector magnificus,
dr. H.C. van der Plas,
in het openbaar te verdedigen
op woensdag 24 juni 1992
des namiddags te vier uur in de aula
van de Landbouwuniversiteit te Wageningen.

VOORWOORD

Het schrijven van een proefschrift is niet slechts de zaak van een promovendus alleen. Zonder de steun en inzet van velen zou het niet mogelijk zijn geweest een dergelijk werk te voltooien. Via deze weg wil ik iedereen bedanken die aan het tot stand komen van dit proefschrift heeft bijgedragen. Aan verschillende personen is echter een bijzonder woord van dank verschuldigd.

Als eerste wil ik mijn promotor Bert Wartena bedanken. Bert was een van de eersten die nadrukkelijk op het belang van een onderzoek naar de fysische uitwisselingsprocessen binnen een OTC heeft gewezen. Zijn kennis en inzicht in de materie waren een bron van inspiratie voor mij.

Als tweede wil ik mijn co-promotor Adrie Jacobs bedanken. Hij was degene die het meest bij mijn werk betrokken was. Bij Adrie kon je altijd terecht voor theoretische of praktische problemen, waarbij hij altijd positief tegen deze problemen bleef aankijken, ook al waren deze nog zo lastig op te lossen. Adrie, het doorleeswerk voor het proefschrift zit er op, nu op naar de afzonderlijke artikelen.

De KEMA, in het bijzonder Maria Janssen (MO) wil ik bedanken voor de financiële en materiële ondersteuning van deze promotieplaats. Ruud Steenkist (MO) wil ik bedanken voor zijn werk als contactpersoon bij de KEMA.

Met name bij de voorbereiding en uitvoering van de experimenten zijn vele personen betrokken geweest. Het experimentele gedeelte is uitgevoerd op het waarnemingsveld van de vakgroep Meteorologie aan de Haarweg te Wageningen. Ik wil Dick Welgraven bedanken voor zijn hulp bij de vele grote en kleine karweitjes die rondom de experimenten uitgevoerd dienden te worden. Verder wil ik alle medewerkers van de fijnmechanische en electronische werkplaats van de oude vakgroep Natuur en Weerkunde bedanken voor hun hulp bij het opzetten en afbreken van de experimenten. Met name Anton Jansen, Willy Hillen, Teun Jansen, Peter Jansen, Frits Antonysen, Kees van Asselt en Kees van den Dries. Paul van Espelo wil ik bedanken voor zijn hulp bij de rookexperimenten. Van KEMA-zijde dienen met name genoemd te worden Peter Gamelkoorn (MMD) voor zijn hulp bij

1. Het op grote schaal inzetten van OTC's ten behoeve van CO₂-begassingsexperimenten is slechts van beperkte waarde zonder een gedetailleerde fysische karakterisering van de gebruikte OTC.
Dit proefschrift.
2. Observaties aan planten dienen in het midden van een OTC uitgevoerd worden daar hier de verschillen in microklimaat het kleinst zijn.
Dit proefschrift.
3. Het door van der Eerden et al. (1988) geschatte economische verlies aan gewasopbrengst in Nederland ten gevolge van luchtverontreiniging gaat voorbij aan het feit dat de onder OTC-omstandigheden afgeleide blootstellings-effect relaties niet zonder meer voor Nederlandse veldsituaties kunnen worden gebruikt.
Van der Eerden, L.G., A.E.G. Tonneijck & J.H.M. Weijnands (1988). Crop loss due to air pollutants in the Netherlands. Environmental Pollution 53: 365-376.
Dit proefschrift.
4. Doordat de turbulentiegraad bij atmosferische stromingen langs een wand groter is dan bij de meeste technische stromingen kan men, voor het modelleren hiervan, het voor technische stromingen ontwikkelde $k-\epsilon$ stromingsmodel niet zonder meer toepassen.
Detering, H.W. & D. Etling (1985). Application of the $k-\epsilon$ turbulence model to the atmospheric boundary layer. Boundary Layer Meteorology 33: 113-133.
Dit proefschrift
5. De interactie tussen een gascomponent en het gewas verloopt bij experimenten met veldbegassingssystemen anders dan onder natuurlijke omstandigheden. Een studie naar de gasuitwisselingsprocessen bij dit soort experimenten is daarom noodzakelijk.
Dit proefschrift
6. Voor het verkrijgen van redelijk nauwkeurige gegevens met betrekking tot latente en sensible warmtestroomdichtheden aan het aardoppervlak zijn nauwkeurige temperatuurmetingen noodzakelijk. De toepassing van driedraads-weerstandsmetingen voor het meten van temperatuurverschillen in de atmosfeer is op grond hiervan verwerpelijk.
7. Het gebruik van modelplanten ter bepaling van de uitwisselingsprocessen in een vegetatie is een beperkte weergave van slechts enkele aspecten van de werkelijkheid en dient daarom in alle gevallen kritisch benaderd te worden.

8. De geschiedenis van de OTC-ontwikkeling toont eens te meer aan dat het betrekken van natuurkundigen bij experimenten met planten absoluut noodzakelijk is.
9. Goed wetenschappelijk werk vergt tijdschalen die veel langer zijn dan de tijdschalen van de politieke belangstelling. Dit leidt er toe dat niet de beste onderzoekers, maar veeleer de beste politici onder de onderzoekers overleven.
10. Een pragmatische politieke besluitvorming doet partij-idealen vervagen.
11. De gemiddeld hogere opkomstpercentages bij gemeenteraadsverkiezingen in plaatsen van minder dan 10000 inwoners in vergelijking tot die in grotere gemeenten zijn niet zozeer een gevolg van een grotere betrokkenheid van de burger bij lokale vraagstukken maar veeleer van de aantrekkingskracht van bepaalde personen.
12. Daar aan de negatieve effecten van ziekte- en plaagbestrijdingsmiddelen op het milieu voor de producent van een bepaald middel meestal geen prijskaartje verbonden is hebben middelen met grote negatieve effecten een onterecht prijsvoordeel op meer milieuvriendelijke middelen.
13. Het gebrek aan scholing in het omgaan met tekstverwerkingspakketten leidt tot een lage kritische instelling ten aanzien van de wijze van toepassing van deze pakketten. Dit heeft als gevolg dat de tijd die een gemiddelde student nodig heeft voor de opmaak van een onderzoeksverslag positief is gecorreleerd met zijn of haar kennis van tekstverwerkingspakketten. Scholing verdient derhalve meer aandacht.
14. Het reisgedrag van Nederlanders in onveilige streken in het buitenland kenmerkt zich door een overschatting van de invloed van het Nederlandse staatsburgerschap.
Toerisme is vol risico's. De Volkskrant, T.R.A.J.E.C.T, biz. 5, 14 maart 1992.
15. De opwinding over incidentele computervirussen is er de oorzaak van dat de groeiende dreiging van deze virussen ten onrechte wordt gebagatelliseerd.
Computervirussen worden steeds geraffineerder. De Volkskrant, WETENSCHAP, biz. 15, 14 maart 1992.

Stellingen behorende bij het proefschrift van T.H. Jetten:

"Physical description of transport processes inside an Open Top Chamber in relation to field conditions"

Wageningen, 24 juni 1992.

het uitvoeren van de luchtverontreinigingsmetingen en Bennie Stortelder (MO) voor de technische coördinatie.

Studenten hebben aan verschillende gedeelten van het hier beschreven werk een belangrijke bijdrage geleverd. I thank Roel Henderickx, Mark Irvine (University of Strathclyde) en Patrick Bocken for their contribution to this thesis.

De discussies met Anno van Dijken en Marcel Bottema (TUE) met betrekking tot verschillende aspecten van respectievelijk het bodem-gewas-atmosfeer model en het FLUENT-model zijn zeer zinvol geweest en hebben in meer of minder belangrijke mate bijgedragen tot het hier gepresenteerde eindresultaat. Computerberekeningen met FLUENT vonden plaats bij de sectie Fysische Technologie van de afdeling TFO van de KEMA. Bij deze wil ik alle medewerkers van deze sectie bedanken voor de genoten gastvrijheid. Met name Ad Braam en Peter Jansen wil ik bedanken voor hun hulp.

Alle medewerkers van de huidige vakgroep Meteorologie en de toenmalige vakgroep Natuur en Weerkunde wil ik bedanken voor de zeer plezierige en stimulerende werkomgeving. Onder meer de gesprekken in de koffiegroep van 15.00 uur en het zaalvoetbalteam zorgden er vaak voor dat er een heel ander licht op bepaalde problemen geworpen werd. Cor Jacobs, Ad van den Berg, Leo Kroon en Bert Heusinkveld wil ik bedanken voor de laatste correcties op het manuscript en hun advies bij het tot stand komen van diverse figuren.

De ontembare energie van mijn kamergenoot Rushdi El-Kilani gecombineerd met zijn doorlopend optimisme waren een bijzondere stimulans voor mij. De discussies over vele aspecten van dit onderzoek waren zeer nuttig.

Het voltooien van een dergelijk proefschrift is niet mogelijk zonder de steun en medeleven van familieleden en vrienden. Met name wil ik hierbij noemen Pa, Ma, Monique, Gertrud, Jos, Johan, Frank en de harde kern van Marijkeweg B4. Een speciaal woord van dank voor Jolande. Je steun en vertrouwen gedurende de laatste paar maanden van dit onderzoek vormden een speciale bron van inspiratie voor mij.

TABLE OF CONTENTS

1	INTRODUCTION	1
	1.1 General	1
	1.2 Historical background to the present study	3
	1.3 Objectives of the present study	4
	1.4 Organization of the thesis	6
2	OPEN TOP CHAMBERS (OTC's), AN OVERVIEW	9
	2.1 General	9
	2.2 Technical description of the OTC construction	11
	2.2.1 The chamber	11
	2.2.2 The air-supply system	12
	2.3 Microclimate OTC	14
	2.4 Technical description of the KEMA-type OTC	20
3	THEORY	23
	3.1 Governing equations	23
	3.1.1 Conservation of mass	23
	3.1.2 Conservation of momentum	24
	3.1.3 Conservation of energy	28
	3.1.4 Conservation of a scalar quantity	32
	3.2 Scaling of the flow inside an OTC	33
	3.3 Models used	42
	3.3.1 The FLUENT model	42
	3.3.1.1 Physical background of the FLUENT model	43
	3.3.1.2 Numerical background of the FLUENT model	48
	3.3.1.3 Simulations	52
	3.3.1.4 Modelling of plants in the FLUENT model	54
	3.3.2 The OTC-resistance model	57
	3.3.2.1 The OTC-system model	58
	3.3.2.2 The soil-vegetation model	68
4	EXPERIMENTAL SET-UP	81
	4.1 General	81
	4.2 Experiments dealing with the flow field in and around an OTC	82
	4.3 Experimental set-up and data acquisition continuous experiments	84

5	RESULTS	91
	5.1 Flow regime	91
	5.2 Radiation	101
	5.3 Temperature	103
	5.4 Humidity	107
	5.5 Ozone	109
	5.6 Energy and mass exchange between soil-vegetation and atmosphere	110
6	FINAL REMARKS AND CONCLUSIONS	115
	6.1 Introduction	115
	6.2 Model computations	115
	6.3 The KEMA-type OTC system	117
	6.4 Conclusions	123
	APPENDIX 1 Sensors used	129
	APPENDIX 2 Case studies OTC-resistance model	131
	SUMMARY	139
	SAMENVATTING	143
	REFERENCES	147
	LIST OF SYMBOLS	153
	CURRICULUM VITAE	159

CHAPTER 1 INTRODUCTION

1.1 General

Gases and other substances are emitted into the atmosphere as a result of human activities. The input of pollutants from man's activities on a regional scale may far exceed those from natural sources, so that significant changes result in the budget of depositing substances. It was not until 1982 that public opinion in Europe became aware of the dramatic large-scale effects of acid rain on vegetation. Nevertheless, scientific experiments to study the effect of air pollutants on nature have been carried out for more than 100 years. It is now assumed that photochemical oxidants, primarily ozone, in combination with acidifying components, may play an important role in damaging plants and forests in Europe (Hov et al., 1986, 1987). Ozone is produced by reactions requiring sunlight, nitrogen oxides and volatile organic components. Van der Eerden et al. (1988) estimated air pollution losses in the Netherlands to be 5% of total crop volume. Approximately 70% of these losses were caused by ozone. Yearly net consumer losses were estimated to be US \$320 million.

The impact of air pollutants on plants in natural vegetations cannot be described by simple exposure-yield response relationships. Outdoor experiments in which plants are exposed to ambient air pollutant levels yield conflicting results from year to year because the interacting environmental effects are complex and not constant. The best way to study the effects of air pollutants on plants is still one of the issues scientists are dealing with. An oft-used approach is the application of one or more types of environmental stresses in combination with air pollutant stresses. The experimental set-up plays an important role in extrapolating experimental results to real field conditions.

To determine the impact of air pollutants on a crop requires growing conditions, which are as natural as possible, combined with the simultaneous control of ambient pollutant levels. Various experimental set-ups to study the effect of air

pollutants on plants have been developed over the last few decades. The set-ups can be grouped roughly into three types; laboratory chambers, open-air fumigation systems and field chambers (Ormrod et al., 1988).

Laboratory chambers

By creating a laboratory chamber, the researcher introduces a degree of artificiality into the experimental set-up but the experimental precision is high since various input parameters can be controlled. Laboratory chambers allow the use of a wide range of pollutant treatments in combination with a wide range of treatments resulting in other types of environmental stress. However, there may be large differences between the environmental stress in these systems and actual field conditions.

Open-air fumigation systems

The second type of set-up includes open-air fumigation experiments, with plants being exposed to air pollutants under ambient conditions. Open air-fumigation uses natural environmental and soil conditions. However, these experiments have the disadvantage that only the addition of a pollutant is possible. Natural pollutant concentrations in the environmental air cannot be excluded without changing the microclimate and physical exchange processes within a crop. Environmental stresses are less controllable than in laboratory chambers and instantaneous air pollutant concentrations at a particular position may fluctuate widely as a result of atmospheric turbulence. Furthermore, the replicability of the experiments is doubtful. In addition, replication of treatments requires a large investment in space and material. There are now some fumigation systems which can achieve both reasonable spatial uniformity and temporal control of the fumigant concentration. The operation and management of such systems is, nevertheless, beset by uncertainties (McLeod et al., 1985; Colls and Baker, 1988; Heagle, 1989).

Field chambers

The third type of experimental set-up to study the effect of air pollutants on plants involves the use of field chambers. The Open Top Chamber (OTC) is the type most widely used at present. The original objective of the open top chamber design was

to create an environment that more closely resembled field conditions than the environment found in closed systems. At the same time air quality could be controlled. This was obtained by constructing a unit in which plants grow, with an open top through which filtered or non-filtered ambient air was blown by a fan. Gaseous air pollutants could be added simultaneously to the incoming air. The present study deals with the OTC research. Attention is focused primarily on OTC's used by KEMA¹⁾.

1.2 Historical background to the present study

OTC's are used for research throughout the world. The development of open-air fumigation systems had already started when OTC's were chosen as a main research tool for several projects. However, the inadequate control of gaseous air-pollutant concentrations within the experimental area precluded the use of this kind of system at that time.

The U.S. National Crop Loss Assessment Network (NCLAN) was the first to use open top chambers on a large scale. This institution consisted of government and non-government organisations cooperating to determine the immediate and potential effects of air pollution on crop production. The major NCLAN objective was to obtain valid relationships between seasonal exposures to various ozone levels and the yield of important agricultural crops. During a series of meetings in 1980, OTC's were chosen as the major research tool in the U.S. NCLAN research programme (Heagle et al., 1988) since the chambers:

- allowed adequate control of a range of ozone concentrations regardless of wind direction,
- allowed for a control treatment (less than ambient ozone level),
- allowed treatment replication at a moderate cost,
- did not cause a major change of microclimate inside the chamber.

The European Community (EC) coordinates several experiments within the framework of their programme of environmental protection. Their main topic is the effect of air pollution on agricultural crops and trees. One of the projects involves

setting up a European network of OTC-experiments. Several valuable experiments with OTC's were already under way in various European countries when this project was initiated. Furthermore, the specific objectives of the various experiments obviously differed from site to site. The primary objective of the EC programme is, however, not to assess agricultural crop losses at the community level (as in the NCLAN programme); emphasis is placed on the coordination of current experiments to investigate the mechanisms of injury in relation to the variety of pollution climates that characterize Europe, and on the study of interacting factors (Mathy, 1988).

The study described in the present thesis is part of an ongoing KEMA research project. The main objective of this research project is to determine the effects of air pollution on natural vegetation, in particular on the biomass production of agricultural crops in the Netherlands. Three main experimental set-ups were chosen: gas-exchange chambers, OTC's and field experiments. The gas exchange experiments were described by Aben (1990) and the field experiments by van Pul (1992).

The OTC-experiments at KEMA started in 1983. Various plant species, bred in a greenhouse, were exposed to realistic outdoor ozone concentrations (40-200 μgm^{-3} for eight hours per day) in four OTC's for periods of 2-4 weeks. The biomass production and other parameters of the plants were measured at the end of the exposure period. Differences were observed in the amount of plant biomass between non-filtered OTC's and ambient plots.

1.3 Objectives of the present study

A sub-project of the KEMA-OTC research deals with the microclimate within an OTC, as compared to field conditions. An important objective of this KEMA study is to find out how the OTC environment affects the growth and development of plants and how the sensitivity of plants to pollutants and other stresses is influenced. This is not only important for extrapolating OTC experiments to field conditions; even if OTC's are only used for comparison of filtered versus non-filtered plots, it is

important to know how OTC's alter the sensitivity of plants to pollutant stresses. In particular, KEMA intends to obtain an insight into the differences in meteorological parameters determining the gas-transport processes under field and OTC conditions. This thesis deals with the physical behaviour of an OTC. The study was started in cooperation with the Department of Meteorology of the Agricultural University of Wageningen (AUW) and is part of the sub-project mentioned above.

The rather complex configuration of the OTC system itself can be considered as a system of sources and sinks of heat, mass and momentum. The whole OTC system is placed in a turbulent flow field which influences the turbulent transport processes taking place inside the chamber. The microclimate around plants grown under OTC conditions differs from the microclimate observed under field conditions. The resulting microclimate inside a chamber is determined by ambient conditions, the OTC system, plants grown inside the chamber and the ventilation rate.

The major aims of the present study are:

- to give a physical description of the transport processes (mass, momentum and energy) inside an OTC in relation to field conditions;
- to determine the influence of the ventilation rate and the atmospheric boundary layer on the turbulent transport processes inside an OTC.

The ultimate aim of the KEMA research is to compare the exchange coefficients under field and OTC conditions. This comparison can be used to estimate the differences in pollutant uptake by plants inside and outside OTC's. In the present study only the effect of plants on the microclimate is studied. Biological effects of the OTC microclimate on plants are not considered. The resulting meteorological parameters found in the present study may contribute to a crop-growth model in which the effects of pollutant-induced stress observed within an OTC can be extrapolated to an effect under field conditions.

As the KEMA OTC's are based on the OTC described by Heagle et al. (1973), most of the results found in this study can be applied to other OTC's of this type.

1.4 Organization of the thesis

This chapter is an introductory chapter dealing with the OTC as a research tool in studying the effects of air pollutants on plants (1.1). The historical background is presented (1.2) and the main objectives of the present study are given (1.3). In this section an outline of the thesis is given.

Chapter 2 gives an introduction in the open top chamber research. After some general remarks (2.1) an overview of the various types of OTC constructions used (2.2) and the changes in microclimate observed in OTC's based on the Heagle-design (2.3) are presented. Chapter 2 ends with a technical description of the KEMA-type OTC (2.4).

The theory is presented in Chapter 3. First the governing equations, which will be used in the present study, are summarized (3.1). Attention is given to the restrictions that determine the use of these equations. The governing equations are applied to the flow within an OTC and a first guess is made at the relative importance of the various terms in these equations for various positions inside the chamber (3.2). This analysis provides us with a basic insight into the exchange processes which take place inside the chamber. Section 3.3 describes the theoretical background to the two models used in the present study. The first model used is based on the flow simulating program FLUENT (3.3.1). The scaling results found in Section 3.2 will be used to derive the equations which form the basis of this model. The model simulates the turbulent exchange processes within an OTC with a "one and a half order" closure model and is used to generate answers to the following questions:

- In what way is mean air flow and turbulence inside the chamber influenced by mean air flow and turbulence outside the OTC?
- What is the influence of the configuration (nozzle, cylindrical model) on mean air flow and turbulence inside a chamber?
- What is the influence of different flow rates on the questions outlined above?
- How do plants influence mean air flow and turbulence inside a chamber?

The second model used is the OTC-resistance model. It describes the mass and energy fluxes in the OTC system in terms of a potential difference and a bulk resistance (3.3.2). The model is composed of two modules. The first module (3.3.2.1) is based on a resistance model for an OTC initially described by Unsworth (1984) and calculates scalar quantities (e.g. temperature, humidity, air pollutant concentration) inside an OTC system with a bulk resistance model. The module is coupled to a module which describes the bulk exchange processes between soil-vegetation and air inside as well as outside an OTC (3.3.2.2).

Chapter 4 gives an overview of the experimental set-up used to characterize the OTC system. The experimental results were used to derive the prior conditions needed for the models used and served as a tool to verify the simulation results. After a general introduction (4.1) incidental experiments dealing with the flow field within and around an OTC are described (4.2). The last section describes the continuous experiments dealing with the microclimate inside and outside an OTC (4.3).

In Chapter 5 the main experimental and model results are summarized. Main aspects of the flow regime (5.1), the short-wave and long-wave radiation loads (5.2), temperature (5.3), humidity (5.4) and ozone concentration (5.5) are briefly described. Finally, an estimation of the energy and mass exchange fluxes between soil-vegetation and atmosphere inside a chamber is made and the simulated ozone fluxes under field and OTC conditions are compared (5.6).

In Chapter 6 theoretical analysis and experimental and model results are related to one another and this leads to the final remarks and conclusions. After an introduction (6.1) the limitations of the models used are briefly discussed (6.2). Section 6.3 discusses the use of the KEMA-type OTC system and suggests some practical improvements. In Section 6.4 the major conclusions of the present study are given. Although not an objective of the study some attention is paid to the biological effects of the OTC microclimate on plants.

During the last four years much research has been carried out using the KEMA-

type OTC system. The present thesis presents only the broad outlines of the theoretical background of the models used and the model and experimental results. More detailed information can be found in Jetten (1991) and Jetten and Stortelder (1990). Nowadays the use of OTC's has shifted from air pollutant exposure experiments to carbon dioxide enrichment experiments. Although the thesis is not dealing with carbon dioxide fumigation experiments some common remarks referring to this point are made in Section 6.4.

¹⁾ KEMA: Environmental Research Department of the Joint Laboratories and other Services of the Dutch Electricity Supply Companies, Arnhem, The Netherlands.

CHAPTER 2 OPEN TOP CHAMBERS (OTC's), AN OVERVIEW

2.1 General

The OTC's are based on two designs developed, simultaneously, at the Boyce Thompson Institute for Plant Research in Yonkers, New York (Mandl et al., 1973), and at the U.S. Department of Agriculture in cooperation with the North Carolina State University and the Environmental Protection Agency (Heagle et al., 1973). There are two main ways of using OTC's:

- By comparing plant growth and development in OTC's supplied with filtered and non-filtered air, the effects of ambient concentrations of pollutants on plant growth and development can be studied.
- By injecting pollutants into OTC's supplied with filtered air, the effects of individual air pollutants or a combination of air pollutants on plants can be studied.

Various OTC-designs have three objectives (Bell and Ashmore, 1986):

- to minimise differences in microclimate within and between chambers,
- to minimise differences in microclimate inside and outside chambers,
- to minimise the incursion of ambient air.

The choice of an OTC-design depends on the plant species used, the experimental site and the experiments conducted. Furthermore, the price of an OTC and factors like durability and portability of an OTC-design have to be considered.

The microclimate inside a chamber should not be influenced by interactions between OTC's or interactions between OTC's, surrounding buildings and other obstacles. In most experiments involving OTC's an array of chambers is set up. This clustering can result in microclimate differences between OTC's depending on the place in the array. Davis et al. (1983) used a wind tunnel to examine the flow field inside and around cylindrical chamber models. This revealed possible effects of OTC's on the microclimate of downwind OTC's due to incursion of ambient air into a chamber.

OTC's have been used with plants grown in the soil beneath the OTC or in some form of container. The growth of a plant in a container allows the soil conditions to be chosen and reduces soil variability between plots. Furthermore, it is easier to study the responses of plant root systems under these conditions. However, containers can restrict root development and can cause abnormal changes of soil temperature. An alternative would be to replace the soil in a chamber by a standard agricultural soil (Bell and Ashmore, 1986). There is circumstantial evidence that fertilizer rates or type of growth medium do not affect relative plant response to ozone (Heagle, 1983; Heagle 1989).

The NCLAN programme employed standard agronomic procedures for planting dates, fertilizer rates and herbicide application. Chambers were placed over field-crops after crop emergence. Plots were selected on plant appearance, size and stand density, and soil uniformity (Heagle et al., 1988). In most of the NCLAN experiments the plants were irrigated to minimise soil water stress. Water stress can cause partial stomata closure and thus a decrease of foliar gas exchange. Therefore, it was expected that pollutant-induced yield loss would be higher if plants were exposed when they were well watered rather than when they were under water stress. Since it is known that parasites and pests affect ozone exposure-yield relationships, plant pests and diseases were controlled before levels became high enough to affect yield (Heagle, 1989). The NCLAN ozone exposure-yield response studies focused on the most economically important agricultural crops (e.g. field corn, soybean, wheat and cotton). Within each crop the most widely grown cultivars within each region were chosen. A summary of the ozone exposure-yield response experiments in open top chambers performed in the NCLAN programme was given by Heagle et al. (1988).

The protocol of the European OTC-programme also recommends that the chambers should be sited in field crops, preferably spring-sown crops (cereals or legumes), using on-site field soils. Furthermore, the European open top chamber protocol recommends preventive sprays, adequate surface irrigation to avoid water stress, and the normal use of fertilizers (Mathy, 1988).

OTC's are composed of an air-supply system and the chamber itself. The air-

supply system provides the air flow through the chamber. This system can be subdivided into three basic components:

- a ventilation unit to provide air flow to the chambers,
- a filter unit to remove air pollutants from the ambient air,
- a system of manifolds or pipes to disperse the air into the chamber.

2.2 Technical description of the OTC construction

2.2.1 The chamber

Most of the OTC's have a cylindrical construction, but rectangular and more-angular configurations are used too. Surface areas of OTC's vary from 1.30 m² (volume 2.85 m³) to 19.5 m² (volume 75 m³). The surface area of the original Heagle-design was about 7 m², the volume was 17 m³. The KEMA-type OTC used in the present study is shown in Figure 2.1. Most chambers consist of a frame made of aluminum, which is light and resistant to corrosion. The frame is kept as small as possible to prevent shading effects. The frame provides support for a transparent covering. Various types of covering are used e.g. polyvinylchlorides-, polyethylene- and teflon films, rigid plastics, polycarbonates, fiberglass or glass. (Bell and Ashmore, 1986; Jäger et al., 1987).

Various types of modifications have been tested to minimise incursion of ambient air into a chamber (Davis and Rogers, 1980; Buckenham et al., 1981; Davis et al., 1983). Davis et al. (1983) found that a collar with a reduced opening, placed vertically above the test area, gives the best results since this type of collar:

- streamlines the air flow over the OTC,
- decreases the open top area,
- prevents turbulent eddies inside the chamber with sizes larger than the diameter of the open top.

The relatively small plot size of an OTC is a serious limitation to OTC experiments. Large variations in results observed were probably due to experimental variability associated with a small sample size. Given a 12%

coefficient of variation and an ozone effect of 10%, 40 OTC duplicates would be required to give a 95% probability of showing a statistically significant treatment effect (Heagle, 1989).

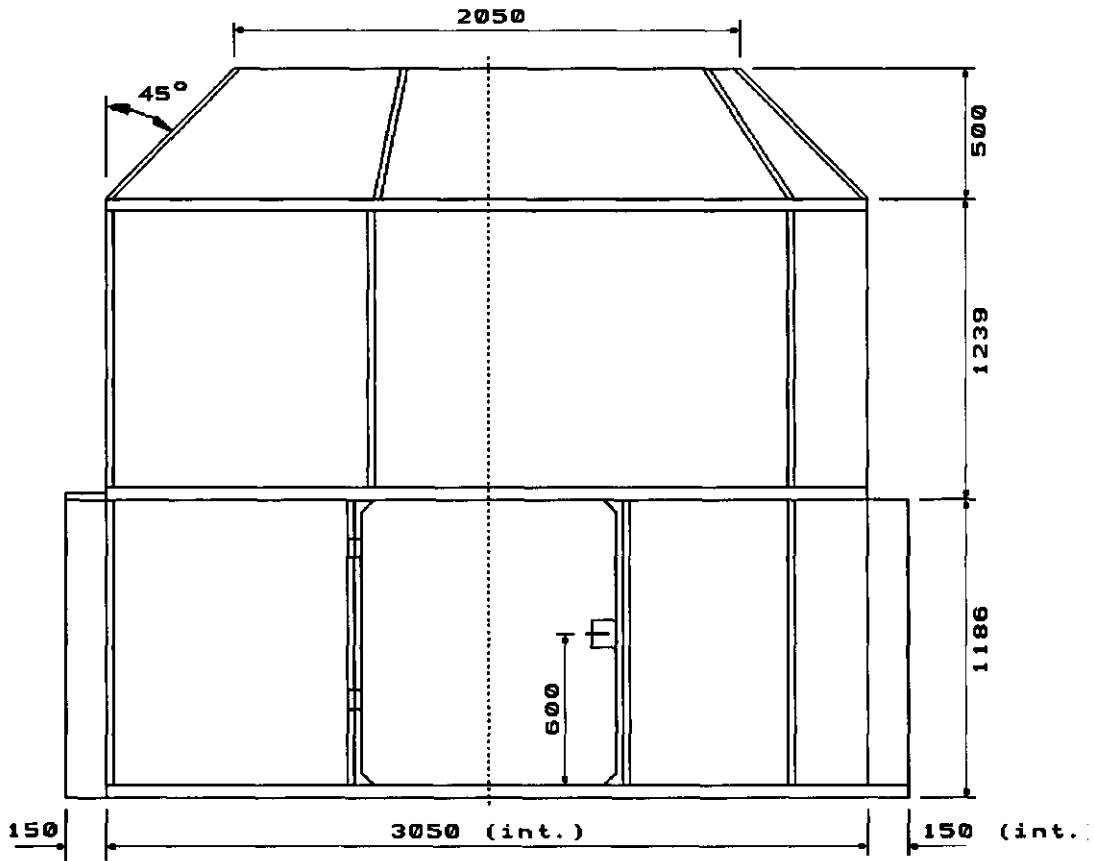


Figure 2.1: Dimensions (in mm) of the KEMA-type Open Top Chamber.

2.2.2 The air-supply system

Ventilation unit

The ventilation unit provides the air flow to the chambers. A fan creates the pressure rise needed for a certain flow rate. The ventilation rates (flow rate to chamber volume) used vary in the range 1.3 - 10 times per minute. Most of the

OTC's based on the Heagle or Mandl design, use a ventilation rate between 2 and 4 air changes per minute corresponding to a flow rate between approximately 0.5 and $1.3 \text{ m}^3\text{s}^{-1}$ (Jäger et al., 1987). The NCLAN research programme employed a ventilation rate of approximately 3 air changes per minute corresponding to a flow rate of approximately $1.18 \text{ m}^3\text{s}^{-1}$ (Heagle et al., 1988). The European open top chamber protocol recommends at least 3 air changes per minute (Mathy, 1988).

Filter unit

The filter unit is meant to remove air pollutants from the ambient air. In most of the present experimental set-ups an activated charcoal filter in combination with a particulate filter is used. The particulate filter is meant to extend the lifetime of the activated charcoal filter. The filter units are arranged in a zigzag pattern to maximise the surface area. The filter efficiency depends on the residence time of the air in the filters. It is important to balance filter efficiency against the capacity of the fan (Bell and Ashmore, 1986). Since activated charcoal filters do not remove nitrogen oxides from the ambient air there is now increasing interest in the use of an activated charcoal filter in combination with a Purafil filter (Bell and Ashmore, 1986, Jäger et al., 1987). Purafil is a combination of activated alumina, potassium permanganate and a small amount of free water. Purafil adsorbs sulphur dioxide, ozone and nitrogen oxides but some nitrogen monoxide is released as nitrogen dioxide. To adsorb this nitrogen dioxide it is necessary to install an activated charcoal filter after the Purafil filter.

Air flow into the chamber

The air flow into the chamber is controlled by a system of manifolds or pipes. The method used to distribute air within the chamber is one of the major design features of an OTC. A review of the most used air distribution systems was given by Bell and Ashmore (1986):

- The lower part of the chamber is composed of two walls. Air is blown between the walls and enters the chamber through holes in the inner wall. This design is used in the NCLAN programme.
- Parallel pipes are attached to an air-supply system, with air flow directed from holes both upwards and downwards.

- A perforated false floor is installed above manifolds of various configurations.
- One or more manifolds are attached to various points on a vertical inlet pipe. This distribution system can be modified according to the height of a particular species and can be changed as a crop grows. The European open-top chambers protocol recommends the use of a perforated annulus adjusted so that it can be 10 to 15 cm above developing crops.
- Air flows from one side of the chamber to the opposite side. To prevent incursion of ambient air via the open top, a part of the air flow is discharged from a collar around the top.

2.3 Microclimate OTC

The microclimate inside an OTC is determined by a combined effect of:

- (1) ambient conditions,
- (2) modification of the air inside the air-supply system,
- (3) incursion of ambient air via the open top,
- (4) the properties of the chamber walls,
- (5) the plants within the chamber.

Ambient conditions

Ambient air flows into the OTC via the air-supply system. The position of the air-inlet of the air-supply system in relation to the properties of the ambient air determines the properties of the air at the beginning of the air-supply system (e.g. temperature, humidity, air pollutant concentration).

Modification of the air inside the air-supply system

Exchange processes between the air within the air-supply system on one hand, and the walls of the air-supply system, the fan and the filters on the other hand can change the properties of the air, e.g. the temperature. The filters within the air-supply system can remove or release components, e.g. water vapour.

Incursion of ambient air via the open top

Incursion through the open top of a chamber can change the temperature pattern,

humidity pattern and the gaseous-pollutant pattern inside a chamber. Schmitt and Ruck (1987) have shown that the air flow out of the top is not uniform but very complex.

Properties of the chamber wall

The properties of the chamber wall can modify the air in the chamber (e.g. temperature, humidity, air pollutant concentration). The chamber wall transmits only a part of the incoming direct and diffuse radiation; the rest is reflected or absorbed. The incidence angle, spectrum of the incoming radiation, thickness of the wall and wall properties (absorption, reflectance, emissivity) play an important role. Furthermore, focusing effects due to the configuration (circular) and shading effects caused by the frame have to be taken into account. The properties of the chamber wall can change with the exposure time.

Plants within the chamber

The microclimate within a chamber affects the growth and development of plants and the uptake of pollutants by these plants. On the other hand, plants influence the microclimate since:

- they are obstacles in an air flow,
- they change the energy balance at the chamber floor,
- they act as a sink or source of carbon dioxide (CO_2), oxygen (O_2), water (H_2O) and pollutants like ozone (O_3).

The flow rate plays an important role in the determination of the resulting microclimate inside a chamber. If the flow rate decreases, the temperature-difference between OTC and field increases. The combination of flow rate and wind velocity outside an OTC plays a major role in the determination of the degree of incursion. The flow rate needed to prevent incursion is a non-linear function of the wind velocity outside the OTC (Schmitt and Ruck, 1987).

In the coming pages a review is given of the microclimate changes observed in OTC's based on the Heagle-design used in the NCLAN programme. Unless this is

stated, the OTC's are not modified by a collar. The microclimate effects can be divided into the following categories: air flow in a chamber, radiation, temperature, humidity, rainfall, dew and air pollutants.

Air flow in a chamber

The air flow through a canopy inside a chamber differs in many ways from field conditions. The wind profile found in chambers is an arbitrary result of the ventilation geometry, the ambient wind field, position inside the chamber and flow rate. Experiments conducted by Heagle et al. (1979) showed slightly smaller wind speeds near the centre of the chamber than towards the periphery. Higher wind speeds can be observed close to an air-inlet hole. This can result in border effects on plants (Jäger et al., 1987).

According to Roberts et al. (1983) the continuous turbulent air flow through a crop inside a chamber plays an important role in the uptake of air pollutants by the crop. Unsworth et al. (1984) measured boundary layer resistances within an OTC using model soybean leaves. They found boundary layer resistances ranging from 10-20 sm^{-1} which was rather small in comparison to those found under field conditions. The mean wind speed within field crops is seldom more than 1 ms^{-1} . To get the same boundary layer resistance as found within chambers a wind speed within a crop of 2-5 ms^{-1} would be, theoretically, needed.

Radiation

Olszyk et al. (1980) reported a reduction of Photosynthetic Active Radiation (PAR) intensity compared to ambient PAR of maximum 20% (vinyl chloride plastic film) depending on solar height and azimuth and the position in the chamber. Weinstock et al. (1982) reported reductions of mean global radiation intensity within a chamber from 10% of ambient in June to 24% in August for the same type of wall-material. Buckenham et al. (1981) reported reductions of direct radiation of up to 40% in areas shaded by the framework (chamber with collar). The intensity in the rest of the chamber was rather uniform and 10-20% less than outside. Heagle et al. (1979) reported significant position and height effects during a day. Olszyk et al. (1980) reported an increase of PAR radiation intensity at canopy height (0.38 m)

due to reflection of radiation by the inner surface of the plastic walls. Heagle et al. (1988) reported higher radiation levels at the north side of the chamber compared to the south side (northern hemisphere). Under field conditions canopy closure usually occurs during vegetative growth and lower leaves become shaded. However, in OTC's chamber walls cause an overall decrease in light intensity within the chamber but can cause an increased light intensity in lower portions of the plant canopies near chamber walls (Heagle et al., 1988).

The reduction of PAR radiation inside a chamber is important for canopy photosynthesis. However, it is the net radiation that is the term most relevant to the energy balance of a canopy. The incoming and outgoing short-wave and long-wave radiation determine the net radiation balance. Since the chamber walls are approximately at chamber air temperature the incoming long-wave radiation within a chamber will be higher than outside (Unsworth et al. 1982, 1984, 1986; Sanders et al., 1991). Unsworth (1986) reported differences in net radiation between an OTC modified with a collar and field conditions up to 120 Wm^{-2} .

Temperature

Inside OTC's, air, leaf and soil temperature are often higher than under field conditions. The average increase of temperature inside a chamber depends on the weather-type and the ventilation rate. A higher ventilation rate limits the temperature increase inside an OTC. As incursion increases, the temperature differences between inside and outside will decrease. Incursion of ambient air into a chamber, modified with a collar, is less than incursion into a chamber without such a design. Therefore, the temperature increase inside an OTC modified with a collar is slightly more, when receiving the same net radiation (Unsworth et al., 1986). Unsworth (1986) reported a maximum temperature increase inside a Heagle-type chamber design of 2-4 K. The largest temperature increase was observed on calm, sunny and hot days (Heagle et al., 1988). Temperature differences depending on height of the order of 0.5 K (0.45-1.35 m) were reported on sunny days but not on cloudy ones. Highest temperatures were measured near the chamber floor (Heagle et al., 1979). Weinstock et al. (1982) reported mean hourly temperature increases inside the chamber of 0.4-3.7 K (height: 1.5 m).

During clear, calm nights a surface temperature inversion in the field resulted in warmer air being drawn to the OTC's than the colder layer of air near the soil-vegetation surface. A significant effect of horizontal position on the temperature in the lower part of the OTC was not found (Olszyk et al., 1980; Heagle et al., 1979).

The temperature of a leaf depends on the temperature of the ambient air, the radiation balance of the leaf, evaporation of water and the air flow around the leaf. Weinstock et al. (1982) reported chamber leaves to be warmer than ambient leaves by an extent usually attributable to higher chamber air temperatures. Fuhrer et al. (1987) reported higher soil temperatures (+0.4 K at 0.05 m depth) as a result of higher chamber temperatures.

Humidity

A part of the incoming net radiation in well watered plant canopies is used for evaporating water from the plants and the soil. Model calculations described by Unsworth (1982) revealed that evaporation of plants contributes to less than 1% relative humidity under normally employed ventilation rates. Since radiation intensity varies within a chamber, the measured evaporative water can be significantly greater in certain areas of the chambers. Olszyk et al. (1980) measured evaporative water loss from black flat top Bellani atmometers. They found 20% more evaporation in the northern part of the chamber than in the southern area. Weinstock et al. (1982) reported a decrease of relative humidity of 5-10% inside the chamber (height: 1.5 m) compared to field conditions. Heagle et al. (1988) reported an increase or decrease of relative humidity up to 10% depending on ambient conditions, soil moisture and type of plant canopy. The difference was usually less than 5%.

The vapour pressure deficit of the air is an important factor in plant evaporation processes. The amount of water loss from plants is related to the vapour pressure deficit. Furthermore, vapour pressure deficit can modify stomatal response. Weinstock et al. (1982) reported a vapour pressure deficit increase of 1 to 7 mbar inside the chamber (height 1.5 m) compared to field conditions.

Rainfall

Heagle et al. (1973) reported that rainfall patterns within the chamber depended on the wind velocity outside the OTC. The chamber walls, in combination with modifications to decrease incursion cause rain shadows within the chamber. Therefore, irrigation is needed to reduce lateral gradients in soil moisture levels. Care should be taken with the amount of water delivered to a crop, the application period and the chemical composition of the water. During irrigation the micrometeorological conditions should closely resemble field conditions (Johnston et al., 1986).

Dew

During periods of dew outside the OTC, dew formation within an OTC is occasionally reduced or suppressed completely (Weinstock, 1982; Jäger, 1987).

Air pollutants

Under field conditions ozone concentrations within a crop will be lower than above. In OTC's there is no clear canopy induced vertical gradient due to the continuous ventilation. Air pollutant concentrations within the chamber are not completely homogeneous since incursion of ambient air into the chamber and transport of pollutants to walls, soil and plants can take place. The highest fluctuations of ozone concentration within a chamber occur when wind speed outside the chamber is strong and highly variable and the difference in ozone concentration between the air inside the chamber and ambient air is largest (Heagle et al., 1988). An ozone decrease above the air-inlet holes with increased height was observed for chambers fumigated with ozone. Heagle et al. (1979) injected ozone into the airstream going to a chamber. They found mean concentrations of ozone at 1.20 and 1.80 m to be 4 and 16% less, when compared to those at 0.45 m.

The use of OTC's obviously introduces a degree of artificiality which makes it impossible to duplicate field conditions; this has been confirmed by several authors (Last, 1986; Unsworth, 1986; Sanders et al., 1991). The literature mentions several examples of growth differences between non-filtered OTC's and field plots, which

vary with season and plant species (Unsworth, 1986; Heagle et al., 1988).

2.4 Technical description of the KEMA-type OTC

General

Four OTC's have been used in the KEMA research project. They are located at KEMA and used for fumigation experiments in which plants are exposed to various concentrations of pollutants, primarily ozone. There is a reference-field, where plants are grown under field conditions (as a crop), at KEMA. Furthermore, an OTC reference model is available from which the enclosure itself has been removed. The position of the plants, soil conditions and the watering regime are exactly the same in this model as in an OTC.

The chamber

The type of OTC used in the KEMA research project is a modified version of the USDA-EPA type described by Heagle et al. (1973) with, as modification, an added collar and the use of different wall material.

The KEMA-type OTC (fig. 2.1) consists of a cylindrical aluminum frame covered with 1.5 mm lexan (polycarbonate). Lexan does not transmit wavelengths less than 385 nm. There is a sharp decrease in transmittancy at a wavelength of about 2200 nm. In the range 2200-12000 nm almost no radiation is transmitted except for a narrow band around 4000 nm. A collar was constructed to minimise incursion. Wind tunnel experiments conducted at KEMA, in which various types of collars were tested, showed the nozzle-configuration to be the best. The lower half of the chamber is composed of a double wall of lexan forming a rectangular channel. The inner wall is perforated and consists of about 225 air-inlet holes (5 rows, 0.025 m diameter). Incoming air is uniformly distributed over the air-inlet holes. A white painted netting (3.5x1.2 m, 0.05 m mesh) was stretched at the side of the air-supply system (north side). This netting is meant to prevent light spots inside a chamber due to reflection of light against the circular north wall.

The chamber floor is covered with a wooden plate (Betonplex birch) with 36 holes for the plants. These holes are situated in three plant-hole circles of 18 (radius:

0.45 m), 12 (radius: 0.85 m) and 6 holes (radius: 1.25 m), respectively. Plants are grown in pots or loosely woven sacks. Water reaches the plants via a water-supply system. Therefore, water stress is not a reducing factor in plant respiration. The amount of water supplied can be controlled for each plant hole.

The air-supply system

The air-supply system is situated at the north side of the OTC. A fan draws ambient air via a filter unit and a connecting duct into the perforated channel around the lower half of the OTC (Fig. 2.2). The flow rate is adjustable between $0.4 \text{ m}^3\text{s}^{-1}$ and $3.25 \text{ m}^3\text{s}^{-1}$, and set to $1.4 \text{ m}^3\text{s}^{-1}$. The OTC volume is 20.4 m^3 , so that the ventilation rate is 4.1 per minute. The flow rate is measured using a multipoint pitot-tube station combined with a honeycomb air-equalizing and air-straightening section, which is positioned in the middle of the connecting duct. The air is filtered by means of two activated charcoal filters or by means of an activated charcoal filter (Sutcliffe Speakman, type 207C) in combination with a Purafil filter. Filter efficiencies can be found in Jetten and Stortelder (1990). The mean residence time of the air in the filters is about 0.38 s (flow rate: $1.4 \text{ m}^3\text{s}^{-1}$). Since the filters in the filter unit are removable, the air flow into the OTC can be filtered or non-filtered. A particulate filter (Super Hi-flo 85) is positioned at the beginning of the air-supply system to extend the lifetime of the activated charcoal and Purafil filters.

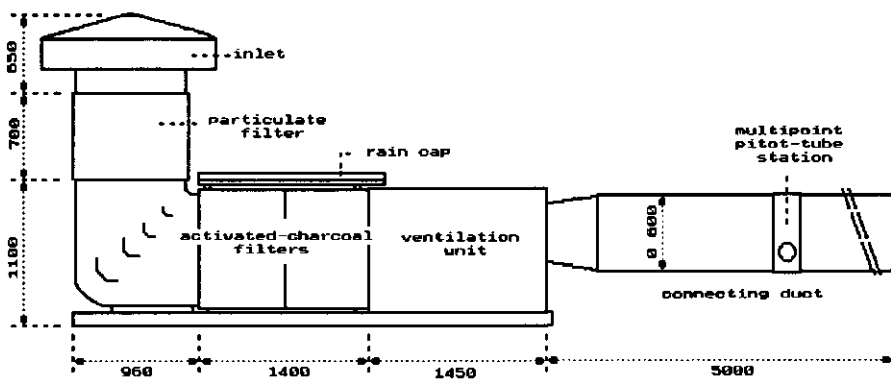


Figure 2.2: The air-supply system of the KEMA-type OTC.

Fumigation system

The plants inside the OTC were exposed to various concentrations of ozone. An ozone generator (Fischer 502) transformed oxygen (from gas cylinders) to ozone. The oxygen flow, and thus ozone production, could be controlled by means of a mass-flow controller. Ozone was injected into the air-supply system just before the fan, insuring good mixing of the ozone. The day and night concentrations of ozone were adjustable and controlled by a computer.

Monitoring of the microclimate

A mast, one metre high, to which temperature, relative humidity, PAR and leafwet-period sensors were attached was placed in the middle of each OTC and in the middle of the OTC reference model. A personal computer read the output of the sensors. Samples of air were continuously aspirated from all OTC's and from the ambient air. Three monitors recorded the concentrations of nitrogen oxides, ozone and sulphur dioxide. More information about the sensors used and the measurement protocol can be found in Jetten and Stortelder (1990). Table 2.1 represents a summary of the main microclimate differences between a KEMA-type OTC and an OTC reference observed over a period of six years. The values given in this table clearly show an OTC effect on the microclimate.

Table 2.1: Open top chamber effects on microclimate during May-September (1983-1988). Flow rate: $1.4 \text{ m}^3\text{s}^{-1}$.

Variable	Effects in chamber
Wind speed	Mean wind speed in lower 0.75 m of the chamber decreased with distance to the chamber wall from 1.20 ms^{-1} at 0.20 m from the wall to 0.85 ms^{-1} at 1.10 m from the wall.
PAR radiation	Mean reduction of PAR radiation over a day at 1 m was 15-30%. On clear days northern positions in the chamber received more PAR radiation than southern positions.
Temperature	The mean temperature increase over a 4-week period was 0.8-2.0 K. Temperature differences could increase to approximately 4.0 K.
Humidity	Mean relative humidity was 4-5% lower than under field conditions.
Dew	Mean vapour pressure deficit was 1-2 mbar higher in the chamber. No dew formation was seen on the leaves of plants grown under OTC conditions during periods of dew outside the OTC.
Ozone concentration	Ozone concentration differences over the chamber were less than 15%.

CHAPTER 3 THEORY

3.1 Governing equations

A basic knowledge of the flow regime inside an OTC is needed in order to understand the differences and similarities between the exchange processes taking place under field and OTC conditions. In this section the governing equations which will be used in the present study are summarized and the restrictions governing the use of these equations are briefly discussed.

The physical aspects of a fluid (liquid or gaseous medium) are governed by three fundamental principles:

- mass is conserved,
- momentum is conserved,
- energy is conserved.

These fundamental principles can be expressed in terms of mathematical equations, which in their most general form are partial differential equations. The theory used in this chapter can be found in Hinze (1959), Monin and Yaglom (1965), Stull (1988) and Tennekes and Lumley (1972). All the equations are given using the Eulerian approach.

3.1.1 Conservation of mass

The conservation of mass leads to the continuity equation.

$$\underbrace{\frac{\partial \rho}{\partial t}}_{\text{I}} + \underbrace{\frac{\partial \rho U_i}{\partial X_i}}_{\text{II}} = 0 \quad (3.1)$$

where

- Term I : Time change.
 Term II : Convection.

- U_i : Component of velocity vector in i -direction [ms^{-1}].
 X_i : Distance in i -direction [m].
 i : Subscript denoting the direction of the velocity vector (1,2,3).
 t : Time [s].

ρ : Density [kgm^{-3}].

In the case of gaseous media in steady motion the variation of density due to the variations of pressure can be ignored if the velocity at any point in the flow is small in comparison with the velocity of sound. In general, for unsteady motions, variations of the density will be negligible if the following condition is fulfilled:

$$\tau > \frac{L}{c} \quad (3.2)$$

where

- L : Characteristic length scale in which the velocity of the fluid undergoes a perceptible change [m].
 c : The speed of sound [ms^{-1}].
 τ : Characteristic time scale in which the velocity of the fluid undergoes a perceptible change [ms^{-1}].

If incompressibility is assumed Eq. (3.1) reduces to

$$\frac{\partial U_i}{\partial X_i} = 0. \quad (3.3)$$

3.1.2 Conservation of momentum

Newton's second law describes the conservation of momentum, which reads for a fixed point in space

$$\frac{\partial \rho U_i}{\partial t} + \frac{\partial \rho U_i U_j}{\partial X_j} = -\frac{\partial P}{\partial X_i} - 2\rho \varepsilon_{ijk} \Omega_j U_k + \frac{\partial \tau_{ij}}{\partial X_j} + \rho F_i \quad (3.4)$$

where

- P : Hydrostatic pressure [Nm^{-2}].
 F_i : Body force per unit mass in i -direction [Nkg^{-1}].
 j, k : Subscript denoting the direction (1,2,3).
 τ_{ij} : Force per unit area in the X_j -direction acting on the face that is normal to the X_i -direction [Nm^{-2}].
 ε_{ijk} : Alternating unit tensor [-].
 Ω_j : Component of angular velocity vector of the rotation of the earth [s^{-1}].

The terms $\frac{\partial \tau_{ij}}{\partial X_j}$ in Eq. (3.4) represent the viscous stress terms. The flow inside an OTC is considered to be a Newtonian flow in which the viscous shear stress is

linear dependent on the shear. The stress for a Newtonian medium is given by

$$\tau_{ij} = \mu \left(\frac{\partial U_i}{\partial X_j} + \frac{\partial U_j}{\partial X_i} \right) - \left(\frac{2}{3} \mu \right) \frac{\partial U_k}{\partial X_k} \delta_{ij} \quad (3.5)$$

where

- δ_{ij} : Kronecker delta [-].
 μ : Dynamic viscosity [$\text{kg s}^{-1} \text{m}^{-1}$].

The assumption of incompressibility leads to a modified version of Eq. (3.4).

$$\underbrace{\frac{\partial U_i}{\partial t}}_I + \underbrace{U_j \frac{\partial U_i}{\partial X_j}}_{II} = - \underbrace{\frac{1}{\rho} \frac{\partial P}{\partial X_i}}_{III} - \underbrace{2 \varepsilon_{ijk} \Omega_j U_k}_{IV} + \underbrace{\nu \frac{\partial^2 U_i}{\partial X_j \partial X_j}}_V + \underbrace{F_i}_{VI} \quad (3.6)$$

where

- Term I : Time change.
 Term II : Convection.
 Term III : Pressure gradient forces.
 Term IV : Coriolis effect (the influence of the earth's rotation).
 Term V : Viscous stress.
 Term VI : Body forces per unit mass.

- ν : Kinematic viscosity [$\text{m}^2 \text{s}^{-1}$].

In turbulent flows, a description of the flow at all points in time and space is not feasible. Therefore, Reynolds developed governing equations of mean quantities by expressing variables into a mean and a turbulent part. Expanding all the dependent variables in Eq. (3.3) into a mean and turbulent part and time averaging leads to

$$\frac{\partial \bar{u}_i}{\partial X_j} = 0 \quad (3.7)$$

$$\frac{\partial u'_i}{\partial X_j} = 0 \quad (3.8)$$

where

- (\dots) : Time averaging operator [-].
 $(\dots)'$: Deviation from time mean value [-].

Expanding all the dependent variables in Eq. (3.6) into a mean and turbulent part, and averaging the whole equation leads to

$$\frac{\partial \bar{u}_i}{\partial t} + \bar{u}_j \frac{\partial \bar{u}_i}{\partial X_j} = -\frac{1}{\rho} \frac{\partial \bar{p}}{\partial X_i} - \frac{\partial \overline{u'_i u'_j}}{\partial X_j} - 2\epsilon_{ijk} \Omega_j \bar{u}_k + \nu \frac{\partial^2 \bar{u}_i}{\partial X_j \partial X_j} + F_i \quad (3.9)$$

Due to non-linearity of Term II of Eq. (3.6) an extra term, called the turbulent diffusion term, appears in the right hand side of Eq. (3.9). The importance of the various terms in the governing equations can be estimated by using dimensionless numbers composed of characteristic flow scales. For every flow one or more typical length (L), time (τ), velocity (U) and pressure (ΔP) scales can be defined. With these typical scales the various terms in Eq. (3.9) can be made dimensionless.

$$\frac{U}{\tau} \frac{\partial \bar{u}_i}{\partial \bar{t}} + \frac{U^2}{L} \bar{u}_j \frac{\partial \bar{u}_i}{\partial \bar{X}_j} = -\frac{\Delta P}{\rho L} \frac{\partial \bar{p}}{\partial \bar{X}_i} - \frac{\partial \overline{u'_i u'_j}}{\partial \bar{X}_j} - 2U \epsilon_{ijk} \Omega_j \bar{u}_k + \frac{\nu U}{L^2} \frac{\partial^2 \bar{u}_i}{\partial \bar{X}_j \partial \bar{X}_j} + F_i \quad (3.10)$$

where
 (...) : Dimensionless variable.

Dividing Eq. (3.10) by the inertial scale $\frac{U^2}{L}$ and ignoring body forces leads to

$$Sr \frac{\partial \bar{u}_i}{\partial \bar{t}} + \bar{u}_j \frac{\partial \bar{u}_i}{\partial \bar{X}_j} = -\frac{1}{Eu} \frac{\partial \bar{p}}{\partial \bar{X}_i} - \frac{\partial \overline{u'_i u'_j}}{\partial \bar{X}_j} + \frac{1}{Ro} \epsilon_{ijk} \bar{u}_k + \frac{1}{Re} \frac{\partial^2 \bar{u}_i}{\partial \bar{X}_j \partial \bar{X}_j} \quad (3.11)$$

where

Eu : Euler number $\frac{\rho U^2}{\Delta P}$

Re : Reynolds number $\frac{UL}{\nu}$

Ro : Rossby number $\frac{U}{2\Omega_j L}$

Sr : Strouhal number $\frac{L}{U\tau}$

For every direction a typical length and velocity scale can be defined. Furthermore, a scale characterizing the turbulent fluctuations in a particular direction can be defined. Analogous to the derivation of Eq. (3.11) this yields for

the X_a -direction

$$\begin{aligned}
 & \frac{L_a}{U_a \tau} \frac{\partial \bar{u}_1}{\partial t} + \frac{\bar{u}_1}{U_a} \frac{\partial \bar{u}_1}{\partial X_1} + \frac{L_a U_b}{U_a L_b} \frac{\partial \bar{u}_1}{\partial X_2} + \frac{L_a U_c}{U_a L_c} \frac{\partial \bar{u}_1}{\partial X_3} = - \frac{\Delta P}{U_a^2 \rho} \frac{\partial \bar{p}}{\partial X_1} - \frac{u_a u_a}{U_a^2} \frac{\partial \bar{u}_1}{\partial X_1} - \\
 & \frac{L_a u_a u_b}{U_a^2 L_b} \frac{\partial \bar{u}_1}{\partial X_2} + \frac{L_a u_a u_c}{U_a^2 L_c} \frac{\partial \bar{u}_1}{\partial X_3} + \nu \frac{1}{U_a L_a} \frac{\partial^2 \bar{u}_1}{\partial X_1^2} + \nu \frac{L_a}{U_a L_b L_b} \frac{\partial^2 \bar{u}_1}{\partial X_2^2} + \\
 & \nu \frac{L_a}{U_a L_c L_c} \frac{\partial^2 \bar{u}_1}{\partial X_3^2} + F_{cor}
 \end{aligned} \tag{3.12}$$

where

- Term I : Time change.
 Term II : Convection.
 Term III : Pressure gradient forces.
 Term IV : Turbulent diffusion.
 Term V : Viscous stress.
 Term VI : Coriolis forces.

- L_a : Characteristic length scale in a -direction [ms^{-1}].
 U_a : Characteristic mean velocity scale in a -direction [ms^{-1}].
 u_a : Characteristic turbulent velocity scale in a -direction [ms^{-1}].
 a, b, c : Subscript denoting the direction (1,2,3).

Expanding all the dependent variables in Eq. (3.6) into a mean and turbulent part and subtracting the equation for the mean part leaves an equation for a turbulent gust (u'_j). Multiplying this equation by (u'_j) and time averaging leads to an equation for the turbulent kinetic energy. This equation can be written

$$\frac{\partial k}{\partial t} + \bar{u}_i \frac{\partial k}{\partial X_i} = - \bar{u}_i u'_j \frac{\partial \bar{u}_i}{\partial X_j} - \frac{\partial \bar{u}'_j k}{\partial X_j} - \frac{1}{\rho} \frac{\partial \bar{u}'_j p}{\partial X_j} - \nu \frac{\partial \bar{u}'_j{}^2}{\partial X_j} + \frac{\nu}{2} \frac{\partial^2 (\bar{u}'_j u'_j)}{\partial X_j^2} \tag{3.13}$$

where

- Term I : Time change.
 Term II : Convection.
 Term III : Production.
 Term IV : Turbulent transport.
 Term V : Redistribution by pressure perturbations.

Term VI : Loss by viscous stress.

k : Turbulent kinetic energy [m^2s^{-2}].

$$k = \frac{1}{2} (\overline{(u_1')^2} + \overline{(u_2')^2} + \overline{(u_3')^2}) \quad (3.14)$$

Analogous to the equation for turbulent kinetic energy an equation can be derived for the turbulent momentum flux

$$\begin{aligned} \frac{\partial \overline{u_i' u_k'}}{\partial t} + \overline{u_j} \frac{\partial \overline{u_i' u_k'}}{\partial X_j} &= -\overline{u_i' u_j'} \frac{\partial \overline{u_k'}}{\partial X_j} - \overline{u_k' u_j'} \frac{\partial \overline{u_i'}}{\partial X_j} - \frac{\partial \overline{u_i' u_j' u_k'}}{\partial X_j} - \frac{1}{\rho} \left(\frac{\partial \overline{p' u_k'}}{\partial X_j} + \frac{\partial \overline{p' u_i'}}{\partial X_k} \right) \\ &\quad - \overline{\rho' \left(\frac{\partial u_i'}{\partial X_k} + \frac{\partial u_k'}{\partial X_i} \right)} + \nu \frac{\partial^2 \overline{u_i' u_k'}}{\partial X_j^2} - 2\nu \frac{\partial \overline{u_i' \partial u_k'}}{\partial X_j^2} + F_{cor} \end{aligned} \quad (3.15)$$

where

- Term I : Time change.
- Term II : Convection by mean wind.
- Term III : Production by mean wind shear.
- Term IV : Transport by turbulent motions.
- Term V : Transport by pressure correlation term.
- Term VI : Redistribution by return-to-isotropy term.
- Term VII : Molecular diffusion.
- Term VIII : Viscous dissipation.
- Term IX : Coriolis force.

3.1.3 Conservation of energy

At any point in a fluid the amount of energy flowing into a system has to balance the internal energy of the system and the amount of work done by the system. For a gaseous medium the conservation of energy in combination with the perfect gas law

$$PV = nR^* T \quad (3.16)$$

where

- R^* : Universal gas constant (8.3144) [$\text{Jmol}^{-1}\text{K}^{-1}$].
- T : Temperature of the gas [K].
- V : Volume of the gas [m^3].
- n : Amount of gas [mol].

leads to

$$\frac{\partial T}{\partial t} + U_i \frac{\partial T}{\partial X_i} - \frac{1}{\rho C_p} \left(\frac{\partial P}{\partial t} + U_i \frac{\partial P}{\partial X_i} \right) = \frac{\lambda}{\rho C_p} \frac{\partial^2 T}{\partial X_i \partial X_i} + \frac{1}{\rho C_p} (\phi_c + \phi_s + \rho \epsilon) \quad (3.17)$$

I II III IV V

where

- Term I : Time change.
 Term II : Convection.
 Term III : Pressure variation.
 Term IV : Molecular diffusion.
 Term V : Chemical reactions, radiation and viscous dissipation.

- C_p : Specific heat capacity at constant pressure [$\text{Jkg}^{-1}\text{K}^{-1}$].
 ϵ : Viscous dissipation [m^2s^{-3}].
 λ : Molecular thermal conductivity [$\text{Wm}^{-1}\text{K}^{-1}$].
 ϕ_c : Energy production or loss by chemical reactions [$\text{Jm}^{-3}\text{s}^{-1}$].
 ϕ_s : Energy production through absorption of radiation [$\text{Jm}^{-3}\text{s}^{-1}$].

All the dependent variables in Eq. (3.17) are split into a mean and turbulent part. After time averaging the equation is made dimensionless and divided by a temperature convective scale ($\frac{U\Delta T}{L}$) leading to

$$Sr \frac{\partial \bar{T}}{\partial \bar{t}} + \bar{u}_i \frac{\partial \bar{T}}{\partial \bar{X}_i} - \frac{1}{\rho C_p} \left(Sr \frac{\Delta P}{\Delta T} \frac{\partial \bar{p}}{\partial \bar{t}} + \frac{\Delta P}{\Delta T} \bar{u}_i \frac{\partial \bar{p}}{\partial \bar{X}_i} \right) = \frac{1}{Pe} \frac{\partial^2 \bar{T}}{\partial \bar{X}_i \partial \bar{X}_i} - \frac{\partial \bar{T} \bar{u}_i}{\partial \bar{X}_i} +$$

I II III IV V

$$\frac{L}{\Delta T U \rho C_p} (\phi_c + \phi_s + \rho \epsilon) \quad \text{VI} \quad (3.18)$$

where

- Term I : Time change.
 Term II : Convection.
 Term III : Pressure variation.
 Term IV : Molecular diffusion.
 Term V : Turbulent diffusion.
 Term VI : Chemical reactions, radiation and viscous dissipation.

- a : Molecular thermal diffusivity $\frac{\lambda}{\rho C_p}$ [m^2s^{-1}].

- Pe : Péclet number $\frac{UL}{a}$

Again, for every direction a typical length and velocity scale can be defined. Furthermore, a scale characterizing the turbulent fluctuations in a particular direction can be defined. Thus Term II, IV and V of Eq. (3.18) can be written

$$\text{Term II: } \frac{U_a L \bar{u}_1}{UL_a} \frac{\partial \bar{T}}{\partial \bar{X}_1} + \frac{U_b L \bar{u}_2}{UL_b} \frac{\partial \bar{T}}{\partial \bar{X}_2} + \frac{U_c L \bar{u}_3}{UL_c} \frac{\partial \bar{T}}{\partial \bar{X}_3} \quad (3.18a)$$

IIa IIb IIc

$$\text{Term IV: } \frac{aL}{UL_a L_a} \frac{\partial^2 \bar{T}}{\partial \bar{X}_1 \bar{X}_1} + \frac{aL}{UL_b L_b} \frac{\partial^2 \bar{T}}{\partial \bar{X}_2 \bar{X}_2} + \frac{aL}{UL_c L_c} \frac{\partial^2 \bar{T}}{\partial \bar{X}_3 \bar{X}_3} \quad (3.18b)$$

IVa IVb IVc

$$\text{Term V: } \frac{T_{H_a} u_a L}{L_a U \Delta T} \frac{\partial \bar{T}' \bar{u}'_1}{\partial \bar{X}_1} + \frac{T_{H_b} u_b L}{L_b U \Delta T} \frac{\partial \bar{T}' \bar{u}'_2}{\partial \bar{X}_2} + \frac{T_{H_c} u_c L}{L_c U \Delta T} \frac{\partial \bar{T}' \bar{u}'_3}{\partial \bar{X}_3} \quad (3.18c)$$

Va Vb Vc

where T_H : Characteristic scale for the temperature fluctuations [K].

Humidity differences in the air cause density differences which sometimes can not be neglected. To correct for these humidity differences the temperatures in Eqs. (3.17) and (3.18) have to be replaced by virtual temperatures (T_v) and the specific heat capacity for dry air by the specific heat capacity for humid air. The virtual temperature of the air is defined as the temperature of dry air which has the same density as humid air at the same pressure:

$$T_v = T(1 + 0.61 q_a) \quad (3.19)$$

where q_a : Specific humidity of the air [kgkg^{-1}].

The specific heat capacity for dry air can be written

$$C_p = C_{pd} (1 + 0.84 q_a) \quad (3.20)$$

where C_{pd} : Specific heat capacity of dry air at constant pressure [$\text{Jkg}^{-1}\text{K}^{-1}$].

In Eq. (3.11) it was assumed that the velocity of the motion is sufficiently small, to ignore the variations in the density produced by the variations of pressure. However, for temperature differences within a gravitational field Archimedean forces cause an upward buoyancy of the warmer volumes of fluid and a downward

buoyancy of the cooler volumes. The velocity field can be assumed to be completely incompressible if variations of density produced by temperature inhomogeneities are small, i.e. provided the absolute temperature differences over the flow are small in comparison with the mean temperature. For these cases a correction term was introduced by Boussinesq in the right hand side of the momentum equations leading to

$$Sr \frac{\partial \bar{u}_i}{\partial t} + \bar{u}_j \frac{\partial \bar{u}_i}{\partial X_j} = - \frac{1}{Eu} \frac{\partial \bar{p}}{\partial X_i} - \frac{\partial \bar{u}_j \bar{u}_i}{\partial X_j} + \frac{1}{Ro} \epsilon_{ijk} \bar{u}_k + \frac{1}{Re} \frac{\partial^2 \bar{u}_i}{\partial X_j \partial X_j} + \delta_{i3} \frac{1}{Ar} \bar{T}_1 \quad (3.21)$$

where

$$T_1 = T_v - T_{ov}$$

T_{ov} : Virtual temperature at a reference height [K].

T_1 : Virtual temperature difference with virtual temperature at a reference height [K].

Ar : Archimedes number $\frac{U^2}{g\beta\Delta TL}$

$\beta = \frac{1}{T_v}$: Thermal expansion coefficient for a perfect gas [K⁻¹].

The introduction of variations in density produced by variations in temperature leads to an extra term in the equations for turbulent kinetic energy (3.13) and turbulent momentum flux (3.15). Eq. (3.13) changes to

$$\begin{aligned} \frac{\partial k}{\partial t} + \bar{u}_j \frac{\partial k}{\partial X_j} &= -\overline{u'_j u'_j} \frac{\partial \bar{u}_i}{\partial X_j} - \frac{\partial \overline{u'_j k}}{\partial X_j} + g \delta_{i3} \overline{u'_i \left(\frac{T'_v}{T_v} \right)} - \frac{1}{\rho_0} \frac{\partial \overline{u'_i \rho'}}{\partial X_i} - \\ &\nu \left(\frac{\partial \overline{u'_i{}^2}}{\partial X_j} \right) + \frac{\nu}{2} \frac{\partial^2 \overline{(u'_i u'_i)}}{\partial X_j^2} \end{aligned} \quad (3.22)$$

where

g : Acceleration due to gravity [ms⁻²].

ρ_0 : Density of air at reference height [kgm⁻³].

Eq. (3.15) changes to

$$\frac{\partial \overline{u'_i u'_k}}{\partial t} + \bar{u}_j \frac{\partial \overline{u'_i u'_k}}{\partial X_j} = -\overline{u'_i u'_j} \frac{\partial \bar{u}_k}{\partial X_j} - \overline{u'_k u'_j} \frac{\partial \bar{u}_i}{\partial X_j} - \frac{\partial \overline{u'_i u'_j u'_k}}{\partial X_j} - \frac{1}{\rho_0} \left(\frac{\partial \overline{\rho' u'_k}}{\partial X_i} + \frac{\partial \overline{\rho' u'_i}}{\partial X_k} \right)$$

$$\overline{p' \left(\frac{\partial u_i'}{\partial X_k} + \frac{\partial u_k'}{\partial X_i} \right)} + \frac{g}{T_v} (\delta_{k3} \overline{u_i' T'_v} + \delta_{i3} \overline{u_k' T'_v}) + v \frac{\partial^2 \overline{u_i' u_k'}}{\partial X_j^2} - 2v \frac{\partial \overline{u_i' \partial u_k'}}{\partial X_j^2} + F_{cor} \quad (3.23)$$

3.1.4 Conservation of a scalar quantity

A fluid can be composed of various components. Eq. (3.24) can be derived for the conservation of any scalar quantity.

$$\underbrace{\frac{\partial C}{\partial t}}_I + \underbrace{U_i \frac{\partial C}{\partial X_i}}_{II} = \underbrace{D_{sc} \frac{\partial^2 C}{\partial X_i \partial X_i}}_{III} + \underbrace{S_{sc}}_{IV} \quad (3.24)$$

where

- Term I : Time change.
- Term II : Convection.
- Term III : Molecular diffusion.
- Term IV : Source or sink.

- C : Concentration of a scalar quantity [kgm^{-3}].
- D_{sc} : Molecular diffusivity of a scalar quantity [m^2s^{-1}].
- S_{sc} : Production or loss of a scalar quantity (e.g. chemical reactions) [$\text{kgm}^{-3}\text{s}^{-1}$].

All the dependent variables in Eq. (3.24) are split into a mean and turbulent part. After time averaging the equation is made dimensionless and divided by a mass convective scale ($\frac{\Delta CU}{L}$) leading to

$$\underbrace{Sr \frac{\partial \bar{c}}{\partial \bar{t}}}_I + \underbrace{\bar{u}_j \frac{\partial \bar{c}}{\partial \bar{X}_j}}_{II} = - \underbrace{\frac{\partial \bar{c}' \bar{u}'_j}{\partial \bar{X}_j}}_{III} + \underbrace{\frac{1}{Sh} \frac{\partial^2 \bar{c}}{\partial \bar{X}_j \partial \bar{X}_j}}_{IV} + \underbrace{\frac{L}{\Delta CU} S_{sc}}_V \quad (3.25)$$

where

- Term I : Time change.
- Term II : Convection.
- Term III : Turbulent diffusion.
- Term IV : Molecular diffusion.
- Term V : Source or sink.

- Sh : Sherwood number $\frac{UL}{D_{sc}}$

Again for every direction a typical length and velocity scale can be defined.

Furthermore, a scale characterizing the turbulent fluctuations in a particular direction can be defined. Thus Term II, III and IV of Eq. (3.25) can be written

$$\text{Term II: } \frac{U_a L_a \bar{u}_1}{UL_a} \frac{\partial \bar{c}}{\partial \bar{X}_1} + \frac{U_b L_b \bar{u}_2}{UL_b} \frac{\partial \bar{c}}{\partial \bar{X}_2} + \frac{U_c L_c \bar{u}_3}{UL_c} \frac{\partial \bar{c}}{\partial \bar{X}_3} \quad (3.25a)$$

IIa IIb IIc

$$\text{Term III: } \frac{C_n u_a L}{L_a U \Delta C} \frac{\partial \bar{c}' \bar{u}_1}{\partial \bar{X}_1} + \frac{C_n u_b L}{L_b U \Delta C} \frac{\partial \bar{c}' \bar{u}_2}{\partial \bar{X}_2} + \frac{C_n u_c L}{L_c U \Delta C} \frac{\partial \bar{c}' \bar{u}_3}{\partial \bar{X}_3} \quad (3.25b)$$

IIIa IIIb IIIc

$$\text{Term IV: } \frac{D_{sc} L}{UL_a L_a} \frac{\partial^2 \bar{c}}{\partial \bar{X}_1 \bar{X}_1} + \frac{D_{sc} L}{UL_b L_b} \frac{\partial^2 \bar{c}}{\partial \bar{X}_2 \bar{X}_2} + \frac{D_{sc} L}{UL_c L_c} \frac{\partial^2 \bar{c}}{\partial \bar{X}_3 \bar{X}_3} \quad (3.25c)$$

IVa IVb IVc

where
 C_n : Characteristic scale for scalar quantity concentration fluctuations [kgm⁻³].

Eq. (3.25) does not take into account variations in air density. Variations in air density can be incorporated by replacing concentrations of a scalar quantity by specific scalar quantities (kg scalar quantity per kg air).

3.2 Scaling of the flow inside an OTC

The fluid dynamics of the flow inside an OTC is complicated and characterized by the coexistence of various length and velocity scales. The choice of the magnitude of a scale depends on the position in the chamber. It is clear that the scales near the air-inlet holes will be highly determined by the distance to the chamber wall, the sizes of the air-inlet holes and the air-inlet velocity. Towards the middle of the chamber more length and velocity scales can be involved. Near the open top the diameter of the open top itself becomes important. Whirls may penetrate into the chamber via the open top. This is a rather complicated process and depends partly on the length and velocity scales of the flow field outside the OTC.

If no significant transport of mass to the walls and the plants inside a chamber

takes place then the total amount of mass flowing into the chamber equals the amount of mass leaving the chamber. If the flow field is assumed to be incompressible then mean velocity components in various parts of the chamber and the air-supply system can be estimated.

Table 3.1: Typical numbers for the KEMA-type OTC

Subject	Size	Units
Mean flow rate	1.4	m ³ s ⁻¹
Mean vertical velocity air-inlet air-supply system (2.0 m)	0.42	ms ⁻¹
Mean horizontal velocity connecting duct	4.95	ms ⁻¹
Mean horizontal velocity rectangular channel (assuming mean air-inlet velocity is uniform over the chamber)	3.93	ms ⁻¹
Mean inlet velocity air-inlet holes (perpendicular to the chamber wall)	12.88	ms ⁻¹
Mean vertical velocity inside the chamber (height: 1.5 m)	0.19	ms ⁻¹
Mean vertical velocity inside the chamber (open top)	0.42	ms ⁻¹

For three typical positions a first guess of the importance of the various terms in the equations describing the conservation of momentum, energy, ozone and water vapour is made using dimensional analysis.

Air-inlet hole

The flow field near the air-inlet holes is dominated by the existence of an air-inlet jet. Tennekes and Lumley (1972) described the flow of turbulent jets with dimensional analysis. For an axisymmetric jet Eqs. (3.26) and (3.27) were derived.

The constants in these equations were derived from experiments. For $8 \leq \frac{x}{d} \leq 40$

$$\frac{U_s}{U_j} = 6.4 \frac{d}{x} \quad (3.26)$$

$$l = 0.067 x \quad (3.27)$$

where

- x : Distance to orifice in the direction of the mean flow [m].
- d : Orifice height [m].
- l : Distance from the centre line of a jet to the point where the velocity in the direction of the mean flow equals $0.5 U_s$ [m].
- U_s : Mean centre line velocity component of a jet in the direction of the mean flow [ms⁻¹].

U_j : Initial velocity jet in the direction of the mean flow [ms^{-1}].

(see Fig. 3.1)

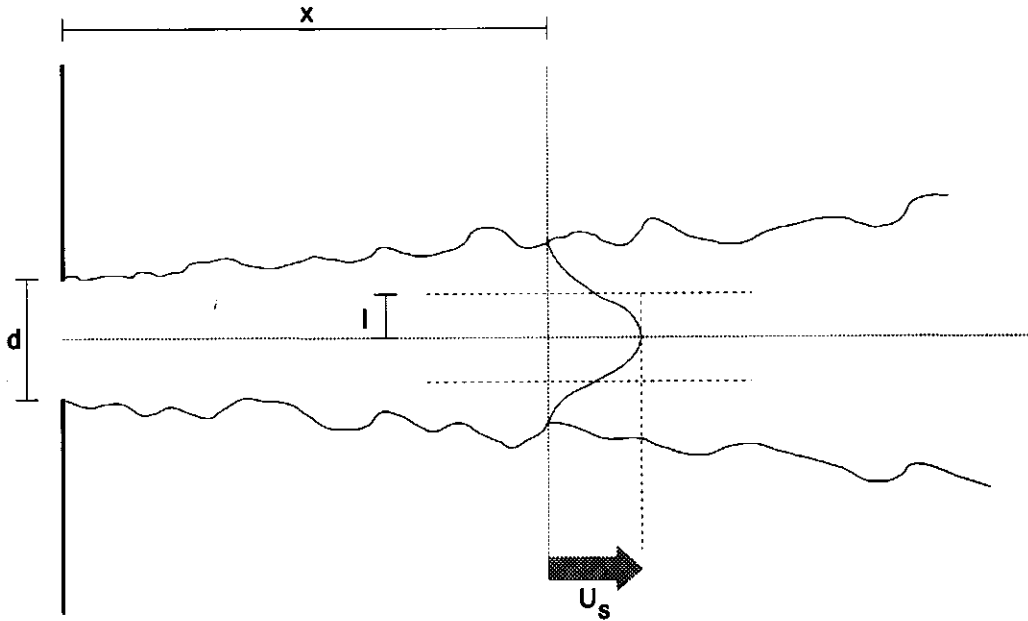


Figure 3.1: Dimensions of the axisymmetric jet (after Tennekes and Lumley, 1972).

Eq. (3.26) can be used to calculate the mean velocity, in the direction of the mean flow at the centre line of a jet at various distances to the chamber wall. Eq. (3.27) calculates l , which says something about the width of a jet (see Table 3.2). However, Eqs. (3.26) and (3.27) are valid under special conditions only. The jet has to be axisymmetric and only a limited number of scales play an important role. The flow regime within an OTC is a multi-scale problem. The flow field around the jet affects the jet itself depending on the position inside the chamber. If the air flow into a chamber is circular symmetric, pressure forces in the middle of the chamber force the air to leave the chamber via the open top. Furthermore, adjacent jets can interfere with each other and recirculation zones between jets and between jets and walls can occur. Therefore, Table 3.2 just gives an impression of some variables within the air inlet jet. How realistic these values really are depends

strongly on the importance of other scales involved.

Table 3.2: Calculated variables of an axisymmetric jet using Eqs. (3.26) and (3.27).
The mean inlet velocity is 12.88 ms^{-1} (see Table 3.1).

x [m]	U_s [ms^{-1}]	l [m]
0.25	8.18	0.017
0.50	4.09	0.034
0.75	2.73	0.050
1.00	2.05	0.067

A first guess of the characteristic length, velocity, pressure, temperature, ozone and water vapour scales is given below. The X_1 -direction is taken perpendicular to the air-inlet hole, The X_3 -direction is the vertical. Since the flow rate is rather constant the time scale for the flow field is considered to be more than 600 s.

- L_a : The distance to the orifice in the direction of the mean flow (0.5 m).
 L_b, L_c : The distance from the centre line of a jet to the point where the velocity in the direction of the mean flow equals $0.5 U_s$ (l : 0.034 m).
 U_a : The mean centre line velocity component in the direction of the mean flow (U_s : 4.09 ms^{-1}).
 U_b, U_c : Of the order of $U_s \frac{l}{X}$ (0.28 ms^{-1}).
 u_a, u_b, u_c : $\frac{U_{a,b,c}^2}{U_s^2}$ of the order of $\frac{l}{X}$ (1.07 ms^{-1}).
 ΔP : Of the order of $0.5 \rho U_s^2$ (10.2 Nm^{-2}).
 ΔT : Of the order of 1 K during sunny periods.
 T_{β} : Of the order of 0.5 K during sunny periods.
 ΔC : Of the order of the concentrations observed inside a chamber (water vapour: 10 gkg^{-1} ; ozone: $20 \text{ }\mu\text{gm}^{-3}$).
 C_{β} : Of the order of 0.5 gkg^{-1} for water vapour and $4 \text{ }\mu\text{gm}^{-3}$ for ozone.

The U and L scale applied in the equations describing the conservation of energy or any other scalar quantity are taken as being equal to U_a and L_a . The molecular diffusivity for water vapour is taken as $23.4 \cdot 10^{-6} \text{ [m}^2\text{s}^{-1}\text{]}$, the molecular diffusivity for ozone is taken as $13.6 \cdot 10^{-6} \text{ [m}^2\text{s}^{-1}\text{]}$.

Middle of an OTC

Within the middle of the chamber various length and velocity scales may be important. However, it is not clear what length and velocity scales play a dominant role. A first guess of the characteristic length, velocity, pressure, temperature, ozone and water vapour scales in the middle of the OTC at a height of 0.5 m is given below. The X_1 -direction is taken perpendicular to the air-inlet hole, The X_3 -direction is the vertical.

- L_a : The radius of the chamber (1.5 m).
- L_b : The complicated flow pattern in the middle of the chamber is partly determined by the distance between the air-inlet holes (of the order of 0.2 m).
- L_c : The distance to the chamber floor (0.5 m).
- U_a, U_b : The interacting air-inlet jets lead to a complicated flow pattern in the middle of the chamber. Therefore, it is not clear which characteristic velocity scale should be used. Measurements have shown that the mean velocity in the middle of the chamber is of the order of 1 ms^{-1} .
- U_c : The mean vertical velocity above the air-inlet holes (0.19 ms^{-1}).
- u_a, u_b, u_c : If an upstream flow contains mixing zones, sudden area changes and bends the turbulence level might be as high as 10% (Hinze, 1959). The turbulent intensity is defined

$$I = \frac{\sqrt{(u')^2}}{U} \quad (3.28)$$

where

I : Turbulent intensity [-].

Therefore, u_a and u_b are chosen 0.1 ms^{-1} , u_c is chosen as 0.02 ms^{-1} .

ΔP : Of the order of $0.5 \rho U_a^2$ (0.6 Nm^{-2}).

The ΔT , T_n , ΔC and C_n scale applied are taken as being equal to the values near the air-inlet hole. The U and L scale applied in the equations describing the conservation of energy or any other scalar quantity are taken as being equal to U_a and L_a . The time scale is considered to be more than 600 s.

Open top area

The flow field in the open top area is determined by the properties of the OTC as well as the properties of the flow field around the OTC. Analogous to the flow field in the middle of the chamber various length and velocity scales can be relevant and it is not clear what length and velocity scales play a dominant role. A first

guess of the characteristic length, velocity, pressure, temperature, ozone and water vapour scales for the open top region is given below. The X_1 -direction is parallel to the mean wind direction over the OTC, The X_3 -direction is the vertical.

- L_a, L_b : The radius of the open top area (1.0 m).
 L_c : The height of the nozzle (0.5 m).
 U_a : The mean horizontal wind velocity outside the OTC (assumed 2 ms⁻¹).
 U_b : The mean wind velocity in the cross wind direction (0 ms⁻¹).
 U_c : The mean vertical velocity at the top of the OTC (0.42 ms⁻¹).
 u_a, u_b, u_c : The turbulent intensities in the free atmosphere are larger than the turbulent intensities in most technical flows. For a thermally neutral surface layer according to Stull (1988)

$$\frac{\overline{(u_i')^2}}{U_*^2} = C_1 \quad (3.29)$$

where

C_1 : Constant (X_1 -direction ≈ 6 ; X_2 -direction ≈ 3 ; X_3 -direction ≈ 1) [-].

U_* : Friction velocity [ms⁻¹].

Assuming a friction velocity of 0.3 ms⁻¹ leads to

u_a : 0.74 ms⁻¹; u_b : 0.52 ms⁻¹; u_c : 0.30 ms⁻¹.

- ΔP : Of the order of $0.5\rho U_a^2$ (2.5 Nm⁻²).
 ΔT : Of the order of the temperature difference between an OTC and its environment during sunny periods (5 K).
 T_{II} : Of the order of 1 K during sunny periods.
 ΔC : Of the order of the concentrations observed inside an OTC (water vapour 10 gkg⁻¹; ozone 20 μ gm⁻³).
 C_{II} : Of the order of the observed differences between an OTC and its environment (water vapour 2 gkg⁻¹; ozone 200 μ gm⁻³).

The U and L scale applied in the equations describing the conservation of energy or any other scalar quantity are taken as being equal to U_a and L_a . The time scale is considered to be more than 600 s. Since the mean crosswind direction is 0 ms⁻¹ the momentum equation in the X_2 -direction is of limited importance.

Results

A first guess of the importance of the various terms in the momentum equation at any position is done using Eq. (3.12). For a latitude of about 50° $2\varepsilon_{ijk}\Omega_j$ is $1.1 \cdot 10^{-4}$ s⁻¹. Therefore, the Coriolis forces are neglected. The inertial terms are balanced by the turbulent diffusion and the pressure gradient term for all three positions studied.

Viscous stresses and time change of mean momentum are negligible (see Table 3.3).

Table 3.3: Magnitude of dimensionless terms of the momentum equation (3.12).

Dir.	Position: 0.5 m perpendicular to air-inlet holes										
	I	IIa	IIb	IIc	III	IVa	IVb	IVc	Va	Vb	Vc
1	0.00	1.00	1.00	1.00	0.50	0.07	1.00	1.00	0.00	0.00	0.00
2	0.00	1.00	1.00	1.00	108	1.00	14.7	14.7	0.00	0.00	0.00
3	0.00	1.00	1.00	1.00	108	1.00	14.7	14.7	0.00	0.00	0.00
	Position: middle of the chamber (height: 0.5 m)										
	I	IIa	IIb	IIc	III	IVa	IVb	IVc	Va	Vb	Vc
1	0.00	1.00	7.50	0.57	0.50	0.01	0.08	0.01	0.00	0.00	0.00
2	0.00	0.13	1.00	0.08	0.50	0.00	0.01	0.00	0.00	0.00	0.00
3	0.00	1.75	13.2	1.00	13.9	0.02	0.14	0.01	0.00	0.00	0.00
	Position: open top area										
	I	IIa	IIb	IIc	III	IVa	IVb	IVc	Va	Vb	Vc
1	0.00	1.00	0.00	0.42	0.50	0.14	0.10	0.11	0.00	0.00	0.00
3	0.00	2.38	0.00	1.00	11.3	0.63	0.44	0.51	0.00	0.00	0.00

Dir. : Direction. Term III : Pressure gradient forces.
 Term I : Time change. Term IV : Turbulent diffusion.
 Term II : Convection. Term V : Viscous stress.

The importance of the various terms in the energy equation describing the temperature at any position is estimated using the dimensionless numbers of Eq. (3.18). Provided that the velocity of a gas is much less than the speed of sound it can be shown that variations in pressure will play a considerably smaller role than variations in temperature. In the OTC case changes of $\frac{dP}{dt}$ will be of the order of 1 while changes in $\frac{\rho C_p dT}{dt}$ will be of the order of 10^3 . Therefore, Term III of Eq. (3.18) is neglected. The term $\frac{\epsilon}{C_p}$, which is part of the turbulent kinetic energy equation, plays an insignificant role in the energy equation and can be neglected. Furthermore, it is assumed that the two source terms (chemical reaction and radiation absorption) can be neglected as well. The molecular diffusion and time

changes of temperature are negligible for all three positions studied. Consequently, inertial terms are balanced by the turbulent diffusion terms (see Table 3.4).

Table 3.4: Magnitude of dimensionless terms of the energy equation (3.18).

Position: 0.5 m perpendicular to air-inlet holes									
I	IIa	IIb	IIc	IVa	IVb	IVc	Va	Vb	Vc
0.00	1.00	1.00	1.00	0.00	0.00	0.00	0.13	1.92	1.92
Position: middle of the chamber (height: 0.5 m)									
I	IIa	IIb	IIc	IVa	IVb	IVc	Va	Vb	Vc
0.00	1.00	7.50	0.57	0.00	0.00	0.00	0.05	0.38	0.03
Position: open top area									
I	IIa	IIb	IIc	IVa	IVb	IVc	Va	Vb	Vc
0.00	1.00	0.00	0.42	0.00	0.00	0.00	0.07	0.05	0.06

Term I : Time change. Term IV : Molecular diffusion.
 Term II : Convection. Term V : Turbulent diffusion.

A first guess of the importance of the various terms in the conservation equation for ozone and water vapour for three positions is done using Eq. (3.25). The content of the lower part of the chamber including the rectangular channel is 10.5 m³. At a flow rate of 1.4 m³s⁻¹ this amount of air is replaced in approximately 7 s. Therefore, the production or loss of ozone and water vapour as a result of chemical reactions is neglected. The molecular diffusion and time changes of ozone and water vapour are negligible for all three positions studied. Consequently, inertial terms are balanced by the turbulent diffusion terms (see Table 3.5 and 3.6).

Buoyancy

The influence of buoyancy on mean movements is characterized by the Archimedes number (see Eq. 3.21). A first guess of the Archimedes number at 0.25 and 0.5 m distance to the air-inlet hole, in the middle of the chamber and at the open top area is given in Table 3.7. As is mentioned before the coexistence of various length and velocity scales complicates the choice of a particular length or velocity scale. Since buoyancy forces are working in the vertical direction only, the

U_c and L_c are used as characteristic velocity and length scales.

Table 3.5: Magnitude of dimensionless terms of the ozone equation (3.25).

Position: 0.5 m perpendicular to air-inlet holes									
I	IIa	IIb	IIc	IIIa	IIIb	IIIc	IVa	IVb	IVc
0.00	1.00	1.00	1.00	0.05	0.77	0.77	0.00	0.00	0.00
Position: middle of the chamber (height: 0.5 m)									
I	IIa	IIb	IIc	IIIa	IIIb	IIIc	IVa	IVb	IVc
0.00	1.00	7.50	0.57	0.02	0.15	0.01	0.00	0.00	0.00
Position: open top area									
I	IIa	IIb	IIc	IIIa	IIIb	IIIc	IVa	IVb	IVc
0.00	1.00	0.00	0.42	3.70	2.60	3.00	0.00	0.00	0.00

Table 3.6: Magnitude of dimensionless terms of the water vapour equation (3.25).

Position: 0.5 m perpendicular to air-inlet holes									
I	IIa	IIb	IIc	IIIa	IIIb	IIIc	IVa	IVb	IVc
0.00	1.00	1.00	1.00	0.01	0.19	0.19	0.00	0.00	0.00
Position: middle of the chamber (height: 0.5 m)									
I	IIa	IIb	IIc	IIIa	IIIb	IIIc	IVa	IVb	IVc
0.00	1.00	7.50	0.57	0.01	0.04	0.00	0.00	0.00	0.00
Position: open top area									
I	IIa	IIb	IIc	IIIa	IIIb	IIIc	IVa	IVb	IVc
0.00	1.00	0.00	0.42	0.07	0.05	0.06	0.00	0.00	0.00

Term I : Time change. Term III : Turbulent diffusion.

Term II : Convection. Term IV : Molecular diffusion.

Close to the air-inlet holes buoyancy forces can be neglected. Towards the middle of the chamber buoyancy forces play a more significant role. However, the temperature scale given here is a maximum one which occurs during sunny periods only. During these periods, especially, buoyancy forces have to be taken into account. At the open top buoyancy forces can not be neglected any more

since temperature gradients of 1-5 K over the open top are common even during night-time.

Table 3.7: Archimedes numbers inside the OTC.

Position	U_c [ms ⁻¹]	ΔT [K]	L_c [m]	Ar
Near air-inlet holes (0.25 m)	0.56	1	0.017	551
Near air-inlet holes (0.50 m)	0.28	1	0.034	69
Middle chamber	0.19	1	0.5	2.2
Open top area	0.42	5	0.5	2.1

A correction for humidity differences is of limited importance. The largest humidity difference is observed between the OTC open top region and the OTC environment (approximately 2.0 gkg⁻¹). If the temperature difference between an OTC and its environment is 5.0 K (temperature outside 293 K) and the specific humidity outside and inside the OTC is 10.0 gkg⁻¹ and 12.0 gkg⁻¹, respectively, then the difference in virtual temperature will be approximately 5.4 K (see Eq. (3.19)). Consequently, the Archimedes number at the open top decreases from approximately 2.1 to 1.9.

3.3 Models used

3.3.1 The FLUENT model

The flow field within an OTC is a complex one characterized by the coexistence of various length and velocity scales (see previous section). Therefore, a model has been used to describe the flow field inside an OTC. For this purpose an already existing technical flow simulating model (FLUENT) was chosen. In Section 3.3.1.1 attention is focused on the physical aspects of this model while the numerical background is outlined in Section 3.3.1.2. The modelling of plants is described in Section 3.3.1.3. The physical background of the theory can be found in the FLUENT manual (Creare, 1987) and in literature (Launder, 1984; Launder

and Spalding, 1974; Rodi, 1976; 1980; 1981; 1984; Tennekes and Lumley, 1972). The numerical background can be found in the FLUENT manual and in Patankar (1980).

3.3.1.1 Physical background of the FLUENT model

The FLUENT model basically describes the conservation of mass, momentum and energy (see Section 3.1). Within the FLUENT programme two model options have been used, the $k-\epsilon$ model and the Algebraic Stress Model (ASM). The local closure technique used by both models can be applied only to situations where the length scale of turbulence is much smaller than the length scale over which mean gradients change. It is assumed that inside a chamber local gradients are closely related to exchange processes and that a local closure method can be applied since:

- large eddies inside an OTC will be mainly caused by the atmospheric boundary layer; eddies of more than 2 metre diameter (open top diameter) are not expected in the chamber,
- the pressure field within the chamber creates a mean upward vertical velocity of approximately 0.42 ms^{-1} which limits the amount of incoming air from outside the chamber.

The $k-\epsilon$ model

The $k-\epsilon$ model option parameterizes the turbulent diffusion terms of the governing equations by employing a "one and a half order" local closure technique. The turbulent diffusion terms of the momentum equation (3.9) are related to a local shear

$$-\overline{u_i u_j} = \nu_t \left(\frac{\partial \overline{u_i}}{\partial X_j} + \frac{\partial \overline{u_j}}{\partial X_i} \right) - \frac{2}{3} k \delta_{ij} \quad (3.30)$$

where
 ν_t : Turbulent viscosity [m^2s^{-1}].

The parameterization of the turbulent viscosity forms the core of the $k-\epsilon$ model. The turbulent viscosity is related to the turbulent kinetic energy and a dissipation

rate by

$$v_t = c_\mu \frac{k^2}{\epsilon} \quad (3.31)$$

where

$$\begin{aligned} c_\mu &: \text{Empirical constant [-]}. \\ \epsilon &: \text{Dissipation rate [m}^2\text{s}^{-3}\text{]}. \end{aligned}$$

The constant c_μ can be derived from local equilibrium shear layers where the production of turbulent kinetic energy equals the dissipation

$$c_\mu = \left(\frac{-\overline{u_1' u_3'}}{k} \right)^2 \quad (3.32)$$

where the X_1 -direction is the mean wind direction and the X_3 -direction is normal to the wall.

Analogous to Eq. (3.30) the turbulent diffusion terms of the conservation equation for any scalar quantity are assumed to be proportional to the gradient of the quantity transported.

$$-\overline{u_i' \phi'} = D_t \frac{\partial \phi}{\partial X_i} \quad (3.33)$$

where

$$\begin{aligned} D_t &: \text{Turbulent diffusivity for heat or mass [m}^2\text{s}^{-1}\text{]}. \\ \phi &: \text{General variable.} \end{aligned}$$

Like the turbulent viscosity the turbulent diffusivity is not a property of the fluid but depends on the properties of the flow field. Experiments have shown that the ratios of the turbulent diffusivities for momentum to heat or mass are approximately equal across a flow and vary little from flow to flow.

$$\sigma_t = \frac{\nu_t}{D_t} \quad (3.34)$$

where

$$\sigma_t : \text{Turbulent Prandtl or Schmidt number [-]}.$$

An exact solution of the turbulent kinetic energy equation (3.13) is not given by the model since unknown correlations appear in the turbulent kinetic energy

equation. At high Reynolds numbers the turbulent kinetic energy equation is further reduced to

$$\frac{\partial k}{\partial t} + \overline{u_j} \frac{\partial k}{\partial X_j} = -\overline{u'_i u'_j} \frac{\partial \overline{u_i}}{\partial X_j} + \frac{\partial}{\partial X_j} \left(\frac{v_i}{\sigma_k} \frac{\partial k}{\partial X_j} \right) - \epsilon \quad (3.35)$$

where the transport due to velocity and pressure fluctuations is assumed to be proportional to the gradient of k .

At high Reynolds numbers with prevailing local isotropy an exact solution of the equation for the dissipation rate can be derived from Eq. (3.6)

$$\frac{\partial \epsilon}{\partial t} + \overline{u_j} \frac{\partial \epsilon}{\partial X_j} = \underbrace{-\frac{\partial}{\partial X_j} \frac{\partial \overline{u'_i \epsilon'}}{\partial X_j}}_{\text{III}} - \underbrace{2\nu \frac{\partial u'_i}{\partial X_k} \frac{\partial u'_i}{\partial X_j} \frac{\partial u'_k}{\partial X_j}}_{\text{IV}} - \underbrace{2 \left(\nu \frac{\partial^2 u'_i}{\partial X_j \partial X_j} \right)}_{\text{V}} \quad (3.36)$$

where

- Term I : Time change.
- Term II : Convective transport.
- Term III : Diffusive transport.
- Term IV : Generation due to vortex stretching.
- Term V : Viscous destruction.

This equation contains complex correlations whose behaviour is little known. Therefore, model assumptions have been introduced in Eq. (3.36) leading to a highly empirical equation. The diffusion term is parameterized with the gradient assumption (3.33). The difference between the production and destruction term is parameterized using two empirical constants.

$$\frac{\partial \epsilon}{\partial t} + \overline{u_j} \frac{\partial \epsilon}{\partial X_j} = \underbrace{\frac{\partial}{\partial X_j} \left(\frac{v_i}{\sigma_\epsilon} \frac{\partial \epsilon}{\partial X_j} \right)}_{\text{III}} + \underbrace{c_{\epsilon 1} \frac{\epsilon}{k} (P)}_{\text{IV}} - \underbrace{c_{\epsilon 2} \frac{\epsilon^2}{k}}_{\text{IV}} \quad (3.37)$$

where

- Term I : Time change.
- Term II : Convection.
- Term III : Diffusion term parameterized with gradient assumption.
- Term IV : Generation of vorticity due to vortex stretching connected with the energy cascade minus viscous destruction of vorticity.

P : Production of turbulent kinetic energy by mean wind shear [$m^2 s^{-3}$].

- $c_{\epsilon 1}$: Empirical constant [-].
 $c_{\epsilon 2}$: Empirical constant [-].
 σ_{ϵ} : Ratio of turbulent viscosity for momentum to turbulent viscosity for dissipation rate [-].

The constant $c_{\epsilon 2}$ has been determined empirically from the measured rate of decay of turbulent kinetic energy behind a grid. Assuming the advection term to be zero and the constants c_{μ} and σ_{ϵ} to be known the constant $c_{\epsilon 1}$ can be derived from Eq. (3.37) for a local equilibrium shear layer according to

$$c_{\epsilon 1} = c_{\epsilon 2} - \frac{\kappa^2}{\sigma_{\epsilon} \sqrt{c_{\mu}}} \quad (3.38)$$

where
 κ : Von Karman's constant [-].

Launder and Spalding (1974) tuned the constants $c_{\epsilon 1}$, σ_{ϵ} and σ_k by computer optimization. The values recommended are given in Table 3.8.

Table 3.8: Values of the constants used in the $k-\epsilon$ model according to Launder and Spalding.

c_{μ}	$c_{\epsilon 1}$	$c_{\epsilon 2}$	σ_{ϵ}	σ_k
0.09	1.44	1.92	1.30	1.00

Rodi (1984) pointed out that there is no complete universality of the constants given in Table 3.8. The rate of spread of an axisymmetric jet is overpredicted by about 30% (in the case of stagnant surroundings) using the constants given in Table 3.8. Therefore, some of the constants require different values. Detering and Etling (1985) applied the $k-\epsilon$ model to the atmospheric turbulent boundary layer. They showed that the constants used in engineering flow problems can differ from the constants valid for atmospheric boundary layers. For the atmospheric boundary layer measurements suggest that in the surface layer

$$k \approx 6.25 U_*^2 \quad (3.39)$$

where
 U_* : Friction velocity [ms^{-1}].

The constant is approximately twice as large as the constant found for technical flows. The model constants recommended by Detering and Etling (1985) are given in Table 3.9.

Table 3.9: Values of the constants used in the k - ϵ model according to Detering and Etling.

C_μ	$C_{\epsilon 1}$	$C_{\epsilon 2}$	σ_ϵ	σ_k
0.025	1.09	1.90	1.30	0.74

The k - ϵ model is based on the assumption that the local state of turbulence can be characterized by one velocity scale and that the eddy viscosity is the same for all Reynolds stresses ($\overline{u_i u_j}$). This may be of limited realism in complex flows. Also the turbulent Prandtl or Schmidt number can be affected by buoyancy, rotation and streamline curvature. In spite of these shortcomings the k - ϵ model has proved to be successful in many practical calculations (Launder and Spalding, 1974; Rodi, 1984).

In order to account for the development of the various Reynolds stresses the equations describing these terms can be derived in exact form. The derivation of the exact equations introduces terms accounting for buoyancy, rotation, streamline curvature and other special effects. However, the equations contain higher order correlations which have to be parameterized in order to get a solvable set of equations. So called Algebraic Stress Models (ASM) have been developed to reduce the differential transport equations to algebraic expressions while at the same time retaining most of their basic features.

The algebraic stress model

The transport terms of the Reynolds stresses are taken proportional to the transport of the turbulent kinetic energy (Rodi, 1976). Furthermore, model assumptions are involved for the buoyancy term, the pressure-strain term (VI) and the dissipation terms (VII and VIII) of Eqs. (3.15) and (3.23). The approximations are valid for high Reynolds number situations only, where small-scale dissipative motion is assumed isotropic.

The resulting equation is written:

$$\overline{u_i u_j} = k \left(\frac{2}{3} \delta_{ij} + \frac{(1-\gamma) \left(\frac{P_{ij}}{\epsilon} - \frac{2}{3} \delta_{ij} \frac{P}{\epsilon} \right) + (1-c_3) \left(\frac{G_{ij}}{\epsilon} - \frac{2}{3} \delta_{ij} \frac{G}{\epsilon} \right)}{c_1 + \frac{P+G}{\epsilon} - 1} \right) \quad (3.40)$$

where

- G : Production of turbulent kinetic energy by buoyancy [m^2s^{-3}].
- G_{ij} : Production of turbulent momentum flux by buoyancy [m^2s^{-3}].
- P : Production of turbulent kinetic energy by mean wind shear [m^2s^{-3}].
- P_{ij} : Production of turbulent momentum flux by mean wind shear [m^2s^{-3}].
- c_1 : Constant (1.5-2.2) [-].
- c_3 : Constant (0.4-0.5) [-].
- γ : Constant (0.55-0.60) [-].

Eq. (3.40) can be used whenever transport of turbulent momentum flux is not very important since this transport is modelled rather crudely.

3.3.1.2 Numerical background of the FLUENT model

In numerical flow simulations the results are often subject to numerical inaccuracies so that it is not the turbulence model alone that is responsible for lack of agreement with experimental evidence.

Within the computational domain of FLUENT the governing equations are discretized using a control volume based finite difference method on a defined grid. The SIMPLE (Semi Implicit Method for Pressure Linked Equations) algorithm is used to solve the governing equations for a staggered grid configuration. The linearized equations are solved line by line. Along each line the equations are solved using TDMA (TriDiagonal Matrix Algorithm). The solving procedure is based on an exact solution of the one dimensional convection diffusion equation using a Power Law scheme. The calculations proceed until convergence criteria have been achieved (Creare, 1987; Patankar, 1980).

False diffusion can occur whenever the main direction of the flow does not align with the grid lines, thus causing numerical contributions to diffusion terms. The FLUENT programme provides the QUICK (Quadratic Upstream Interpolation for Convective Kinematics) option to decrease the numerical errors caused by false

diffusion (Creare, 1987).

The properties of the control volumes along the borders of the computational domain have to be set. Various types of boundary conditions can be selected.

- solid wall control volumes,
- inlet control volumes,
- outlet control volumes,
- symmetry boundary conditions.

These boundary conditions are discussed next.

Solid wall control volume

Within a boundary layer near a wall viscous effects become more important so that high Reynolds number turbulence models are not applicable any more. Therefore, empirical laws are available which connect the wall conditions to the dependent variables just outside the viscous sublayer. In meteorology the resultant mean wind velocity parallel to a wall for thermal-neutral conditions can be written according to

$$\bar{u}_1 = \frac{U_*}{\kappa} \ln\left(\frac{z-d}{z_0}\right) \quad (3.41)$$

$$U_* = \sqrt{-u_1' u_3'} \quad (3.42)$$

where

- U_1 : Wind velocity parallel to a wall in the direction of the main flow [ms⁻¹].
- U_3 : Wind velocity normal to the wall [ms⁻¹].
- d : Displacement length [m].
- z : Distance perpendicular to the wall [m].
- z_0 : Roughness height [m].

Eq. (3.41) is only valid above $z \geq 20z_0$ where the production of turbulent kinetic energy approximately equals the dissipation (Wieringa, 1986). In the FLUENT code the resultant mean wind velocity parallel to a wall is expressed as

$$\bar{u} = \frac{U_*}{\kappa} \ln(Z^* E) \quad (3.43)$$

$$Z^* = \frac{z U_*}{\nu} \quad (3.44)$$

where

- E : Roughness parameter (9.8 for aerodynamically smooth walls).
 Z^* : Dimensionless distance perpendicular to the wall.

Eq. (3.43) is valid within the region where $30 < Z^* < 100$. This equation can not be used in areas near separation or stagnation points but the influence of these areas on the flow field is usually small. When buoyancy does not play an important role and diffusion and advection of turbulent kinetic energy can be neglected, then production of turbulent kinetic energy by mean wind shear approximately equals the viscous dissipation of turbulent kinetic energy. Consequently, turbulent kinetic energy and dissipation rate can be written according to

$$k = \frac{U_*^2}{\sqrt{c_\mu}} \quad (3.45)$$

$$\varepsilon = \frac{U_*^3}{\kappa Z} \quad (3.46)$$

Combining Eqs. (3.41), (3.43) and (3.44) and defining z as the height above the displacement length yields

$$EU_* z_0 = \nu \quad (3.47)$$

When aerodynamically smooth walls are oriented oblique to the grid lines they can be approximated by stepped walls. The grid around these walls is too coarse to resolve the detailed flow field around the steps and the solution procedure just 'sees' the inclined wall.

Inlet control volume

Inlet profiles of velocity, turbulent kinetic energy and dissipation rate can be specified for each control volume at the borders of the computational domain. However, when the inlet profiles of turbulent kinetic energy and dissipation rate are not known the user can specify a turbulent intensity (3.28). The FLUENT code calculates the inlet turbulent kinetic energy according to

$$k = 1.5(UI)^2 \quad (3.48)$$

where

- U : Mean velocity at the inlet [ms^{-1}].

I : Turbulent intensity [-].

The dissipation rate is calculated according to

$$\varepsilon = \frac{(c_{\mu}^2 k)^2}{L} \quad (3.49)$$

where

L : Length scale characterizing the size of large, energy-containing eddies [m].

The FLUENT programme calculates the length scale by computing the inlet area and then defining an equivalent radius for a circle of equal area. The length scale is defined as 0.07 times this equivalent radius, a value that is derived from the mixing length in turbulent pipe flow. FLUENT generates a uniform distribution of turbulent kinetic energy and dissipation rate across each inlet zone. In many cases the inlet turbulent intensity specified will not have a major impact on the predicted flow field, since the generation and dissipation of turbulent kinetic energy within the computational domain are far more important.

Outlet control volume

At the outlet control volumes it is assumed that the flow field downstream of the calculation domain does not influence the solution. This is the case when there is no "inflow" over a part of the outlet plane and the Peclet number is sufficiently large. The value of a variable as well as its flux are then known since they are determined by the flow field itself.

Symmetry boundary conditions

If the flow over the computational domain shows symmetrical features then computation time can be reduced by using symmetry planes without losing any essential information. At a symmetry plane the diffusion and convection fluxes are assumed zero. The flow field can be mirrored over the symmetry plane.

A special type of symmetry planes, called cyclic symmetry planes, can be used whenever the flow pattern is repeated several times over the computational domain. Cyclic cells are paired with cyclic cells on the opposing edge of the computational domain. FLUENT matches the values of the flow variables in a cyclic

cell with the value of the paired cyclic cell at the opposite boundary.

3.3.1.3 Simulations

The number of grid points required to compute the flow field inside and outside a ventilated OTC without losing information about important flow characteristics would exceed the limitations set by the internal memory of the computer and the computation time needed. Therefore, the computational grid to calculate the flow regime inside and around an OTC was split into two parts.

The first part computed the flow field around the OTC and at open top height with a rectangular cartesian coordinates grid employing an upwind logarithmic wind profile as a boundary condition (see Fig 3.2). The first grid point was chosen at 0.1 m from the wall. The distance between the grid nodes inside the chamber was 0.25 m. Therefore, structures of the flow field inside the chamber smaller than 0.25 m were not modelled. A symmetry plane was taken parallel to the mean wind direction through the middle of the chamber. At the windward side and at the top side of the domain an inlet profile was set arbitrarily, based on the experimental data for 26-05-89 (15.20 UTC). On that particular day the mean horizontal wind speed at open top height was approximately 4.5 ms^{-1} while thermal conditions were near-neutral (Richardson gradient number at 1.7 m: -0.023). The friction velocity, U_* , was 0.31 ms^{-1} , the roughness length, z_0 , of the grass cover around the OTC was $8.8 \cdot 10^{-3} \text{ m}$. Consequently, according to Eq. (3.47) the roughness parameter of the grass cover, E , was $5.3 \cdot 10^{-3}$. The chamber walls were assumed to be aerodynamically smooth. The turbulent kinetic energy and viscous dissipation of turbulent kinetic energy were set employing Eqs. (3.45) and (3.46). The constants used in the simulation are the ones suggested by Launder and Spalding (1978; see Table 3.8). The parameters of the air were taken equal to the values for a standard atmosphere (see symbol list; default values used).

The second part of the computational grid calculated in detail the flow field inside the ventilated chamber with a cylindrical polar coordinates grid. The flow regime inside the chamber was assumed to be approximately circularly symmetric. The

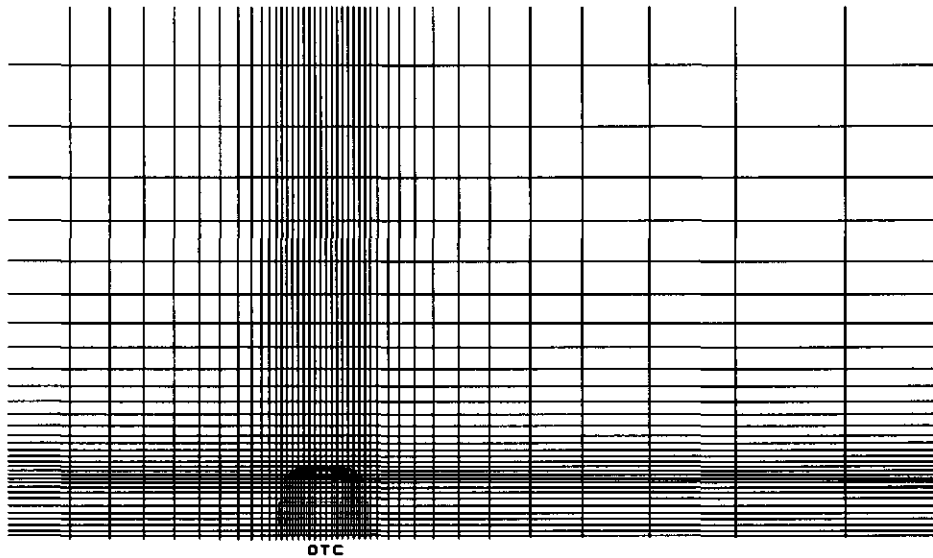


Figure 3.2: Cartesian coordinates grid with OTC

Computational grid plane parallel to the mean wind velocity

Dimensions: 40 m x 12 m x 25 m

Number of cells: 26460 (length:42 x width:18 x height:35)

computational grid for modelling the flow field inside the chamber was constructed using a chamber section of 11.25° . Within every section 5 air-inlet holes were specified (see Fig. 3.3). Within the lower 1.2 m of the chamber the height of the grid cells was 0.025 m. In the upper part of the chamber the height of the cells increased towards the open top. The total inlet area was $9.82 \cdot 10^{-2} \text{ m}^2$. The flow rate was set to $1.4 \text{ m}^3\text{s}^{-1}$. The turbulent kinetic energy and dissipation rate in the inlet area were calculated employing Eqs. (3.48) and (3.49). The turbulence intensity within the air-inlet holes was estimated to be approximately 10% as the upstream flow contains area changes, bends etc. The wall roughness parameter was arbitrarily taken 1.0. Furthermore, it was assumed that the properties of the flow in the lower part of the ventilated chamber are primarily determined by the air-inlet jets and not by the ambient air flowing into the chamber. Therefore, no inlet control volumes were applied to the open top. However, especially in the upper part of the

chamber, flow conditions outside the OTC may influence the properties of the flow inside a chamber (see Section 3.2). To study the influence of the flow outside the OTC on the properties of the flow in the upper part of the ventilated chamber, the computed flow inside the chamber just above the air-inlet holes, using the polar coordinates grid was transformed to input boundary conditions for the cartesian coordinates grid computations. Consequently, the properties of the flow field in the open top region are determined by environmental conditions as well as the properties of the air flow in the lower part of the ventilated chamber.

The behaviour of a scalar quantity was studied introducing a scalar with a molecular mass of 48.0 (equal to that for ozone). The molecular mass of the inerts was set to 28.0. The turbulent Schmidt number was set to 0.7. Transport of the scalar quantity to the chamber walls was neglected.

Section 3.2 has revealed that the inertial terms in the momentum equations are almost completely balanced by the turbulent diffusion and pressure gradient terms. Coriolis forces, viscous stresses and time change of mean momentum are negligible. However, buoyancy effects might play a role. To keep the model as simple as possible the calculations conducted in the present study have been restricted to thermal-neutral conditions. Consequently, the FLUENT model results might deviate from experimental values under non-neutral conditions.

3.3.1.4 Modelling of plants in the FLUENT model

Plants mainly grow within the lower part of the chamber (below 1.2 m). To simulate the behaviour of a flow with plants one can define all the plant elements and assign a roughness value to it. However, within the computational domain needed to simulate the flow field within a chamber there are not enough control volumes available to make a detailed model of a plant. Another way to compute the flow field through a plant community in the lower part of an OTC is to describe the plants as a porous medium.

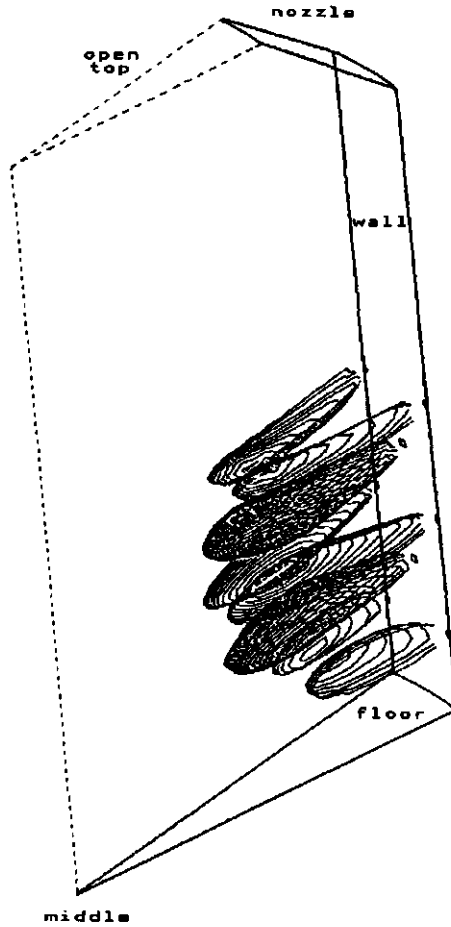


Figure 3.3: Computational domain used for modelling the flow field inside the OTC.

Dimensions: 2.93 m (height) x 1.50 m (radius) x 0.196 radian (angle).

Number of cells: 29172 (66:vertical x 17:radial x 26:angular).

The air-inlet jets are visualised by plotting contour lines of computed turbulent kinetic energy ($0.5 \text{ m}^2\text{s}^{-2}$).

Within the FLUENT code Brinkman's equation is used to simulate the flow through porous media according to

$$\nabla P = -\frac{\mu}{k_p} U + \mu \nabla^2 U + \frac{1}{2} C_D \rho |U| U \quad (3.50)$$

where

- C_D : Inertial resistance coefficient [m^{-1}].
 k_p : Permeability [m^2].
 ∇ : Divergence.
 ∇^2 : Laplacian operator.

Eq. (3.50) can be used to model the pressure gradients in a plant canopy as a result of drag forces. The first term on the right hand side of this equation is ignored by setting the permeability to a very large value. The second term on the right hand side is of the order of $1 \cdot 10^{-5}$ and is small as compared to the third term on the right hand side which is of the order of $1 \cdot 10^{-2}$ or more. The inertial resistance coefficient of Eq. (3.50) can be replaced by a drag coefficient for plants according to

$$\nabla P = \mu \nabla^2 U + \frac{1}{2} \frac{LA}{H_p A_b} c_d \rho |U| U \quad (3.51)$$

where

- A_b : Base area of the chamber [m^2].
 H_p : Height of the plants [m].
 LA : Total leaf area (double-sided) [m^2].
 c_d : Drag coefficient [-].

The drag coefficient is defined according to

$$c_d = \frac{\tau}{0.5 \rho U^2} \quad (3.52)$$

where

- U : Resultant mean wind velocity parallel to a plate [ms^{-1}].
 τ : Force per unit of total leaf surface area in the direction of the flow [Nm^{-2}].

(Monteith and Unsworth, 1990)

Thom (1968) found a value for the drag coefficient of approximately 0.16 for model leaves facing the air flow at an angle of attack of 23 degrees. The height of the plants was taken 0.4 m. The calculations were executed with a leaf area index (single-sided) of 4, leading to an inertial resistance coefficient of 0.44.

3.3.2 The OTC-resistance model

The OTC-resistance model is a bulk resistance model which has been developed primarily to calculate the mass and energy fluxes to or from the various parts of the OTC system. Since bulk resistances are used all the data calculated by the programme represent spatial and time averages.

The model yields information about the temperature, humidity and ozone concentration inside the chamber in relation to field conditions. The model has been used to gain insight into the effects on the microclimate inside the chamber as a result of changes made to the OTC configuration.

Within a resistance model the mass and energy fluxes are the result of a potential difference over a resistance. Eq. (3.53) represents the exchange of heat, water vapour, carbon dioxide or a gaseous pollutant between two locations. The total resistance is composed of component resistances which describe the paths through which the scalar quantity is transported (Monteith and Unsworth, 1990).

$$f_m = \frac{(C_1 - C_2)}{R} \quad (3.53)$$

where

- f_m : Flux density [$\text{Jm}^{-2}\text{s}^{-1}/\text{kgm}^{-2}\text{s}^{-1}$].
- C_x : Concentration at location x [$\text{Jm}^{-3}/\text{kgm}^{-3}$].
- R : Resistance [sm^{-1}].

The OTC-resistance model is composed of two submodels, the OTC-system model and the soil-vegetation model. The OTC-system model is based on a resistance model described by Unsworth et al. (1982, 1984, 1986). The model has been modified and extended with an air-supply system part and a part which describes the energy balance of the chamber walls (Section 3.3.2.1). The OTC-system model was coupled to a second model which describes the bulk exchange processes between the soil-vegetation and the air inside as well as outside an OTC. The bulk exchange processes are described employing a modified parameterization scheme of land surface processes described by Noilhan and Planton (1989) and Jacquemin and Noilhan (1990). Section 3.3.2.2 describes the soil-vegetation model and the modifications made to use this model under OTC

conditions.

3.3.2.1 The OTC-system model

The basic model

The model is based on a steady state scalar quantity balance for an OTC system. Each component of the balanced system is treated as an energy or scalar flux (ozone or water vapour). The ozone or water vapour balance of the chamber is written

$$\frac{C_i - C_c}{R_v} + \frac{C_o - C_c}{R_i} + \frac{F_r}{A_b} = \frac{F_w + F_p + F_s}{A_b} \quad (3.54)$$

where

- A_b : Base area of the chamber [m^2].
- C_c : Mean concentration inside the chamber [kgm^{-3}].
- C_i : Mean concentration at the end of the air-supply system [kgm^{-3}].
- C_o : Mean concentration outside the OTC at open top height [kgm^{-3}].
- F_p : Scalar flux to plants grown under OTC conditions [kgs^{-1}].
- F_r : Production of a scalar as a result of chemical reactions [kgs^{-1}].
- F_s : Scalar flux to chamber floor [kgs^{-1}].
- F_w : Scalar flux to chamber wall [kgs^{-1}].
- R_i : Incursion resistance per unit base area [sm^{-1}].
- R_v : Ventilation resistance per unit base area [sm^{-1}].

The ventilation resistance is written

$$R_v = \frac{A_b}{f_{inl}} \quad (3.55)$$

where

- f_{inl} : Flow rate as a result of ventilation [m^3s^{-1}].

The incursion resistance can not be written in terms of chamber dimensions and flow rate and has to be determined by experiments using

$$R_i = \frac{A_b}{N_i V} \quad (3.56)$$

where

- N_i : The rate of air change due to incursion [s^{-1}].
- V : Chamber volume [m^3].

The incursion resistance depends on the wind speed outside the OTC, the sizes of the chamber and the aerodynamic shape of the open top. Unsworth (1984) measured the decay of a tracer gas concentration inside an OTC immediately after

the fan was stopped and the tracer gas supply cut off. The rate of air change was determined according to

$$\frac{\partial C_c}{\partial t} = -N_i(C_c - C_o) \quad (3.57)$$

This method did not allow for any influence on the incursion resistance, by the fan driven air flow leaving the chamber. However, Unsworth suggested that this influence was probably small.

The energy balance for a chamber is written according to

$$\rho_a C_p \left(\frac{T_i - T_o}{R_v} + \frac{T_o - T_o}{R_i} \right) + \frac{Q_r}{A_b} = \frac{Q_w + Q_p + Q_s}{A_b} \quad (3.58)$$

where

- Q_p : Energy flux to plants grown under OTC conditions [Js^{-1}].
- Q_r : Heat generated by chemical reactions [Js^{-1}].
- Q_s : Energy flux to chamber floor [Js^{-1}].
- Q_w : Energy flux to chamber wall [Js^{-1}].
- T_c : Temperature inside the chamber [K].
- T_i : Temperature at the end of the air-supply system [K].
- T_o : Temperature outside the OTC at open top height [K].

The energy generated by chemical reactions is assumed to be negligible.

The microclimate in a chamber is partly determined by the properties of the air in the air-supply system (C_i, T_i). Furthermore, the chamber walls can play a significant role in the total energy balance of the chamber itself (via Q_w). Therefore, the model was extended with an air-supply system subroutine and a subroutine describing the energy balance of the chamber walls.

Within the air-supply system subroutine the height of the air inlet at the input of the air-supply system, effects caused by the filter unit and the ventilation system, and radiation absorbed by the walls of the air-supply system have been taken into account.

Air inlet

The flow regime around the air inlet of the air-supply system is not known. The height from which the bulk of the air is sucked was determined by correlating the

temperatures measured inside the air inlet to the temperatures measured at various heights outside the OTC. Only the experimental values sampled during conditions of low wind speed (less than 1 ms^{-1} at open top height) and low global radiation intensities (less than 100 Wm^{-2}) were used, in order to obtain high temperature gradients outside the OTC while simultaneously preventing heating of the air inside the air inlet due to radiation absorption by the walls of the air-supply system.

Filter unit

The filter unit is primarily meant for removing gaseous pollutants from the air flowing into the chamber. At the same time the filters adsorb or release water and thus modify the moisture content of the air which passes the filters. This adsorption or desorption behaviour depends on the temperature and relative humidity of the air. The water adsorption and desorption curve for the activated carbon filter used (Sutcliffe type 207C) is not known, however, the curve for the shell based activated carbon type 208C is known (see Fig. 3.4). The main difference between the 207C and 208C type activated carbon is the surface area per g carbon. The 207C type activated carbon has a surface area of $1100\text{-}1200 \text{ m}^2\text{g}^{-1}$ while the 208C type has a surface area of $1200\text{-}1300 \text{ m}^2\text{g}^{-1}$. The filter system of the KEMA-type OTC contains about 290 kg activated carbon. During the course of the day changes in the water content of the filters of 25% can occur which result into changes of specific humidity of more than $1 \cdot 10^{-3} \text{ kgkg}^{-1}$ (flow rate: $1.4 \text{ m}^3\text{s}^{-1}$). Wet and dry bulb temperatures at the air inlet of the air-supply system are used to estimate the relative humidity inside the filter unit. Since a change from adsorption into desorption can result into sudden changes of the equilibrium water content of the filters a combined adsorption/desorption curve was deduced from Fig. (3.4) taking into account the differences between the type 207C and 208C activated carbon. The desorption or adsorption of water is written

$$q_i = q_{inl} + C_{f1}(Hc_{t-\Delta t} - Hc_i) \frac{1}{\rho_a f_{inl}} \quad (3.59)$$

where

- C_{f1} : Filter constant [s^{-1}].
- q_i : Specific humidity of the air at the end of the air-supply system [kgkg^{-1}].
- q_{inl} : Specific humidity of the air at the air inlet [kgkg^{-1}].

- $H_{c_{t-\Delta t}}$: Water content of the filter 1 time step earlier [kg].
 H_{c_t} : Equilibrium water content of the filter [kg].
 Δt : Time step [s].

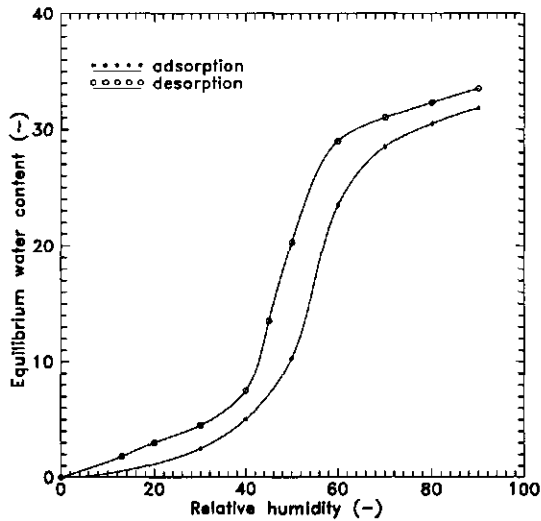


Figure 3.4: Water adsorption by shell based carbon, Sutcliffe type 208C, at 21°C [kg water kg⁻¹ dry filter].

The filter constant C_{f1} expresses the percentage of the difference between the current equilibrium water content (H_{c_t}) and the water content of the filter one time step earlier ($H_{c_{t-\Delta t}}$) which is adsorbed or released by the filters during 1 s (based on 10 minutes mean). This constant was determined by tuning it to the change in specific humidity in the air-supply system.

The condensation or evaporation of water from the filters leads to a temperature change of the air flowing into the OTC. An increase of the specific humidity of the air of $1.0 \cdot 10^{-3} \text{ kg kg}^{-1}$ represents a maximum temperature decrease of approximately 2.5 K. The temperature change is written

$$\Delta T = C_{f2}(q_{in1} - q_t) \frac{L}{C_p} \quad (3.60)$$

where

- C_{f2} : Filter constant [-].
 L : Latent heat [Jkg⁻¹].
 ΔT : Temperature change [K].

The filter constant C_{f2} represents the fraction of the energy needed for evaporation or condensation of water subtracted from or released to the air flowing through the filters.

Ventilation system

The fan used requires a power input of a few kW (maximum 5 kW) dependent on the flow rate and the resistances (i.e. filters, OTC-configuration) before and after the fan. A power input of 5 kW theoretically leads to a maximum temperature increase of 3.0 K (flow rate: $1.4 \text{ m}^3\text{s}^{-1}$). The temperature increase caused by the fan was estimated by comparing the temperatures measured at the end of the air-supply system with the temperatures measured inside the air inlet. To reduce the errors due to adsorption or desorption of water by the filters and absorption of global radiation by the walls of the air-supply system, the temperatures were compared between 04.00 and 06.00 a.m. local time.

Walls of the air-supply system

The walls of the air-supply system absorb short-wave radiation. The amount of global radiation absorbed depends on solar height and azimuth, the orientation of the air-supply system and the properties of the wall. Part of the radiation absorbed is transported to the air inside the air-supply system.

Solar height and azimuth depend on latitude, solar time and day of the year and are estimated with mathematical equations as used by Iqbal (1983). The temperature change caused by A_y m^2 area air-supply system is written

$$\Delta T = \sum_{\text{first wall}}^{\text{last wall}} \frac{C_{1,asp} S_g A_x}{\rho_a C_p f_{in}} \quad (3.61)$$

$$A_x = \frac{A_y}{\tan(\beta)} (\sin(\alpha)) \quad (\text{North south orientation of a wall}) \quad (3.62)$$

$$A_x = \frac{A_y}{\tan(\beta)} (\sin(\frac{1}{2}\pi + \alpha)) \quad (\text{East west orientation of a wall}) \quad (3.63)$$

where

- A_x : Shaded area by a wall of the air-supply system [m^2].
- A_y : Wall surface area of the air-supply system [m^2].
- $C_{1,asp}$: Percentage of the incoming global radiation transported to the air within the air-supply system [-].

- S_g : Global radiation on a horizontal plane [Wm^{-2}].
 α : Azimuth (angle with south) [rad].
 β : Solar height [rad].

During weather conditions with global radiation intensities up to 900 Wm^{-2} with the sun exactly at south and a solar height of 45° a maximum temperature increase inside the air-supply system of 3.5 K can occur (reflection coefficient 0.75; flow rate: $1.4 \text{ m}^3\text{s}^{-1}$).

The constant $C_{1,asp}$ involves a combined effect of the short-wave solar radiation absorbed and the energy transported to the air within the air-supply system. The diffuse radiation is treated in the same way as the direct radiation. The long-wave radiation balance and the energy fluxes through the wall are neglected. Therefore, the estimated value is just a rough estimate as it can vary from place to place and with time depending on the conditions within and around the air-supply system. The constant $C_{1,asp}$ was determined in combination with the constant C_{r2} by tuning it to the temperature change measured within the air-supply system assuming the temperature increase due to the fan to be constant.

Chamber walls

The chamber walls transmit only a part of the direct and diffuse radiation, the rest is reflected or absorbed. Via conduction, convection and radiation, the temperature of the walls affects the temperature of the air inside the chamber.

Since the air flowing into the chamber has to pass the rectangular channel and the netting before it enters the chamber it is assumed that all the energy absorbed by the netting and the chamber side wall of the rectangular channel is transported to the air within the chamber. Furthermore, a part of the energy absorbed at the outer wall of the rectangular channel is transported to the air flowing into the chamber. The following aspects are discussed next:

- the short-wave energy balance,
- the long-wave energy balance,
- convection and conduction.

-Short-wave radiation balance

The absorption of solar radiation by the netting is estimated by the ratio of the

surface area of the netting material to the total netting area (0.36). The absorption percentage of solar radiation for a clear plate of Lexan with a reflection coefficient of 0.09 (General Electric Plastics, 1989) is calculated according to

$$Abs_i = 1 - ((0.91 e^{-k_w x}) + 0.09) \quad (3.64)$$

where

- Abs_i : Percentage of global radiation absorbed by Lexan [-].
- k_w : Extinction coefficient of Lexan (23.569) [m^{-1}].
- x : Path length of a light beam through the Lexan wall [m].

The total absorption by the chamber walls and netting is calculated via the following procedure

- The chamber is divided into 32 slices of 0.10 m width (Fig. 3.5). Arbitrarily the sun is taken at 180° . Consequently, the netting is located between $(294\text{-azimuth})^\circ$ and $(66\text{-azimuth})^\circ$.
- For every slice the length of the area shaded by the front walls, the netting and the back walls or a combination of those is determined according to

$$d_s = \frac{W_h}{\tan(\beta)} \quad (3.65)$$

where

- d_s : Length of the area shaded by a wall [m].
- W_h : Height of a wall [m].

- The absorption of global radiation by the Lexan wall is computed for every slice using Eq. (3.63) where the path length for light is calculated via

$$x^2 = x_{hor}^2 + x_{ver}^2 \quad (3.66)$$

$$x_{ver} = x_{lex} \tan(\beta) \quad (3.67)$$

$$x_{hor} = \frac{x_{lex}}{\sin(\alpha_a)} \quad (3.68)$$

where

- x_{hor} : Total horizontal path length light beam through the Lexan wall [m].
- x_{lex} : Width of the Lexan wall [m].
- x_{ver} : Total vertical path length light beam through the Lexan wall [m].
- α_a : Radius angle calculated from the length of a slice (a_1) and the distance of the slice to the north-south line (a_2) [rad].

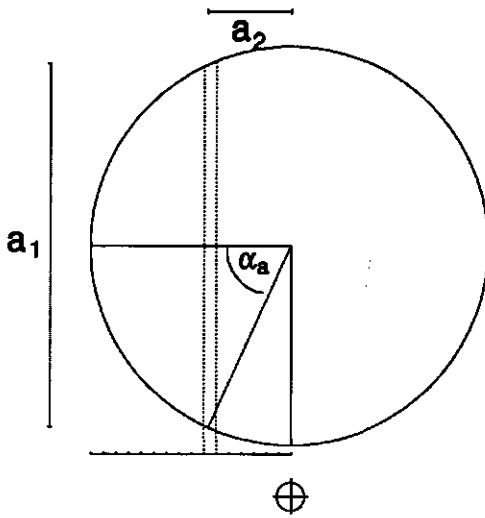


Figure 3.5: Calculation of absorption of global radiation by the chamber walls;
Integration procedure

-The total absorbed radiation for a particular slice is calculated via

$$S_{g,w} = \sum_{i=1}^{i=3} (Abs_w d_i 0.10 S_g) \quad (3.69)$$

where

- $S_{g,w}$: Total global radiation absorbed by the wall [W].
- Abs_w : Percentage of global radiation absorbed by the wall and netting [-].
- d_1 : Length of area shaded by the front wall with or without netting [m].
- d_2 : Length of area shaded by the front and back wall with or without netting [m].
- d_3 : Length of the area shaded by the back wall with or without netting [m].

- The absorption of solar radiation by the chamber walls and netting is integrated over the 32 slices.

The short-wave radiation is split into a direct and a diffuse component using empirical equations described by Spitters et al. (1986). For the direct radiation part the solar height and azimuth are calculated and the absorption is determined via the procedure mentioned above. To determine the absorption of diffuse radiation

an integration over the whole hemisphere was conducted. A uniform overcast sky distribution table over ten degree intervals of inclination angle was used for the diffuse radiation from an overcast as well as a clear sky. The computed diffuse global radiation absorbed by the chamber-side wall and the outer wall of the rectangular channel and the netting was proportional to the diffuse radiation intensity. The energy absorbed by the chamber-side wall of the rectangular channel and the netting is 168 W per 100 Wm² diffuse radiation. The outer wall of the rectangular channel absorbs 50 W per 100 Wm² diffuse radiation.

-Long-wave radiation balance

Since it is assumed that the solar radiation absorbed by the chamber-side wall of the rectangular channel is completely transformed into heat, only the long-wave energy balance of the outer walls is calculated.

The chamber walls are constructed vertical, so the total long-wave radiation from outside is composed of an atmospheric part and a soil part. The absorbed long-wave radiation from the atmosphere is estimated according to (Deardorff, 1978)

$$R_l = 0.5 \epsilon_l [\sigma_c + (1 - \sigma_c) 0.67 (1670 q_a)^{0.08}] \sigma T_a^4 \quad (3.70)$$

where

- q_a : Specific humidity of the air [kgkg⁻¹].
- R_l : Absorbed long-wave radiation from the sky [Wm⁻²].
- T_a : Temperature of the air [K].
- ϵ_l : Emissivity and absorption percentage of long-wave radiation for Lexan (0.9) [-].
- σ : Stefan-Boltzmann constant (5.67 10⁻⁸) [Wm⁻²K⁻⁴].
- σ_c : Cloud fraction [-].

The absorbed long-wave radiation from the soil is written

$$0.5 \epsilon_l \epsilon_s \sigma T_s^4 \quad (3.71)$$

where

- T_s : Temperature of the soil surface [K].
- ϵ_s : Emissivity of the soil (0.95) [-].

The temperature of the soil surface is estimated by the dry bulb temperature measured at a height of 0.5 m above grass. The emitted energy to the soil and atmosphere is calculated according to

$$\epsilon_l \sigma T_w^4 \quad (3.72)$$

where
 T_w : Temperature of the wall [K].

The net absorbed long-wave radiation from the inside of the chamber is written

$$\epsilon_i A \sigma (0.5(T_i + T_w))^3 (T_i - T_w) \quad (3.73)$$

where the temperature of the chamber-side wall of the rectangular channel is taken equal to the temperature of the air at the end of the air-supply system.

-Convection and conduction

Absorption of short-wave and absorption or emission of long-wave radiation causes a temperature change of the chamber wall. The convective heat exchange coefficients describing the energy fluxes from the chamber wall to its surrounding flow field were derived from a general relation valid for describing heat loss by forced convection from infinitely long planes and cylinders

$$Nu = f(Re, Pr) \quad (3.74)$$

$$Nu = \frac{Q L}{\lambda \Delta T A} = \frac{\alpha_h L}{\lambda} \quad (3.75)$$

$$Pr = \frac{\nu}{a} \quad (3.76)$$

where
 Nu : Nusselt number (exchanged energy / by molecular heat conduction exchangeable energy).
 Pr : Prandtl number.
 A : Characteristic surface area [m²].
 Q : Energy exchanged [Js⁻¹].
 L : Characteristic length scale [m].
 α_h : Convective heat exchange coefficient [Wm⁻²K⁻¹].

The convective heat exchange between the air inside the rectangular channel and the outer chamber wall is described via a Nusselt-Reynolds relation valid for forced convection over a flat plate (Monteith and Unsworth, 1990)

$$Nu = 0.032 Re^{0.8} \quad (3.77)$$

As a characteristic length scale half of the circumference is used (5.26 m). The mean velocity inside the rectangular channel is used as a typical velocity scale. The convective heat exchange between ambient air and the outer chamber wall is described via a Nusselt-Reynolds relation valid for forced convection over a

cylinder (Monteith and Unsworth, 1990)

$$Nu = 0.024 Re^{0.81} \quad (4.10^4 < Re < 4.10^5) \quad (3.78)$$

As a characteristic length scale the outer diameter of the chamber is used (3.35 m). The mean wind velocity at 0.5 metre outside the OTC is used as a typical velocity scale. The contribution of the molecular heat conductivity of the Lexan ($140 \text{ Wm}^{-2}\text{K}^{-1}$) wall to the heat exchange coefficient of the outer wall is neglected since the convective heat exchange coefficient is of the order of $10 \text{ Wm}^{-2}\text{K}^{-1}$.

3.3.2.2 The soil-vegetation model

The model initially described by Noilhan and Planton (1989) was adopted to describe the bulk-exchange processes between soil-vegetation and atmosphere under field as well as under OTC conditions. This model has been developed to reduce as much as possible the number of input parameters. Simultaneously, it attempts to preserve the physics which control the bulk-exchange processes (Jacquemin and Noilhan, 1990). The model employs a rather simple parameterization scheme thus making it relatively easy to modify some parts of it, which has been necessary for using this model for OTC conditions. Experiments at KEMA were focused on the effects of ozone uptake by plants. Therefore, the model has been used to make a first guess at the consequences of various aspects of changed environmental conditions on the ozone uptake under OTC conditions.

The basic model

The original parameterization scheme employs two layers in the soil and a single bulk canopy layer. The energy balance for the whole soil-vegetation system is composed of four terms.

$$R_n + H + LE - S = 0 \quad (3.79)$$

$$R_n = S_g(1 - Alb) + \epsilon_s(Lw_i - \sigma T_s^4) \quad (3.80)$$

where

- Alb : Albedo [-].
- H : Sensible heat flux density to soil-vegetation medium [Wm^{-2}].
- LE : Latent heat flux density to soil-vegetation medium [Wm^{-2}].
- Lw_i : Incoming long-wave radiation [Wm^{-2}].

- R_n : Net radiation from sky [Wm^{-2}].
 S : Flux density into the soil and heat storage in the vegetation medium [Wm^{-2}].
 T_s : Surface temperature of the soil-vegetation medium [K].
 ϵ_s : Emissivity of the surface [-].

The albedo and the emissivity represent values for the combined soil-vegetation medium. The sensible heat flux density for thermally neutral situations is expressed as

$$H = \rho_a C_p \frac{T_{z,r} - T_s}{R_{a,h}} \quad (3.81)$$

$$R_{a,h} = \frac{1}{U_{z,r} K^2} \ln\left(\frac{z_r - d}{z_{0,m}}\right) \ln\left(\frac{z_r - d}{z_{0,h}}\right) \quad (3.82)$$

where

- $R_{a,h}$: Bulk aerodynamic resistance to heat transport [sm^{-1}].
 $T_{z,r}$: Temperature of the air at reference height [K].
 $U_{z,r}$: Mean wind speed at reference height [ms^{-1}].
 z_r : Reference height [m].
 $z_{0,h}$: Roughness height for heat [m].
 $z_{0,m}$: Roughness height for momentum [m].

The bulk aerodynamic resistance expresses the resistance to the transport of heat from a reference height to the height ($d+z_{0,h}$) where the virtual source or sink for heat can be found. However, the bulk aerodynamic resistances to the transport of heat and mass can differ significantly from the corresponding resistance to momentum exchange (Chamberlain, 1966; Garrat and Hicks, 1973; Owen and Thomson, 1963; Thom, 1972; 1975). Bluff body forces acting on individual foliage elements increase the total drag force to a canopy generated by skin-friction drag alone. Since the transport of heat and mass is restricted to the mechanism of skin friction drag alone, an additional resistance to heat and mass exchange over that to momentum can be found.

Garrat (1978) suggested that for practical purposes the relation

$$\ln \frac{z_{0,m}}{z_{0,h}} \approx 2 \quad (3.83)$$

can be used leading to an additional resistance of $\frac{2}{U_* \kappa}$.

To correct for the influence of thermal stability on the heat and mass transport correction functions proposed by Holtslag and Beljaars (1988), Louis (1979) and Louis et al. (1982) are used for thermal-unstable conditions and thermal-stable conditions, respectively. Both correction functions use the bulk Richardson number as an independent variable

$$Ri_B = \frac{g(z_r - d - z_{0,m}) \Delta T}{\bar{T} U_{z,r}^2} \quad (3.84)$$

$$\Delta T = T_{z,r} - T_s$$

where

Ri_B : Bulk Richardson number [-].

Since both correction functions use a roughness length for momentum transport Eq. (3.83) has been used to make a correction for the difference between the roughness height for momentum and heat transport. Consequently, Eq. (3.82) changes into

$$R_{a,h} = \left(U_{z,r} Cd_m \left(1 - \frac{15 Ri_B}{1 + 75 Cd_m \sqrt{|Ri_B| \frac{z_r - d}{z_{0,m}}}} \right) \right)^{-1} + \frac{2}{\kappa U_*} \quad (3.85a)$$

(thermal-unstable conditions)

$$R_{a,h} = \left(\frac{U_{z,r} Cd_m}{1 + 10 Ri_B (1 + 8 Ri_B)} \right)^{-1} + \frac{2}{\kappa U_*} \quad (3.85b)$$

(thermal-stable conditions)

$$Cd_m = \frac{\kappa^2}{\ln\left(\frac{z_r - d}{z_{0,m}}\right)} \quad (3.85c)$$

where

Cd_m : Bulk exchange coefficient for momentum during thermal-neutral conditions [-].

In the model computations the roughness height for momentum transport was taken as 10% of the canopy height. The displacement length for momentum as well as scalar transport was taken as 63% of the canopy height.

A prognostic equation for the surface temperature is obtained from the force restore method used by Bhumralkar (1975) and Blackadar (1976).

$$\frac{\partial T_s}{\partial t} = C_T S - \frac{2\pi}{\tau_d} (T_s - T_2) \quad (3.86)$$

where

- C_T : Coefficient [Km^2J^{-1}].
 T_2 : Time averaged mean surface temperature [K].
 τ_d : Daily period (86400) [s].

The coefficient C_T depends on soil texture, soil moisture content and on the fraction of the soil shielded by the vegetation. In our simulations the time averaged surface temperature for a particular day was calculated from experimental values. The first term on the right hand side of Eq. (3.86) represents the diurnal forcing of the surface temperature by the net radiation corrected for a sensible and latent heat flux. The second term on the right hand side of Eq. (3.86) tends to restore the surface temperature to the time averaged mean surface temperature. For a complete plant cover the surface temperature is calculated as the solution of the surface energy balance without any heat storage by plants.

The latent heat flux density is composed of the evaporation of the soil surface and the evapotranspiration of the vegetation. The evaporation of the soil surface depends on the surface temperature of the soil, the specific humidity of the air, the soil moisture content of the upper layer of the soil and the bulk aerodynamic resistance to water vapour transport. The bulk aerodynamic resistance to water vapour transport is assumed to be equal to the bulk aerodynamic resistance to heat transport. The soil moisture content is calculated employing the force restore model described by Deardorff (1978). The force restore model is based on a sinusoidal surface water flux within a daily cycle. It divides the soil into two layers: an arbitrarily chosen thin upper layer interacting with the atmosphere and a bulk soil column of a particular depth at which the soil moisture flux becomes negligible for a period of about one week. The water needed for transpiration is extracted from this bulk layer. The soil parameters within the soil-vegetation module are determined using thermo-hydric equations. The soil is classified according to the eleven soil types of the USDA textural classification. The critical moisture contents for various soils were given by Jacquemin and Noilhan (1990). The estimated and calibrated soil coefficients of the thermo-hydric equations were given by Noilhan and Planton (1989).

The evapotranspiration of the canopy is written

$$E_v = \sigma_v \rho_a \left(\delta \frac{q_{z,r} - q_{sat}(T_s)}{R_{a,v}} + (1 - \delta) \frac{q_{z,r} - q_{sat}(T_s)}{R_{a,v} + R_{s,v}} \right) \quad (3.87)$$

where

- E_v : Evapotranspiration of the vegetation [$\text{kgm}^{-2}\text{s}^{-1}$].
- $R_{a,v}$: Bulk aerodynamic resistance to water vapour transport [sm^{-1}].
- $R_{s,v}$: Bulk surface resistance to transpiration [sm^{-1}].
- q_{sat} : Saturated specific humidity [kgkg^{-1}].
- $q_{z,r}$: Specific humidity of the air at reference height [kgkg^{-1}].
- δ : Fraction of the foliage covered by intercepted water [-].
- σ_v : Fraction of the soil shielded by the vegetation [-].

The fraction of the foliage covered by intercepted water depends on the ratio between the actual moisture content and the maximum moisture content of the canopy. The moisture content of the canopy depends on the amount of intercepted rain and evaporation or condensation of water. The maximum moisture content is related to the one-sided leaf area index.

The transpiration of plants depends on the bulk surface resistance. This bulk surface resistance is defined as the resistance to the transfer of water from the root zone to the leaf surfaces. The bulk surface resistance is related to the stomatal resistance through the leaf area index (Jarvis, 1976). Fractional conductances represent the influence of solar radiation (Dickinson, 1984), soil moisture (Thompson et al., 1981), vapour pressure deficit (Dorman and Sellers, 1989; Sellers et al., 1986) and air temperature (Dickinson, 1984) on stomatal resistance.

$$R_{s,v} = \frac{R_{s,min}}{LAI F_1 F_2 F_3 F_4} \quad (3.88)$$

$$F_1 = \frac{\left(\frac{R_{s,min}}{R_{s,max}} \right) + f}{1 + f} \quad (3.89a)$$

$$f = 0.55 \frac{S_g}{S_{gt}} \frac{2}{LAI} \quad (3.89b)$$

$$F_2 = \frac{W_2 - W_{wilt}}{W_{fc} - W_{wilt}} \quad 0 \leq F_2 \leq 1 \quad (3.90)$$

$$F_3 = 1 - \alpha_1 (q_{sat}(T_a) - q_a) \quad (3.91)$$

$$F_4 = 1.0 - 0.0016(298.0 - T_a)^2 \quad (3.92)$$

where

- LAI : Leaf Area Index [m^2 (one-sided leaf surface) m^{-2} (soil area)].
 F_1, F_2 : Fractional conductances describing the influence of solar radiation,
 F_3, F_4 soil moisture, water vapour pressure deficit and air temperature,
 respectively.
 $R_{s,max}$: Maximum stomatal resistance observed (2000) [sm^{-1}].
 $R_{s,min}$: Stomatal resistance observed at high solar intensities, well irrigated
 soil, saturated air and optimal ambient temperature (200) [sm^{-1}].
 f : Dimensionless term representing the incoming photosynthetically
 active radiation on a foliage, standardized by a species-dependent
 limit value.
 S_{gl} : Species-dependent limit value (100) [Wm^{-2}].
 W_{wilt} : Wilting point volumetric moisture content [m^3m^{-3}].
 W_{fc} : Field capacity volumetric moisture content [m^3m^{-3}].
 W_2 : The mean volumetric moisture content of a bulk soil column [m^3m^{-3}].
 α_1 : Species-dependent empirical parameter (40) [-].

Modifications for OTC conditions

The OTC conditions differ from field conditions in various aspects. Three main aspects have been taken into consideration within the soil-vegetation model:

- the chamber floor,
- the incoming long-wave radiation,
- exchange processes between soil-vegetation and the air inside the chamber.

-The chamber floor

The chamber floor is covered with a wooden plate made of betonplex birch with 36 holes for plants. Plants are grown in pots or loosely woven sacks. The model splits the floor area into two parts. The first part, denoted by subscript *A*, describes the behaviour of the part of the chamber floor shielded by the vegetation (plant cover). The second part, denoted by subscript *B*, describes the non-shielded part of the chamber floor.

-Incoming long-wave radiation

The chamber walls cause the long-wave radiation at the chamber floor to deviate from field conditions. The incoming long-wave radiation at the chamber floor is determined according to

$$Lw_i = \epsilon_w \sigma T_c^4 \quad (3.93)$$

where

Lw_i : Incoming long-wave radiation [Wm^{-2}].
 ϵ_w : Effective emissivity chamber wall [-].

The temperature of the chamber walls was taken as being equal to the spatial mean temperature of the air in the lower part of the chamber. The effective emissivity was determined by comparing the measured long-wave radiation at the chamber floor with the calculated one.

-Exchange processes between soil-vegetation and the air inside the chamber.

The exchange processes between soil-vegetation and the air inside an OTC can not be described by bulk aerodynamic resistances in the same way as those for field conditions. The air in the OTC is assumed to be well-mixed. Therefore, the only relevant resistance in the transport of heat, water vapour and gaseous air pollutants from the chamber air to a leaf surface and the reverse is the so-called leaf boundary layer resistance.

At the surface of plant material the exchange processes with the atmosphere take place via a thin layer of air, the leaf boundary layer, within which the velocity increases away from the surface. Exchange processes from a plant surface to the environment are controlled by molecular as well as turbulent diffusion. Molecular diffusion plays an important role in the transport of molecules through the sub-stomatal cavities and in the skin of air forming the boundary layer around a leaf. Turbulent exchange processes play an important role in the free atmosphere but can play an important role in the boundary layer around a leaf too. It is still not clear whether the boundary layer of a leaf in a canopy should be regarded as laminar or turbulent. Finnigan and Raupach (1987) state that leaf boundary layers are almost invariably laminar but very unsteady.

Two main types of convection are distinguished: forced convection and free convection. The transport of heat by forced convection depends on the flow properties close to the leaves. The transport of heat by free convection is a result of differences in air density, caused by temperature differences which can occur above heated or cooled surfaces. Experimental results of heat exchange by forced convection from planes, cylinders and spheres have been described by Eq. (3.74).

Experimental results of heat exchange by free convection from planes, cylinders and spheres have been described by the general relation (Monteith and Unsworth, 1990)

$$Nu = f(Gr, Pr) \quad (3.94)$$

$$Gr = \frac{g\beta(T_s - T_a)L^3}{\nu^2} \quad (3.95)$$

where

- Gr : Grashof number
 L : Characteristic length scale [m].

In many natural systems a combination of both free as well as forced convection occurs. As a rough criterion for distinguishing the two regimes, the ratio Gr to Re^2 can be used. This ratio represents the ratio of the buoyancy forces to the inertial forces. If $Gr < 0.1 Re^2$ the forced convection functions can be applied (Gates, 1980). The Grashof number for a leaf, with a characteristic diameter of 0.04 m and a temperature of about 2 K higher than the surrounding air, is $2.0 \cdot 10^4$. At a characteristic mean wind speed under OTC conditions of 1 ms^{-1} the Reynolds number is $2.7 \cdot 10^3$. Consequently, the ratio Gr to Re^2 is $2.7 \cdot 10^{-3}$. Therefore, within an OTC free convection of a leaf is relatively small and the forced convection functions have been used. The leaf boundary layer resistance to forced convection of heat for a one-sided leaf surface is written according to

$$R_{b,h} = C_1 \left(\frac{L}{U}\right)^{0.5} \quad (3.96)$$

where

- C_1 : Coefficient = 306 (theory laminar boundary layer); 188 (Pearman et al., 1972); 173 (Gates, 1980); 122 (Parlange et al., 1971) [$\text{s}^{0.5}\text{m}^{-1}$].
 $R_{b,h}$: Leaf boundary layer resistance to heat transfer [sm^{-1}].

For a two-sided leaf surface half of the C_1 given above is taken. In the present study a value for C_1 of 180 was used (one-sided). The characteristic length scale for leaves was taken as 0.02 m.

The energy balance at the chamber floor is written according to

$$R_n = \sigma_v R_{n,A} + (1 - \sigma_v) R_{n,B} \quad (3.97)$$

$$R_{n,A} + H_A + LE_A - S_A = 0 \quad (3.98)$$

$$R_{n,B} + H_B + LE_B - S_B - S_p = 0 \quad (3.99)$$

where
 S_P : The energy absorbed by the wooden floor-plate [Wm^2].

The $R_{n,A}$ and $R_{n,B}$ are calculated employing Eq. (3.80) using the surface temperature of the combined soil-plate-plant medium and the surface temperature of the wooden floor-plate, respectively. Since no water transport through the floor-plate occurred $LE_B = 0$. The heat storage in the soil medium under the floor-plate is written

$$S_B = \alpha_P(T_P - T_{s,B}) \quad (3.100)$$

where
 S_B : The heat transport to the soil medium under the wooden floor-plate [Wm^2].
 $T_{s,B}$: The temperature of a thin upper layer of the soil just below the floor-plate [K].
 T_P : The temperature of the floor-plate [K].
 α_P : Heat transfer coefficient describing the energy transport between the floor-plate and the upper layer of the soil [Wm^2K^{-1}].

The total sensible heat flux density is written

$$H = \sigma_v H_A + (1 - \sigma_v) H_B \quad (3.101)$$

H_A is calculated employing Eq. (3.81) using parallel connected resistances describing the leaf boundary layer heat transport and the heat transport between the pot surface (or the wooden floor-plate) and the chamber air. The heat exchange between the soil medium in the pot and the chamber air was computed employing Eq. (3.96) using a constant C_1 of 180 and a characteristic length scale of 0.18 m (diameter pot).

H_B describes the heat exchange between the wooden floor-plate and the air inside the chamber. The boundary layer resistance to heat exchange between the floor-plate and the air above it was computed employing Eq. (3.96). The constant C_1 was arbitrarily taken as 306. The length scale was assumed to be proportional to the mean distance between the plant holes (0.42 m). The characteristic length scale was estimated in combination with the heat transfer coefficient of Eq. (3.100) by tuning simulated values of the soil heat flux density and the temperature of the floor-plate to experimental data. The prognostic equation describing the temperature change of the floor-plate is written

$$\frac{\partial T_p}{\partial t} = \frac{S_p}{L_p \rho_p C_{w,p}} \quad (3.102)$$

where

- L_p : Thickness of the floor-plate (0.018) [m].
 $C_{w,p}$: Heat capacity floor-plate (1368) [Jkg⁻¹K⁻¹].
 ρ_p : Density of the floor-plate (650) [kgm⁻³].

Mass transfer to or from objects in an air flow is analogous to heat transfer by convection. The boundary layer resistance to the transport of a scalar is related to the boundary layer resistance to heat transport by

$$\frac{R_{b,sc}}{R_{b,h}} = \left(\frac{a}{D_{sc}}\right)^{0.67} = C_r \quad (3.103)$$

where

- C_r : Ratio (ozone: 1.32; water vapour 0.93) [-].
 $R_{b,sc}$: Boundary layer resistance to transfer of scalar [sm⁻¹].

The water gift to the plants grown under OTC conditions is supplied directly to the pot surface (10.8 kg per day). No water flows through the wooden floor-plate. Therefore, the moisture content of the soil directly under the floor-plate is assumed to be at the wilting point or less. A part of the water gift will evaporate from the pot surface, a part will evaporate via transpiration by plants and a part will flow to deeper soil layers below pot level (0.17 m). Assuming total evaporation of the water gift within 12 hours, the mean latent heat flux density is 84 Wm⁻² resulting in a mean temperature decrease inside the chamber of 0.4 K. The maximum mean increase of specific humidity inside the chamber due to the water gift is approximately 0.15 gkg⁻¹ (flow rate: 1.4 m³s⁻¹).

The ozone transport to the chamber walls is calculated using a boundary layer resistance of 32000 sm⁻¹ (Aben, 1990). Experiments conducted by Aben (1987) in a gas-exchange chamber have shown that the ozone uptake by broad bean plants (variety Metissa) can be explained adequately by the ratio of an ozone exposure and the sum of a leaf boundary layer and stomatal resistance for ozone. The ozone concentration within the plant was taken as 0. The uptake and turnover by the mesophyll cells did not limit the ozone uptake. Adsorption by the epidermis and transport through the cuticula were negligible.

The bulk surface resistance to ozone transport is calculated from the bulk surface

resistance to water vapour transport according to

$$R_{s,O_3} = R_{s,v} \frac{D_{H_2O}}{D_{O_3}} \quad (3.104)$$

where

$R_{s,v}$: Bulk surface resistance to water vapour transport [sm^{-1}].
 R_{s,O_3} : Bulk surface resistance to ozone transport [sm^{-1}].

The soil-vegetation model has been used to study the consequences of various aspects of changed environmental conditions on the ozone uptake under OTC conditions.

Simulations

The instantaneous air temperature, specific humidity, ozone concentration and wind speed at reference height under field conditions were determined using linear interpolation between measured values. The instantaneous air temperature and specific humidity inside the chamber were determined using linear interpolation between spatial mean values measured in the lower part of the chamber. The mean global radiation at the chamber floor was estimated experimentally. The height of the plants, the fraction of the soil shielded by the vegetation and the leaf area index under field conditions were taken as being equal to the ones observed under OTC conditions. The fraction of the soil shielded by the vegetation and the leaf area index were estimated. The mean height of the plants was measured weekly. Case studies were executed using the input values given in Table 3.10.

Table 3.10: Input parameters soil-vegetation model.

Input Parameter	Open top chamber		Field
	Vegetation	Floor-plate	
Soil type	Sandy loam	Sandy clay	Sandy clay
Initial soil moisture content	Saturated	Wilting point	Field capacity
Depth upper layer soil	0.02 m	--	0.02 m
Depth bulk soil layer	0.17 m	--	0.50 m
Water supply / precipitation time / amount	irrigation 08.00/11.83kgm ⁻²	no water exchange	precipitation 08.00/1.48kgm ⁻²
Time mean surface temperature (T _s) averaged over one day	spatial mean air temperature in lower part of the chamber	spatial mean air temperature in lower part of the chamber	mean air temperature 0.5 m
Reference height (z _r)	--	--	2.93 m
Global radiation	80% of field conditions	80% of field conditions	measured
Albedo	0.20	0.20	0.20
Emissivity (soil-vegetation)	0.95	0.95	0.95

CHAPTER 4 EXPERIMENTAL SET-UP

4.1 General.

The experiments executed by KEMA did not deliver sufficient material for a detailed analysis of the physical characteristics of the OTC system. Furthermore, the OTC's used by KEMA were situated in rather hilly terrain with buildings and other obstacles in the direct neighbourhood. This complicated a characterization of the OTC environment and its influence on the chamber microclimate. Therefore, the need arose for an extended experiment situated in a flow field without obstacles. The experimental results have been used to derive the prior conditions needed for the models developed (see Chapter 3). Furthermore, the experimental results have been used to verify these models. Since weather conditions over a summer period can vary considerably the experimental period was two to three months in order to cover as many weather types as possible.

The experiments executed in the OTC were partly carried out using plants. Therefore, broad bean (*Vicia faba* variety *metissa*) was selected since these plants had also been used by Aben (1990). The plants were sown and grown under greenhouse conditions for a period of about two weeks. There were three plants per pot. The plants were well supplied with water (about 0.3 l per pot per day at 08.00 local time). Therefore, soil moisture did not limit plant growth and development.

An OTC identical to the KEMA-type OTC was situated at the weather station of the Meteorological Department at the Agricultural University, about one kilometre west of Wageningen. The surroundings of this OTC were flat and the area was covered with short grass (height less than 0.15 m). There were no big obstacles that could disturb the flow field to the OTC within a radius of about 80 m.

Occasional experiments dealing with the flow field within and around an OTC, the degree of incursion and the flow rate are described in Section 4.2. The continuous

experiments dealing with the microclimate inside and outside an OTC are described in Section 4.3. Since it was not feasible to describe the flow field exactly at every moment in time and space the experiments were restricted to time mean measurements at fixed positions. This involved measurements of mean wind speed, temperature, humidity, short-wave and long-wave radiation, net radiation and soil heat flux density, inside as well as outside an OTC. An experimental set-up was constructed in 1989 for continuous monitoring of the microclimate at various positions within and outside the OTC. These experiments were conducted in an OTC without plants. The experiments were repeated during May-July 1990 in an OTC with plants. That year the experiments were extended by the monitoring of ozone and nitrogen oxides. Turbulence parameters were measured occasionally. Characteristic days were chosen for that purpose i.e. cloudy days with high wind speeds (thermal-neutral conditions) or clear days with low wind speeds (thermal-unstable conditions). The sensors used in 1989 and 1990 are described in Appendix 1.

4.2 Experiments dealing with the flow field in and around an OTC.

The features of the flow within and outside an OTC were visualised using white smoke. Since the generation of this smoke causes heat to be produced, the interpretation of the smoke patterns was used only to make the general features of the flow regime visible. The smoke was generated using smoke powder (KAT-Leiden) in a cylinder (length 0.38 m; diameter 0.08 m) or on a flat plate (diameter 0.15 m).

The flow rate plays a major role in the determination of the resulting flow regime within an OTC. Therefore, an accurate determination of this flow rate is necessary. The flow rate inside the air-supply system was measured using a multipoint pitot-tube station. However, this measuring device gives reliable results only when swirl or cross flow in the connecting duct are of minor importance. Testing of the multipoint pitot-tube station revealed that the use of this measuring device can lead to an underestimation or overestimation of the flow rate depending on the OTC configuration and the flow rate applied. The use of a special air flow controlling

valve at the beginning of the connecting duct by KEMA complicated the usefulness of this type of air flow measuring station. Therefore, this valve was not used in our experiments. To monitor the flow rate accurately a cup anemometer was placed in the centre of the duct at the end of the connecting duct. The accuracy of the cup anemometer was tested by comparing the observed mean wind speed to measurements executed with a hot wire anemometer (Lambrecht 641N; accuracy: 5% of reading) across the connecting duct. The spatial mean wind velocity parallel to the walls was within $\pm 5\%$ of the horizontal wind speed measured by the cup anemometer.

The rectangular channel around the lower part of the chamber has been developed to achieve a uniform flow into a chamber. To verify the uniformity of this flow inlet velocities were measured. This was done by measuring the pressure difference between a Prandtl tube (diameter 0.04 m) placed at a distance of 0.01 m perpendicular to the centre of an air-inlet hole and a reference pressure just above the soil outside the OTC. The reference pressure was composed of a Prandtl tube in combination with a pneumatic low pass filter with a first order time constant of 70 s. The pressure difference was measured by a differential manometer (Datametrics, type 590 Barocel in combination with a type 1400 electronic manometer), the accuracy was 0.05% of reading, the operating range was 0-981 Nm². The flow rate applied was approximately 1.4 m³s⁻¹.

Measurements of time mean wind speed inside the chamber were restricted to fixed positions. Apart from these continuous measurements at fixed positions some experiments were conducted in which the variation of air flow within a chamber was measured. The measurements were performed with a hot wire anemometer (Lambrecht 641N).

The rate of incursion in relation to the ten minutes mean wind speed outside the OTC was estimated employing Eq. (3.57) using the ozone concentration of ambient air. Immediately after the fan is stopped the concentration of ozone inside the chamber changes as a result of incursion. Assuming a good mixing of the ozone inside the chamber and no influence on incursion by the fan driven air flow leaving

the chamber, the incursion resistance can be estimated. The ozone concentration was monitored continuously at a height of 1 m in the centre of the chamber. The rate of change of the ozone concentration was integrated over the period 10-70 s after switching off the fan. The incursion resistance was calculated taking into account the ozone concentration inside the chamber at the moment the fan was switched off, and the ozone concentration outside the chamber (height 2 m). Ozone transport to the chamber walls was neglected. The time mean horizontal wind speed outside the OTC was measured at open top height using a cup anemometer.

4.3 Experimental set-up and data acquisition continuous experiments.

Experimental set-up outside the OTC

The properties of the flow field outside the OTC were monitored using sensors attached to three masts (see Table 4.1). One mast (height: 4 m) was situated at about 20 m from the OTC and was used to measure mean profiles of horizontal wind speed, temperature and humidity. The wind direction was measured at the top of this mast. These measurements and measurements of net radiation, global radiation and soil heat flux density were used primarily to characterize the OTC microclimate in relation to field conditions. Furthermore, the experimental data served as input conditions to the OTC-resistance model and were used to calculate a Richardson gradient number which characterized the thermal stability of the surface layer (Stull, 1988).

The sensors for monitoring turbulence parameters were attached to a mast at a distance of 30 m from the OTC. The height of this mast, 6 m in 1989, was increased to 20 m in 1990. The occasional experiments involved measurements of mean fluctuations of wind velocity and temperature, and the spectra of these signals. A comparison of the standard deviations within and outside an OTC yielded information about the degree to which whirls from outside the OTC could penetrate into the chamber.

A third mast (height: 3 m) was used to sample air from outside the OTC through

a heated teflon tube that was connected, via a valve system, to an ozone and nitrogen oxides monitor. The maximum length of these tubes was limited to 30 m. The ozone and nitrogen oxides monitors were placed in a Portocabin at the north side of the air-supply system.

Table 4.1: Sensor configuration outside the OTC (1989/1990).

measurement	sensor (number)	height (m)	1989	1990
1a. dry bulb temperature	LUW-psychrometer (3)	0.50,1.50,2.93	+	+
1b. wet bulb temperature	LUW-psychrometer (3)	0.50,1.50,2.93	+	+
2. dry-wet bulb temperature	Stigter psychrometer (1)	1.50	+	-
3. horizontal wind speed	cup anemometer (4)	0.50,0.90,1.50,2.93	+	+
4. wind direction	wind vane (1)	4.00	+	+
5. net radiation	pyrradiometer (1)	1.00	+	+
6. soil heat flux density	soil heat flux meter (1)	-0.05	+	+
7. global radiation	pyranometer (1)	1.25	+	-
global radiation	pyranometer (1)	3.00	-	+
8. ozone /nitrogen oxides	teflon tubes (1)	2.00	-	+
<i>turbulence measurements</i>				
9. temperature fluctuations	thermocouple (2)	2.93,6.00	+	-
temperature fluctuations	thermocouple (6)	0.50,1.50,2.93, 5.00,10.00,20.00	-	+
10. wind velocity fluctuations	3D-sonic (1)	6.00	+	-
11. vertical wind velocity fluctuations	1D-Sonic (1)	6.00	-	+

Experimental set-up inside the OTC

A mast was constructed inside the chamber; the frame elements had a diameter of 0.028 m. The sensors that were to be attached to this construction had to be as small as possible, because they could disturb the typical 3-dimensional flow pattern within the OTC. Furthermore, precautions had to be taken against the impact of radiation on the measurements themselves. The experimental set-up shown in Figure 4.1 and 4.2 and Table 4.2 was a compromise given these requirements. The total configuration was designed to be flexible and could easily be changed depending on the wind direction and other requirements. In 1989 the flow rate applied was set at approximately $1.4 \text{ m}^3\text{s}^{-1}$. In 1990 the flow rate applied was set at approximately 1.2 or $1.6 \text{ m}^3\text{s}^{-1}$.

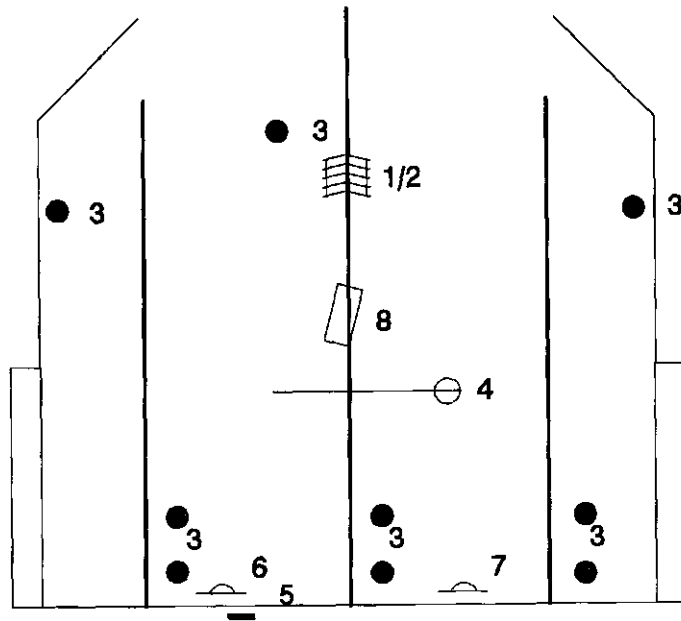


Figure 4.1: Sensor configuration in the chamber (1989).

1/2 = LUW psychrometer (wet and dry bulb temperature); 3 = set of thermocouple, heat bulb anemometer and Stigter psychrometer; 4 = pyrradiometer; 5 = soil heat flux meter; 6 = pyranometer; 7 = pyrgeometer; 8 = infrared thermometer.

Data acquisition

The data acquisition for continuous measurements in the OTC system was done with a data acquisition and control unit from Hewlett Packard (HP 3852A) combined with a HP-Vectra Personal Computer. A measurement cycle was conducted by the data acquisition unit each thirtieth second. Mean values were calculated after each 10-minute period and stored on hard disk. The PC controlled the valves connecting the four air-sampling tubes to the ozone and nitrogen oxides monitor simultaneously. Every 1-1.5 minutes (depending on the sampling position), another air-sampling tube was connected to the monitors and a valve-switching cycle was performed every fifth minute. Experimental values were checked by means of tables or graphs every 12 hours without stopping the data acquisition. Furthermore, a backup to floppy disk was made every 24 hours.

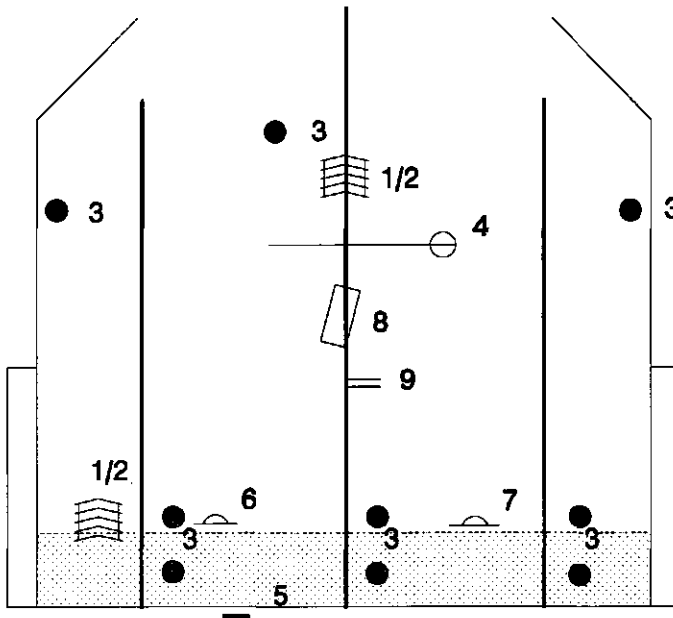


Figure 4.2: Sensor configuration in the chamber (1990).

1/2 = LUW psychrometer (wet and dry bulb temperature); 3 = heat bulb anemometer; 4 = pyradiator; 5 = soil heat flux meter; 6 = pyranometer; 7 = pyrgeometer; 8 = infrared thermometer; 9 = air sampling tube.

The 5½-digit integrating voltmeter with a guard terminal was used for measuring DC-voltage and 4-wire ohms resistance (built in current source) with an integration time of 0.02 seconds. One channel was used for measuring the offset of the voltmeter and a multiplexer chart. The voltage values measured were corrected for this offset. The accuracy of the DC-voltage measurements in the 30 mV range was 0.02 % of the reading +8 μV. The accuracy of the 4-wire-resistance measurements in the 300 Ω range was 0.015 % of the reading +8 mΩ. A 16 channel digital input card was used as a counter (Hewlett Packard, 1988). The ozone and the nitrogen oxides monitors were calibrated weekly.

Table 4.2: Configuration of the sensors inside the OTC (1989-1990).

measurement	sensor (number)	height (m)	1989	1990
1a. dry bulb temperature	LUW-psychrometer (1)	0.50-2.50	+	-
1b. dry bulb temperature	LUW-psychrometer (4)	just above crop (3), 2.00 (1)	-	+
1c. wet bulb temperature	LUW-psychrometer (1)	0.50-2.50	+	-
1d. wet bulb temperature	LUW-psychrometer (4)	just above crop (3), 2.00 (1)	-	+
2. dry bulb temperature	thermocouple (9)	0.15-0.25 (3), 0.60 (3), 2.00-2.40 (3)	+	-
3. dry-wet bulb temperature	Stigter psychrometer (9)	0.15-0.25 (3), 0.60 (3), 2.00-2.40 (3)	+	-
4a. wind speed	heat bulb anemometer (9)	0.15-0.25 (3), 0.60 (3), 2.00-2.40 (3)	+	-
4b. wind speed	heat bulb anemometer (9)	half way crop (3), just above crop (3), 2.00-2.40 (3)	-	+
5a. net radiation south side chamber	pyrradiometer (1)	1.00	+	-
5b. net radiation south side chamber	pyrradiometer (1)	1.80	-	+
6a. soil heat flux density in plant-hole	soil heat flux meter (1)	-0.05	+	-
6b. soil heat flux density under floor plate	soil heat flux meter (2)	-0.05	+	+
7. global radiation south side chamber	pyranometer (2)	0.15-2.00	+	+
8. long-wave radiation	pyrgeometer (1)	0.15	+	+
9a. wall temperature	infrared thermometer (1)	1.90	+	-
9b. leaf/wall temperature	infrared thermometer (1)	1.50	-	+
10. ozone/nitrogen oxides	teflon tubes (2)	0.20-2.00	-	+
<i>turbulence measurements</i>				
11a. dry bulb temperature fluctuations	thermocouple (9)	0.15-0.25 (3), 0.60 (3), 2.00-2.40 (3)	+	-
11b. dry bulb temperature fluctuations	thermocouple (7)	half way crop (3), just above crop (3), 1.50-2.00 (1)	-	+
<i>air-supply system</i>				
12. pressure drop	differential pressure gauge (1)	over dust filter	+	+
13. mean flow rate	multipoint pitot-tube station (1)	middle connecting duct	+	+
14. mean flow rate	cup anemometer (1)	end connecting duct	-	+
15. dry bulb temperature	4-wire-resistance (1)	end connecting duct	-	+
16. ozone/nitrogen oxides	teflon tube (1)	end connecting duct	-	+

The measurement van equipment of the Agricultural University's Meteorological Department was used for occasional measurements during which turbulence parameters were sampled. Use of this van made it possible to monitor various channels at high frequencies (10 Hz or more) simultaneously. The signals were recorded on tape. The calculated standard deviations, covariances and correlations were corrected for a linear trend in the signal during the averaging period.

CHAPTER 5 RESULTS

5.1 Flow regime

The flow regime in the lower part of a ventilated chamber is primarily determined by the way air enters the chamber, the flow rate and the OTC-configuration. Prandtl tube measurements revealed that air-inlet velocities were rather uniform over the chamber. Differences between air-inlet velocities were within 2% of the measured values. Smoke experiments revealed a complicated flow pattern where adjacent air-inlet jets interfere with each other and recirculation zones between air-inlet jets and between jets and walls occur. The mean wind speed decreases with increasing distance to the chamber wall, especially in the first 0.5 m from the wall (see Table 5.1).

Table 5.1: Mean wind speed in the lower part of the chamber.

distance from wall	number of measurements	wind speed [ms^{-1}]	
		mean	range
0.27	90	1.52	0.3->5
0.67	66	0.75	0.3-2.7
1.07	22	0.65	0.2-1.6

The results represent a mean value calculated from measurements with a heat wire anemometer at a height of 0.15, 0.25 and 0.60 m.

The position of the measurement location with regard to the air-inlet holes is the most important factor in determining the wind speed at a particular location. The individual air-inlet jets can be clearly recognized within the outer plant-hole circle. Ten-minutes mean wind speed, measured within the broad bean crop showed some changes in time. The maximum variation over one day at a particular position was 0.2 ms^{-1} (mean wind speed less than 1.5 ms^{-1} , flow rate: $1.2\text{-}1.6 \text{ m}^3\text{s}^{-1}$). Small changes in flow rate during a day appeared to have some influence on the mean wind speed inside a chamber.

Above the air-inlet holes smoke experiments and measurements of time mean

wind speed (vertical velocity magnitude above 1 ms^{-1}) revealed the existence of a vertically organised circular flow pattern.

The FLUENT simulations for a ventilated chamber (see Fig. 5.1) show a similar flow regime. The individual air-inlet jets can be recognized within a distance of 1 m from the chamber wall. Computations show that a recirculation zone near the chamber floor exists with mean wind speeds of more than 1 ms^{-1} . The air-inlet jets in the lower part of the chamber are the driven forces for the vertical circulation pattern observed above the air-inlet holes. Most of the ventilated air leaves the chamber via the middle part of the open top. A part of the ventilated air, which can be mixed with some ambient air, flows via the chamber wall to the lower part of the chamber.

A sensitivity analysis for

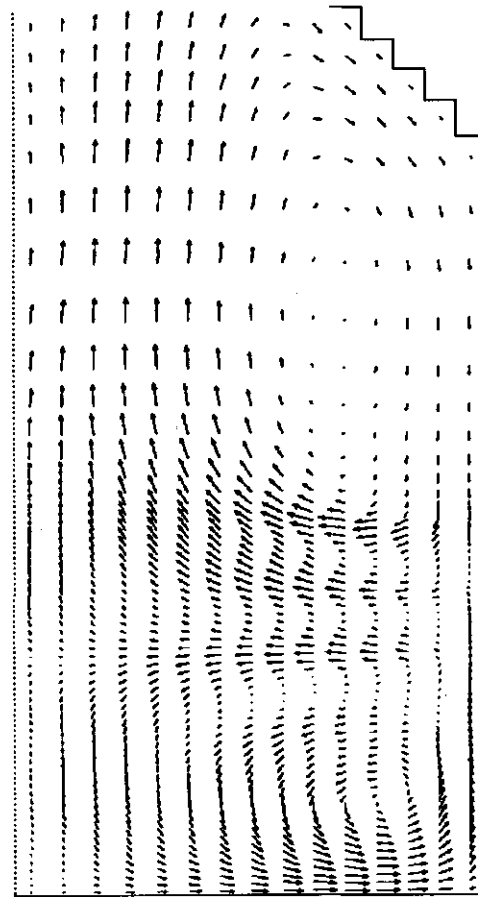
- a different wall roughness setting (10% of its original value),
- the use of the interpolation method QUICK,
- the use of model constants according to Detering and Eting,
- the use of the Algebraic Stress Model (ASM),

did not show major qualitative changes of the simulated flow regime. The most obvious change has been the use of ASM which shows a decreased rate of spread of the air-inlet jets. The global similarity between the various model calculations suggests that for a qualitative analysis the regular $k-\epsilon$ model can be used. A quantitative comparison between velocity magnitudes obtained from model computations and experimental values is given in Table 5.2.

When the ventilation is switched off the flow inside the chamber changes drastically. Figure 5.2 shows the results of the FLUENT simulation for the case study with a non-ventilated chamber. Within the chamber a whirl with the size of the chamber is seen. Air moves along the leeward wall to the base of the chamber, along the base of the chamber to the windward wall and along the windward wall to the top of the chamber. The position of the reattachment point and the existence of an organised circulation pattern within the chamber are similar to the features found by the smoke experiments. These experiments showed a reattachment point at a distance between 0.75 to 1.5 times the height of the chamber at the leeward

side. Incursion of ambient air into the chamber could be observed irregularly at the leeward side of the open top.

Figure 5.1:
Velocity vectors simulated by FLUENT inside a ventilated chamber (flow rate: $1.4 \text{ m}^3\text{s}^{-1}$). The figure represents a vertical plane between the air-inlet holes. The velocity magnitude is represented by the length of the vector. The arrow below the figure represents 1 ms^{-1} .



middle 1 ms^{-1} wall

Table 5.2: Computed and experimental spatial mean velocity magnitudes below 0.7 m in the chamber. KEMA and AUW represent the measured values at KEMA and in the present study, respectively (see Jetten and Stortelder, 1990).

Distance from wall [m]	KEMA [ms^{-1}]	AUW [ms^{-1}]	$k-\epsilon$ FLUENT [ms^{-1}]	ASM FLUENT [ms^{-1}]
0.2	1.20	-	1.15	1.16
0.3	1.10	1.52	1.11	1.11
0.7	0.90	0.75	0.71	0.72
1.1	0.85	0.65	0.56	0.67

Comparison of experimental and computed wind speeds for this case study shows differences between the measured and simulated values of more than 50% of the measured values. There is an underestimation of the measured velocity magnitudes especially in the corners of the chamber.

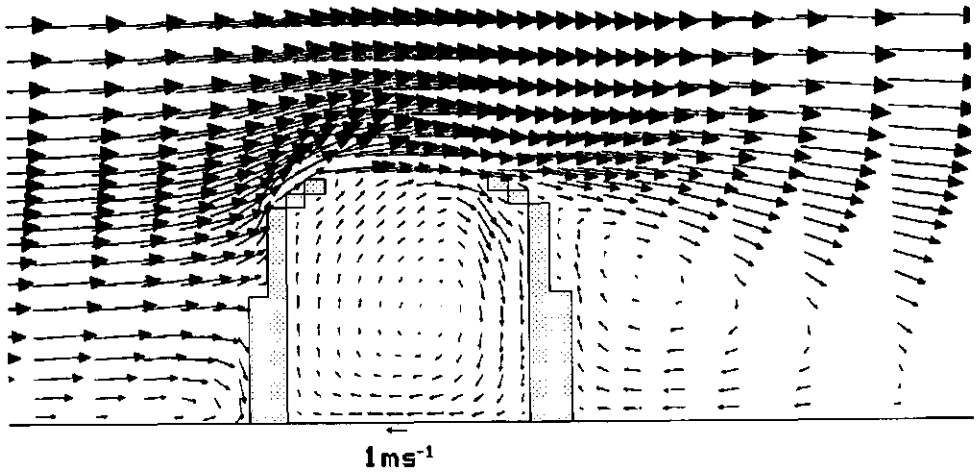


Figure 5.2: Velocity vectors simulated by FLUENT around and inside a non-ventilated chamber. The figure represents a vertical plane through the middle of the chamber. The plane is orientated parallel to the horizontal mean wind velocity. The velocity magnitude is represented by the length of the vector. The arrow below the figure represents 1 ms^{-1} .

The FLUENT simulations for the open top region of a ventilated chamber (flow rate: $1.3 \text{ m}^3\text{s}^{-1}$) show a flow outside the OTC which suppresses the vertical wind velocity at the windward side of the open top resulting in higher vertical velocities at the leeward side (see Fig. 5.3). The computed turbulent kinetic energy at the open top is highest at the windward side. Therefore, the most likely place for incursion is the windward side of the open top.

The empirical relationship found between the mean horizontal wind velocity and the incursion resistance is given by

$$R_i = 63.1 e^{(-0.74U)} \quad (5.1)$$

where

R_i : Incursion resistance [sm^{-1}].

U : Time mean horizontal wind velocity at 2.93 m [ms^{-1}].

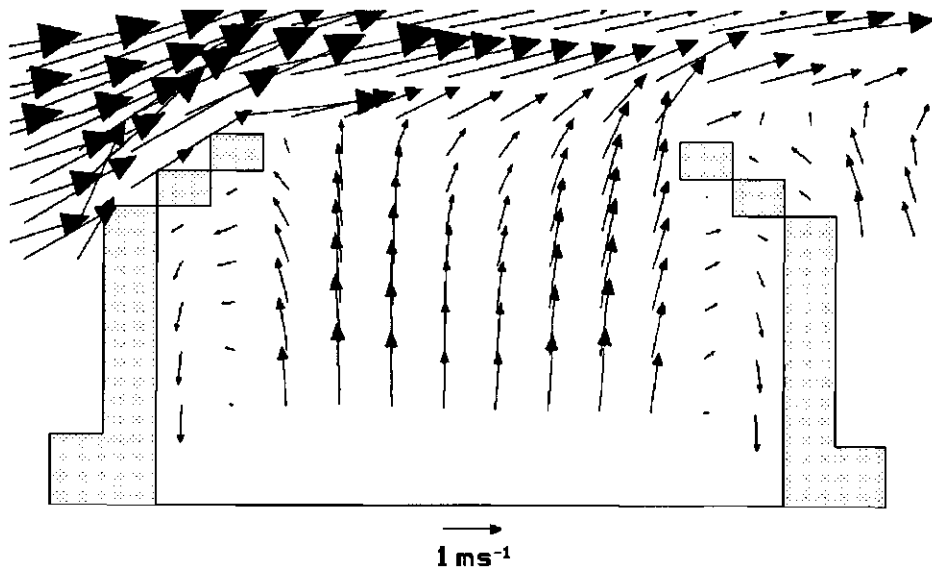


Figure 5.3: Velocity vectors simulated by FLUENT within the open top region of a ventilated chamber (flow rate: $1.3 \text{ m}^3\text{s}^{-1}$). The figure represents a vertical plane through the middle of the chamber. The plane is orientated parallel to the horizontal mean wind velocity. The velocity magnitude is represented by the length of the vector. The arrow below the figure represents 1 ms^{-1} .

Despite the availability of only a limited number of experimental values the shape of the present best fit is similar to the one found by Unsworth (1984). However, this technique did not allow for any influence on the incursion resistance by the fan driven air flow leaving the chamber. Consequently, the empirical relationship found can not be incorporated into the OTC-resistance model directly. Furthermore, FLUENT simulations and experiments have shown that the degree to which the flow field outside the OTC influences the flow field inside a ventilated chamber (flow rate: $1.2\text{-}1.6 \text{ m}^3\text{s}^{-1}$) is limited:

- The FLUENT simulations show scalar concentrations inside a ventilated chamber of less than 0.1 % of the concentrations defined outside the OTC (flow rate: $1.3 \text{ m}^3\text{s}^{-1}$).

- Smoke experiments showed no visual incursion into a ventilated chamber (flow rate: $1.2 \text{ m}^3\text{s}^{-1}$) at ambient mean horizontal wind velocities up to 4 ms^{-1} (height: 10 m).
- The ten minutes mean wind speed measured at heights below 2.4 m inside the chamber showed no relation to mean horizontal velocity (height: 2.93 m; mean wind velocity less than 5 ms^{-1}), vertical wind velocity fluctuations or gradient Richardson number measured above the grass cover outside the OTC.
- The temperature of ambient air is lower than the temperature of the air inside the chamber. Particularly in the open top region temperature fluctuations larger than those in ambient air are expected due to incursion. However, measured turbulent fluctuations showed no incursion effect (see Fig. 5.4).
- The ozone concentrations in the middle of the ventilated chamber (height: 0.9 m) and at the end of the air-supply system showed no clear incursion effect at mean horizontal wind velocities outside the OTC below 5 ms^{-1} (flow rate: $1.2\text{-}1.6 \text{ m}^3\text{s}^{-1}$). At mean horizontal wind velocities above 5 ms^{-1} and a flow rate of $1.2 \text{ m}^3\text{s}^{-1}$ an increase of incursion with mean wind velocity can be seen (see Fig. 5.5).

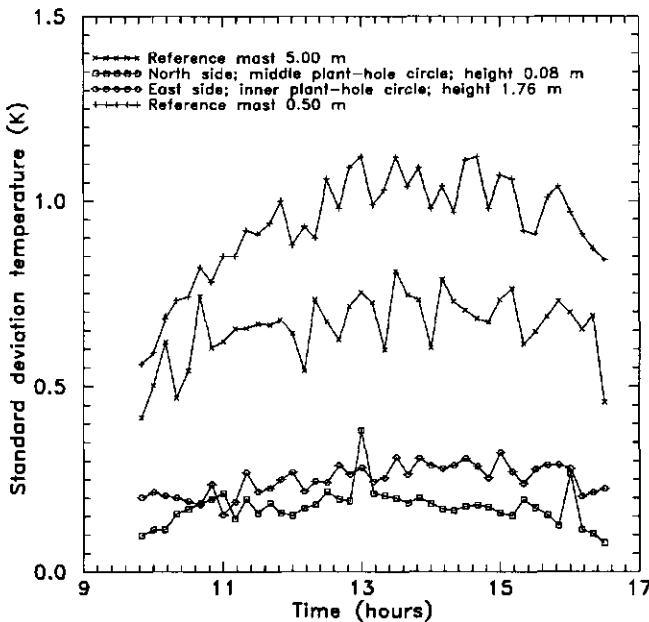


Figure 5.4: Standard deviation temperature measured at two positions within the ventilated chamber and at two heights in the reference mast. Canopy height: 0.38 m; date: 14-07-90; flow rate: $1.6 \text{ m}^3\text{s}^{-1}$.

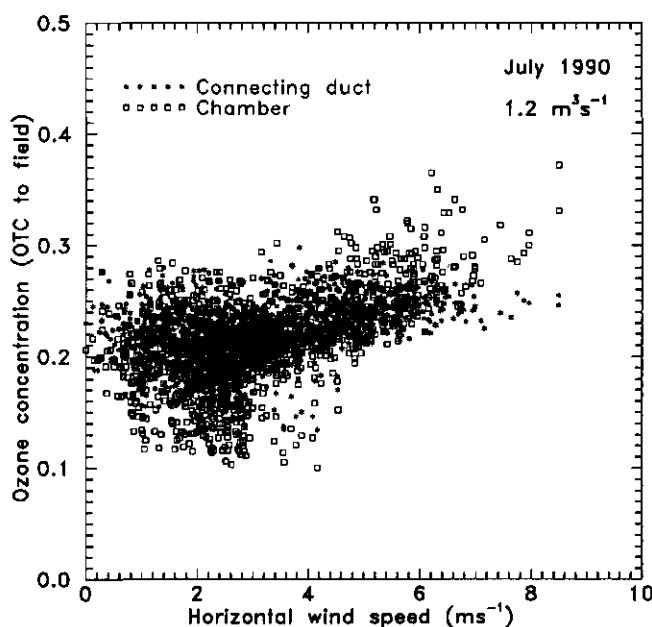


Figure 5.5: Ratio of the measured ozone concentration in the middle of the ventilated chamber (height: 0.9 m) and at the end of the air-supply system to the ozone concentration of ambient air (height: 2.0 m) in relation to the mean horizontal wind velocity outside the OTC (height: 2.93 m) during July, 1990 (flow rate: $1.2 \text{ m}^3\text{s}^{-1}$).

A decrease of the flow rate from $1.3 \text{ m}^3\text{s}^{-1}$ to $1.1 \text{ m}^3\text{s}^{-1}$ does not have a major impact on the calculated flow regime in the open top region. A reduction of the flow rate by approximately 15% resulted into a 1000 times increase of the FLUENT-calculated concentrations inside the chamber but concentrations inside the chamber were still less than 1% of ambient concentrations.

The FLUENT simulations clearly show the importance of the use of a nozzle. In Figure 5.6 and 5.7 the velocity vectors and scalar concentrations for the no-nozzle situation are shown. It is obvious that a nozzle is effective in preventing incursion of ambient air. Scalar concentrations inside the OTC of 1-5% of the ambient concentrations have been computed for the no-nozzle situation. The highest concentrations can be observed at the leeward side of the open top region.

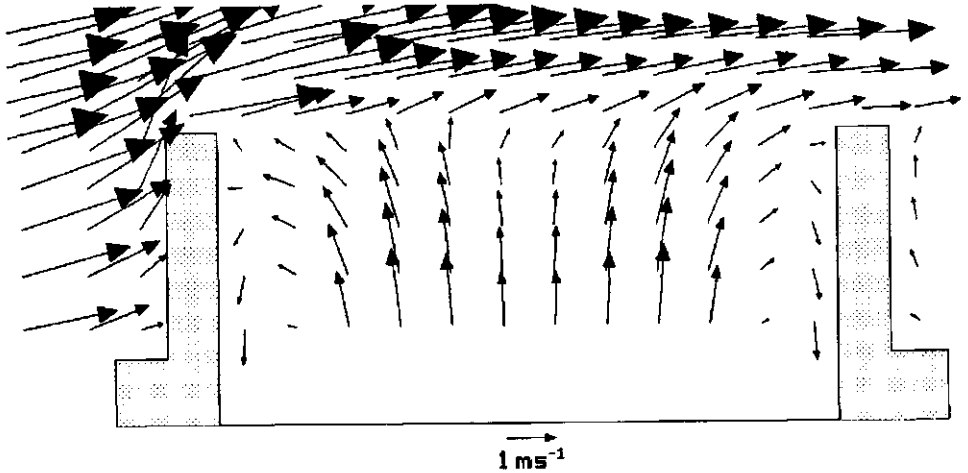


Figure 5.6: Velocity vectors calculated by FLUENT within the open top region of a ventilated chamber without a nozzle (flow rate: $1.3 \text{ m}^3\text{s}^{-1}$). The figure represents a vertical plane through the middle of the chamber. The plane is orientated parallel to the horizontal mean wind velocity. The velocity magnitude is represented by the length of the vector. The arrow below the figure represents 1 ms^{-1} .

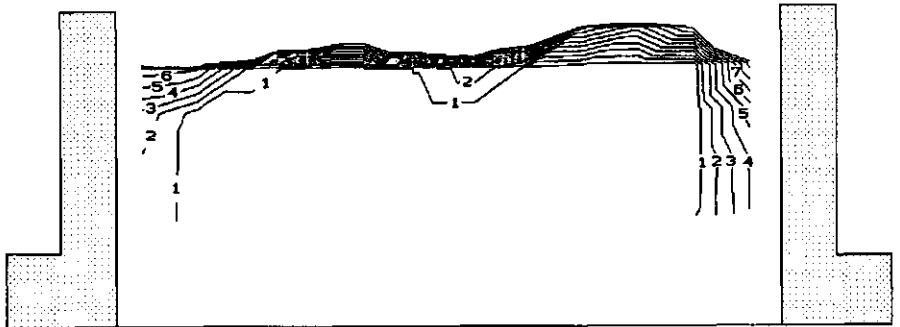


Figure 5.7: Contours of proportional scalar concentration [%] in the open top region of a ventilated chamber without a nozzle (flow rate: $1.3 \text{ m}^3\text{s}^{-1}$). The figure represents a vertical plane through the middle of the chamber. The plane is orientated parallel to the mean wind velocity.

1: 0.3%; 2: 0.9%; 3: 1.5%; 4: 2.1%; 5: 2.7%; 6: 3.3%; 7: 3.9%

Plants grown under OTC conditions are exposed to various magnitudes and directions of wind speed depending on their position with regard to the air-inlet

holes. Plants grown in the middle and the outer plant-hole circle are particularly exposed to an inhomogeneous flow regime where velocity magnitude and turbulent kinetic energy vary from place to place (see Fig. 5.8 and 5.9).

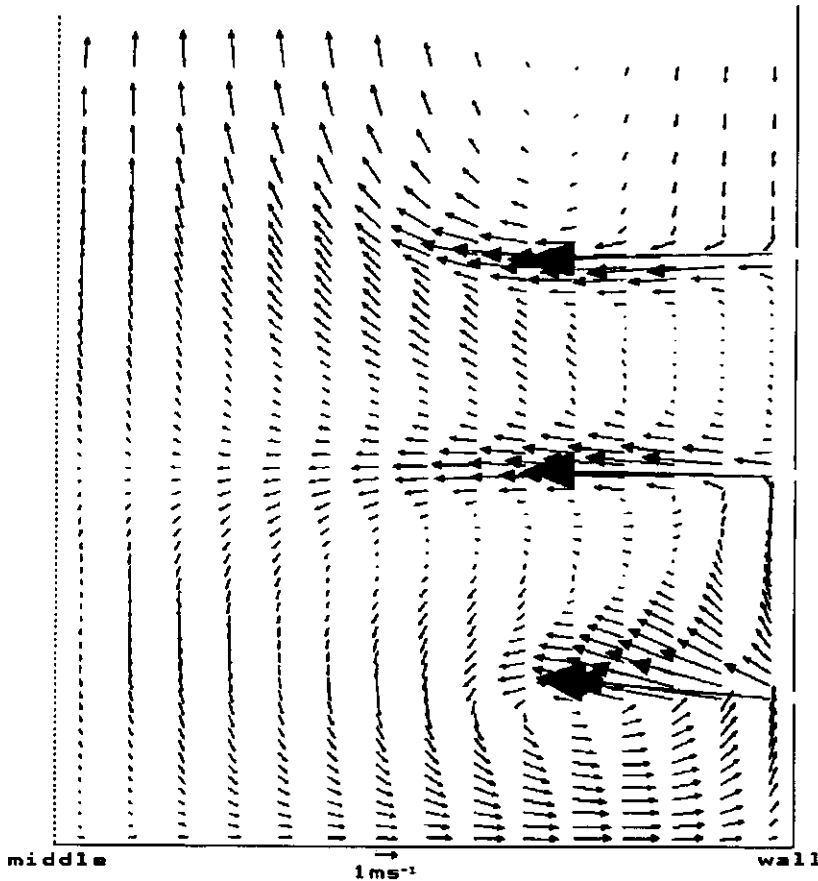


Figure 5.8: Velocity vectors calculated by FLUENT inside the lower part of a ventilated chamber (flow rate: $1.4 \text{ m}^3\text{s}^{-1}$) using the regular $k-\epsilon$ model. The figure represents a vertical plane with three air-inlet holes. The velocity magnitude is represented by the length of the vector. The arrow below the figure represents 1 ms^{-1} .

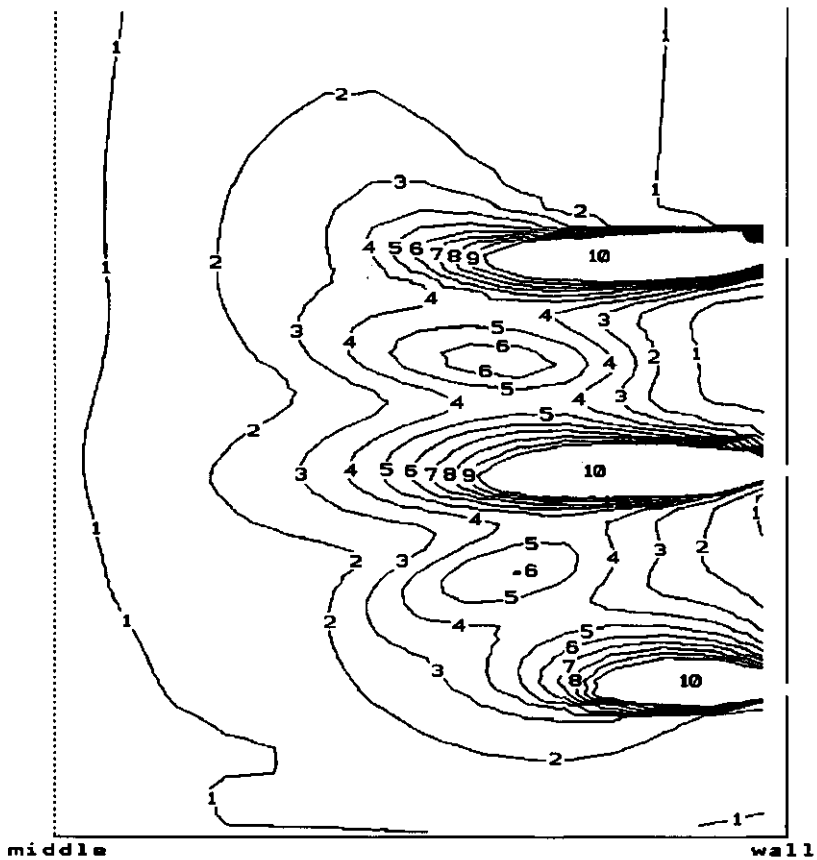


Figure 5.9: Contours of turbulent kinetic energy calculated by FLUENT inside the lower part of a ventilated chamber (flow rate: $1.4 \text{ m}^3\text{s}^{-1}$). The figure represents a vertical plane with three air-inlet holes.

1: $0.05 \text{ m}^2\text{s}^{-2}$; 2: $0.15 \text{ m}^2\text{s}^{-2}$; 3: $0.25 \text{ m}^2\text{s}^{-2}$; 4: $0.35 \text{ m}^2\text{s}^{-2}$; 5: $0.45 \text{ m}^2\text{s}^{-2}$; 6: $0.55 \text{ m}^2\text{s}^{-2}$; 7: $0.65 \text{ m}^2\text{s}^{-2}$; 8: $0.75 \text{ m}^2\text{s}^{-2}$; 9: $0.85 \text{ m}^2\text{s}^{-2}$; 10: $0.95 \text{ m}^2\text{s}^{-2}$.

FLUENT computations show that plants decelerate the flow in the lower part of the OTC due to drag forces and at the same time cause a larger recirculation vortex near the chamber floor (see Fig. 5.10). This results in an increase or decrease of mean velocity magnitude at a particular position near the chamber floor depending on the measurement location, height of the plants and LAI. The computed flow regime for the situation with plants does not show major qualitative changes for the upper part of the chamber.

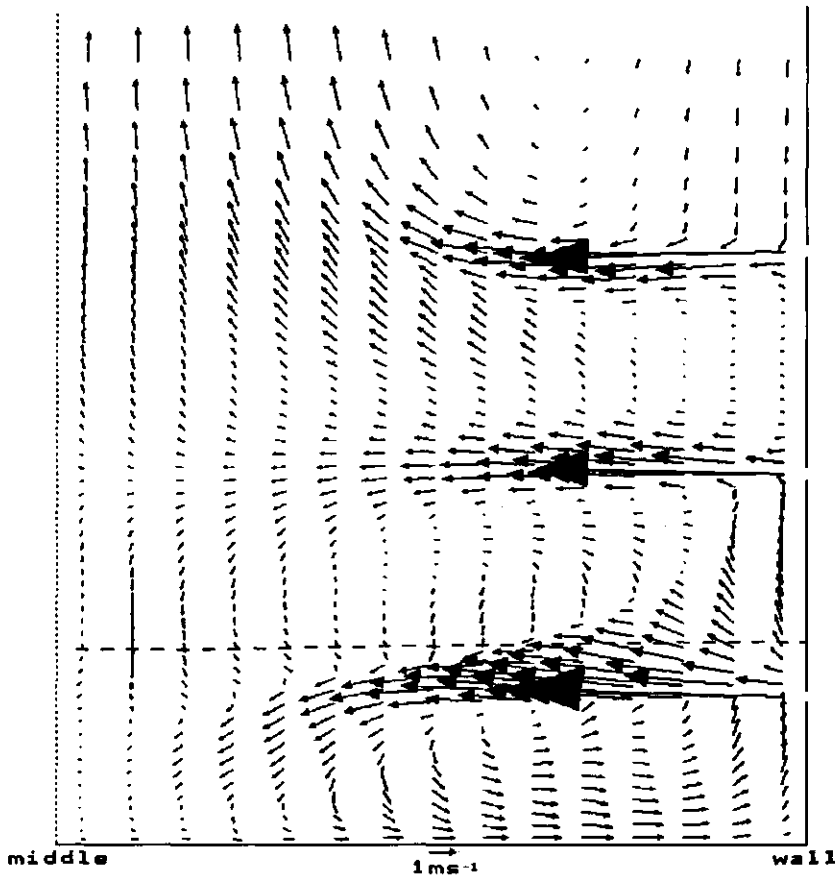


Figure 5.10: Velocity vectors calculated by FLUENT in the lower part of a ventilated chamber (flow rate: $1.4 \text{ m}^3\text{s}^{-1}$) using the regular $k-\epsilon$ model with a porous medium (LAI: 4; plant height: 0.4 m). The figure represents a vertical plane with three air-inlet holes. The velocity magnitude is represented by the length of the vector. The arrow below the figure represents 1 ms^{-1} .

5.2 Radiation

The spatial mean reduction of global radiation intensity at canopy height (just above the broad bean crop: 0.2-0.4 m) inside the chamber compared to field conditions was 15-30%. Shading effects due to the frame were not taken into account. Momentary reductions for a particular location depend on solar height and

azimuth, the measurement location and the weather type. The pattern of the ratio between measured global radiation intensities inside and outside a chamber changes continuously, in time (see Fig 5.11) as well as in space.

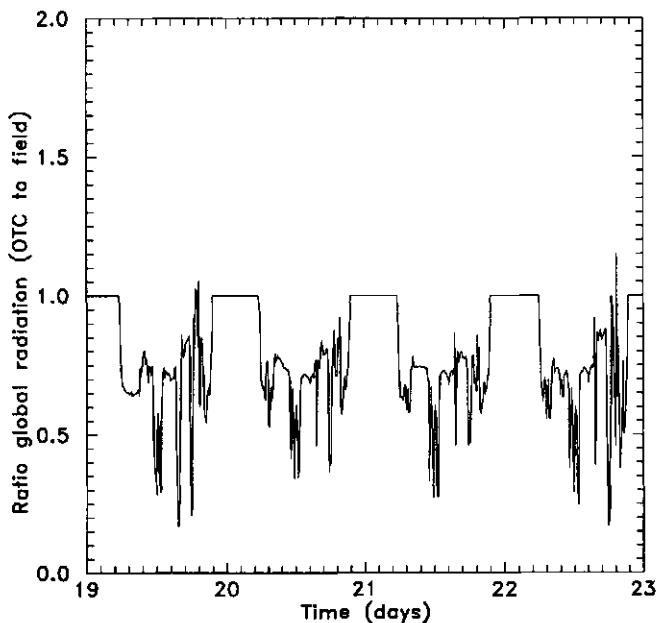


Figure 5.11: Ratio between the measured global radiation intensity inside and outside an OTC. Position: south-east, 0.95 m from wall at canopy height (0.4 m). Period: 19-07-90 to 23-07-90.

Reflection of direct radiation against the inner walls of the chamber causes an increase in global radiation intensities, especially at the north side of the chamber. Furthermore, spots of increased radiation intensity of often less than a few centimetres in diameter have been observed due to the focusing effects of the chamber walls. Shading effects due to the frame can cause a sudden decrease in global radiation intensity. Local reductions of 40-80%, lasting for more than one hour, are common. Neglecting these shading effects the mean reduction of global radiation recorded by a sensor at the south side of the chamber was about 30%. However, at 2.0 m, the reduction decreased to approximately 10% caused mainly by single wall absorption of global radiation. Taking into account an increase in global radiation intensity (canopy height) at the north side of the chamber caused

by single wall absorption and reflection, the spatial time mean reduction of global radiation intensity at canopy height has been estimated to be approximately 20%. Analysis of the model calculations with the OTC-resistance model has shown this has been a reasonable guess.

The incoming long-wave radiation within an OTC is higher than that under field conditions due to a chamber wall effect. Experimental results showed that the incoming long-wave radiation close to the chamber floor can be written (see Eq. 3.93)

$$0.998\sigma T_c^4 \quad (5.2)$$

The short-wave and long-wave radiation balance, in combination with a soil heat flux determine the net radiation balance. The measured soil heat flux was only a small percentage of the net radiation due to a floor-plate effect. The absolute soil heat flux density never exceeded 20 Wm^{-2} . With clear skies the net radiation intensity under OTC conditions during the night is less negative than under field conditions due to incoming long-wave radiation of the chamber walls. The emission of long-wave radiation by the chamber walls is sufficiently high in the early morning and late afternoon to balance a reduction in short-wave radiation. During the day the differences between the measured net radiation inside and outside an OTC increase to a maximum value. However, the percentage of reduction of net radiation inside an OTC is less than the reduction of global radiation. Figure 5.12 shows the ratio between the net radiation intensity under OTC and field conditions for the same period as shown in Figure 5.11. For this position the measured net radiation intensity under OTC conditions was even more than that under field conditions.

5.3 Temperature

The average temperature increase inside an OTC depends greatly on the weather type and the flow rate. At a flow rate of approximately $1.2 \text{ m}^3\text{s}^{-1}$ the spatial mean temperature increase at canopy height compared to ambient air (0.5 m) over May and July 1990 was approximately 2.3 K. At a flow rate of $1.6 \text{ m}^3\text{s}^{-1}$ the spatial mean

temperature increase was 2.1 K. The maximum temperature increase found was 5 K. Observed temperature differences at canopy height over the chamber were within 0.5 K. In cloudy conditions the temperature increase inside the OTC system decreased to 1-2 K. The temperature increase inside the OTC system is caused both by the chamber itself and by the air-supply system (see Fig. 5.13).

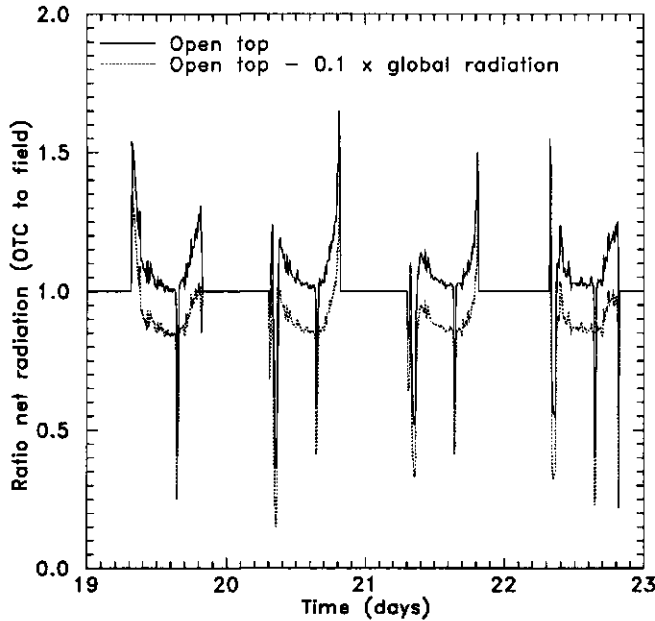


Figure 5.12: Ratio between the measured net radiation intensity inside and outside an OTC. Position: south, between inner and middle plant-hole circle, height 1.94 m. Period: 19-07-90 to 23-07-90.

The figure only represents the data where the net radiation intensity under field conditions was higher than 50 Wm^{-2} . The values were corrected for long-wave radiation through the open top. The dashed line represents the ratio corrected for 10 percent more reduction of global radiation (related to global radiation under field conditions) at canopy height.

During day-time global radiation is the main reason for the temperature increase observed inside the chamber itself (see Fig 5.14). During periods of intermittent cloudiness step changes of temperatures inside the OTC system can be observed. The maximum temperature increase caused by incoming solar radiation was about 3 K. When all the incoming global radiation is used for heating of air inside the chamber, the temperature increase expected at a flow rate of 1.2 and $1.6 \text{ m}^3\text{s}^{-1}$ is

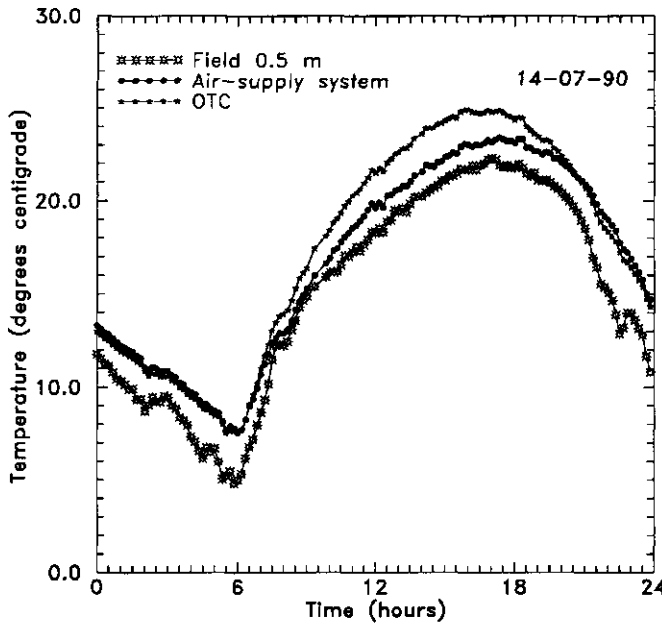


Figure 5.13: Measured temperature inside and outside OTC system. Date: 14-07-91. Flow rate: $1.6 \text{ m}^3\text{s}^{-1}$.

$0.0039 \text{ KW}^1\text{m}^2$ and $0.0029 \text{ KW}^1\text{m}^2$, respectively. The energy balance of the chamber walls and the soil, incursion effects and evaporation of water from the plants cause the temperature increase to deviate from the values mentioned above.

The observed mean temperature increase due to the ventilation system at a flow rate of approximately $1.2 \text{ m}^3\text{s}^{-1}$ and $1.6 \text{ m}^3\text{s}^{-1}$ was 1.42 K ($=2.06 \text{ kW}$) and 1.39 K ($=2.68 \text{ kW}$), respectively (May-July 1990). Evaporation or condensation of water inside the filter unit caused a temperature change of the order of 1 K . However during the day, warming of the air inside the air-supply system by intercepted global radiation almost completely balanced the temperature decrease due to evaporation of water. Tuning of simulated data to experimental results (6220 measurements sampled during May and July 1990) showed that approximately 50% of the energy associated with evaporation or condensation of water vapour caused a temperature change of the air inside the filter unit. Approximately 40% of the energy of intercepted global radiation was transported to the air within the air-supply system. A comparison of the data analysis for the two months did not show

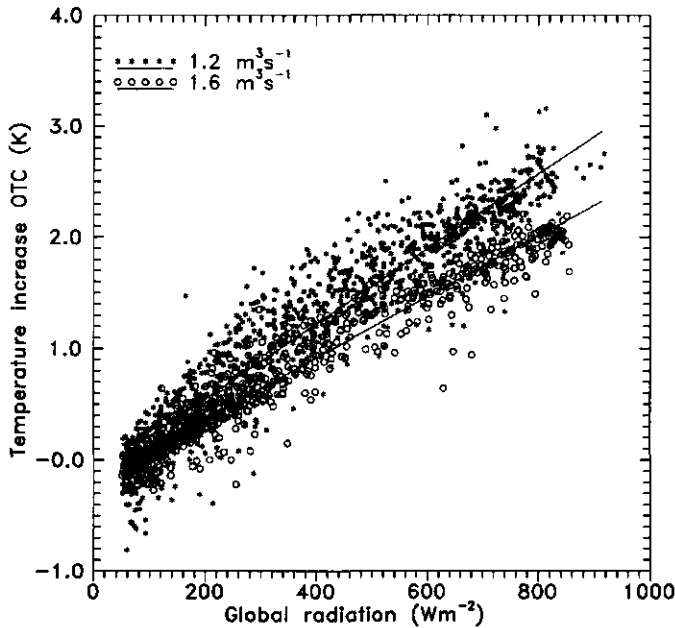


Figure 5.14: Temperature increase inside the KEMA-type chamber (mean of 3 sensors at canopy height) in relation to the global radiation intensity outside the OTC at two flow rates during July, 1990.

Flow rate = 1.2 m³s⁻¹; regression analysis: temperature increase = $-0.128 + 0.00337 \times \text{global radiation}$
 $R^2 = 0.891$

Flow rate = 1.6 m³s⁻¹; regression analysis: temperature increase = $-0.183 + 0.00274 \times \text{global radiation}$
 $R^2 = 0.937$

major differences for the tuning results. The height of the air-inlet of the air-supply system in relation to the temperature profile outside the OTC has to be taken into special consideration. The temperature at 1.50 m under field conditions was found to give the best correlation with the temperature measured at the air-inlet. Consequently, the temperature measured at this height was assumed to give the best estimate of the temperature of the air just before it enters the air-supply system.

During night-time the temperature increase inside the OTC system decreases during cloudy and windy conditions since the temperature change inside the chamber itself is of the order of maximum 0.5 K. However, during clear and calm nights the less negative net radiation inside the chamber, the position of the air-

inlet at 2.0 m and the continuous air flow prevent radiative cooling at the chamber floor. Consequently, the observed maximum temperature increase inside the OTC system compared to ambient air (0.5 m) was about 3 K.

The model results of temperature, specific humidity and ozone concentration are given in Appendix 2. The major part of the temperature difference between observed and measured values was due to model inaccuracies within the air-supply system. The two filter constants (C_{f1} , C_{f2}) and the percentage of intercepted global radiation transported to the air within the air-supply system ($C_{i,asp}$) are empirical constants which have been modelled rather crudely. Furthermore, the constants were derived from data analysis for two months only and fluctuations were smoothed over the whole measurement period.

5.4 Humidity

The difference between spatial mean specific humidity measured inside the chamber at canopy height and ambient air (0.5 m) was usually within 1.0 gkg^{-1} (see Fig. 5.15). The maximum difference observed was about 2.0 gkg^{-1} . The difference decreased during the night. The filters behave as buffers. During the day they usually release water that has been absorbed during the night. Tuning of simulated data to experimental results showed that approximately 2.7% of the difference between the current water content of the filter and the equilibrium water content of the filter is adsorbed or desorbed during a period of 10 minutes (C_{f1} ; Eq. 3.59). At a flow rate of $1.2 \text{ m}^3\text{s}^{-1}$ the spatial mean specific humidity increase at canopy height compared to ambient air (0.5 m) over May and July 1990 was 0.21 gkg^{-1} .

At a flow rate of $1.6 \text{ m}^3\text{s}^{-1}$ the increase was 0.20 gkg^{-1} . Approximately 30-50% of this increase can be explained by the water supply to the plants (0.09 gkg^{-1} at $1.2 \text{ m}^3\text{s}^{-1}$; 0.06 gkg^{-1} at $1.6 \text{ m}^3\text{s}^{-1}$). Since the OTC system is a closed system the remaining part of the increase is related to experimental errors:

- The psychrometers do not measure fluid water droplets. Filters can adsorb this fluid water and release it as water vapour. This water vapour is measured by the psychrometers within the chamber.

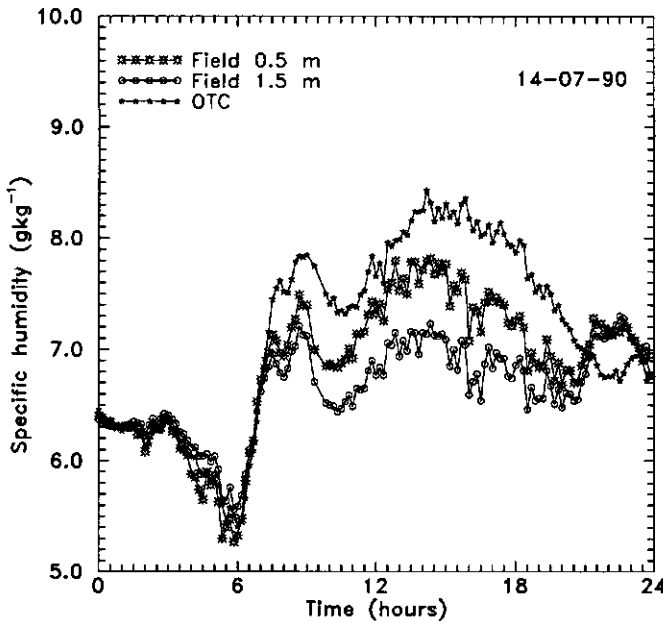


Figure 5.15: Measured specific humidity inside a KEMA-type chamber (mean of 3 sensors at canopy height) and ambient air (height: 0.5/1.5 m). Date: 14-07-90. Flow rate: $1.6 \text{ m}^3\text{s}^{-1}$

- The psychrometers inside the chamber were positioned in a flow field which differs from atmospheric conditions in both direction, velocity magnitude as well as velocity fluctuations. In combination with high radiation loads this can result in systematic errors of approximately 0.1 K between the difference of wet and dry bulb temperature measured by psychrometers located inside a chamber and above grass. Consequently, inaccuracies of measured specific humidity of about 0.1 g kg^{-1} are expected.

The combined effect of humidity and temperature measurements is expressed in the vapour pressure deficit (see Fig. 5.16). At a flow rate of $1.2 \text{ m}^3\text{s}^{-1}$ the spatial mean vapour pressure deficit increase at canopy height compared to ambient air (0.5 m) was 2.7 mbar. At a flow rate of $1.6 \text{ m}^3\text{s}^{-1}$ the increase was 2.2 mbar. Occasionally the specific humidity difference between chamber and ambient air (0.5 m) increased to about 7 mbar.

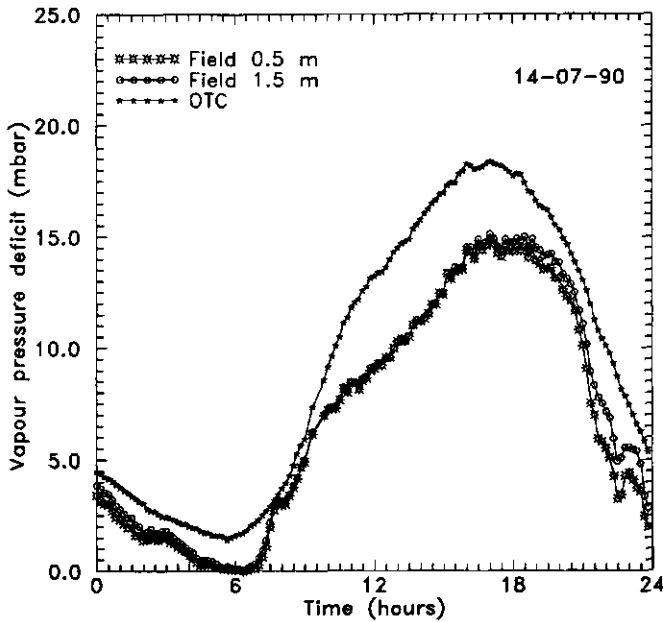


Figure 5.16: Measured vapour pressure deficit inside a KEMA-type chamber (mean of 3 sensors at canopy height) and ambient air (height 0.5/1.5 m). Date: 14-07-90. Flow rate: $1.6 \text{ m}^3\text{s}^{-1}$.

Dew formation was frequently observed, but only on the outside of the chamber walls facing the environment. No dew formation was seen on the leaves of plants grown under OTC conditions during a dew period outside the OTC.

5.5 Ozone

The mean observed ozone concentration inside the chamber was approximately 20% of the concentration observed outside the chamber (concentration higher than $40 \cdot 10^6 \text{ gm}^{-3}$). At a concentration below $20 \cdot 10^6 \text{ gm}^{-3}$ the mean filter efficiency decreased from 80% to 60%. The experiments did not reveal a significant difference between mean filter efficiency at a flow rate of 1.2 and $1.6 \text{ m}^3\text{s}^{-1}$, respectively. Ozone concentration differences over the chamber were less than $4 \cdot \mu\text{gm}^{-3}$.

5.6 Energy and mass exchange between soil-vegetation and atmosphere

The modified soil-vegetation model was used to make an estimate of the energy and mass fluxes between soil-vegetation and the air in the chamber. The original soil-vegetation model was used to make an estimate of these fluxes under field conditions.

A sensitivity analysis (see Table 5.3) has shown that the cumulative daily energy flux per m^2 chamber floor area is most sensitive to variations in canopy configuration (e.g. fraction shielded soil area or LAI). Furthermore, the transmissivity of the walls, the albedo and the boundary layer resistances determining the exchange processes between the air inside the chamber and the chamber floor (upper layer pot soil or floor plate) are important. Emissivity, leaf boundary layer resistance and soil parameters play a limited role.

Changes in parameters which determine the bulk surface resistance have a particular influence on the water and ozone exchange between a canopy and the air inside the chamber. Minimum and maximum stomatal resistance, LAI and fractional conductances affect this bulk surface resistance (see Eq. 3.88). The fractional conductances depend on global radiation intensity, temperature, vapour pressure deficit and soil moisture content. The use of different input parameters under field and OTC conditions, leading to different fractional conductances, results in a change of the ratio of the cumulative daily ozone and water flux density under OTC conditions to those under field conditions.

The vapour pressure deficit inside a chamber appeared to be one of the most important factors in determining the bulk surface resistance difference between field and OTC conditions. An increase of 7 mbar leads to a decrease of fractional conductance of 0.175. An extreme situation, where vapour pressure deficit inside a chamber increases to 25 mbar, results into a reduction of fractional conductance inside the chamber of 32% compared to field conditions. A typical chamber reduction of global radiation intensity of 20% results in a reduction of fractional conductance of 10% at 200 Wm^{-2} to 5% at 900 Wm^{-2} . The maximum temperature increase inside the chamber is approximately 5 K. Consequently, a temperature under field conditions (0.5 m) of 10, 15 and 20 degrees centigrade results into an

increase of fractional conductance inside the chamber compared to that under field conditions of 31%, 14% and 4%, respectively. A temperature under field conditions of 25 degrees centigrade results in a reduction of fractional conductance of 4% inside the chamber. The fractional conductance which represents the effects of soil moisture on stomatal resistance is close to 1 since the soil water content under OTC as well as under field conditions is not a limiting factor (volumetric moisture content higher than field capacity).

Table 5.3: Sensitivity analysis soil-vegetation model

Input parameter	Ratio daily cumulative flux density for:	Ozone $\text{gm}^{-2}(\text{gm}^{-2})^{-1}$	Latent heat $\text{Jm}^{-2}(\text{Jm}^{-2})^{-1}$	Sensible heat $\text{Jm}^{-2}(\text{Jm}^{-2})^{-1}$
Transmissivity chamber walls: 0.70 - 0.90		0.96 - 1.04	0.97 - 1.03	0.83 - 1.18
Emissivity soil-vegetation: 0.93 - 0.97		1.00 - 1.00	1.00 - 1.00	1.00 - 1.00
Albedo: 0.15 - 0.25		1.00 - 1.00	1.01 - 1.00	1.09 - 0.91
Length scale leaf: 0.015 - 0.020 m		1.01 - 1.00	1.00 - 1.00	1.00 - 1.00
Characteristic velocity scale chamber: 0.8 - 1.2 ms^{-1}		1.00 - 1.00	0.95 - 1.04	1.02 - 0.98
Upper layer pots: 0.015 - 0.025 m		1.00 - 1.00	1.00 - 1.00	1.00 - 1.00
Bulk layer pots: 0.15 - 0.19 m		1.00 - 1.00	1.00 - 1.00	1.00 - 1.00
Heat transfer coefficient floor-plate - soil: 2 - 4 $\text{Wm}^{-2}\text{K}^{-1}$		1.00 - 1.00	1.00 - 1.00	1.01 - 1.00
Length scale floor-plate: $\times 0.1 - \times 10$		1.00 - 1.00	0.99 - 1.00	1.03 - 0.93
Length scale pot: $\times 0.5 - \times 2$		1.00 - 1.00	1.18 - 0.87	0.91 - 1.07
LAI: 3 - 4		0.89 - 1.08	0.95 - 1.04	1.03 - 0.98
Fraction soil shielded by vegetation: 0.28 - 0.48		0.74 - 1.26	0.85 - 1.15	1.07 - 0.93
Deviation from daily mean surface temperature of shielded area: -2.0 - +2.0 K		1.00 - 1.00	1.00 - 1.00	1.00 - 1.00
Deviation from daily mean surface temperature below floor-plate: -2.0 - +2.0 K		1.00 - 1.00	1.00 - 1.00	0.99 - 1.01
Maximum stomatal resistance: 1500 - 3000 sm^{-1}		1.05 - 0.95	1.02 - 0.98	0.99 - 1.01
Minimum stomatal resistance: 180 - 220 sm^{-1}		1.09 - 0.92	1.05 - 0.96	0.98 - 1.02

The values given in the table represent the ratio of the cumulative daily ozone, latent heat and sensible heat flux density to the flux density found for a standard setting of parameters (see Table 3.11 and A2.1). Air temperature and specific humidity inside the chamber were determined using linear interpolation between spatial mean values at canopy height which were measured every hour. The ozone flux was calculated using the ozone concentration measured under field conditions. Date: 14-07-90.

For most case studies the simulated mean ozone conductance under field conditions was less than the mean ozone conductance under OTC conditions. The ozone conductances were computed using the same plant configuration under field as well as OTC conditions (LAI, height canopy, fraction vegetation). The bulk aerodynamic resistance term computed under field conditions is the main reason for the higher conductance found under OTC conditions. The effect of fluctuating mean wind speed on ozone conductance under field conditions is shown in Figure 5.17. A temporary decrease of ten minutes mean horizontal wind velocity from 2.6 ms^{-1} to 1.7 ms^{-1} at 16.00 hours can be clearly seen within the figure. During the afternoon the differences between field and OTC conductance decrease due to an increase of vapour pressure deficit inside the chamber while simultaneously the difference between the temperature under field conditions and the optimum temperature value decreases.

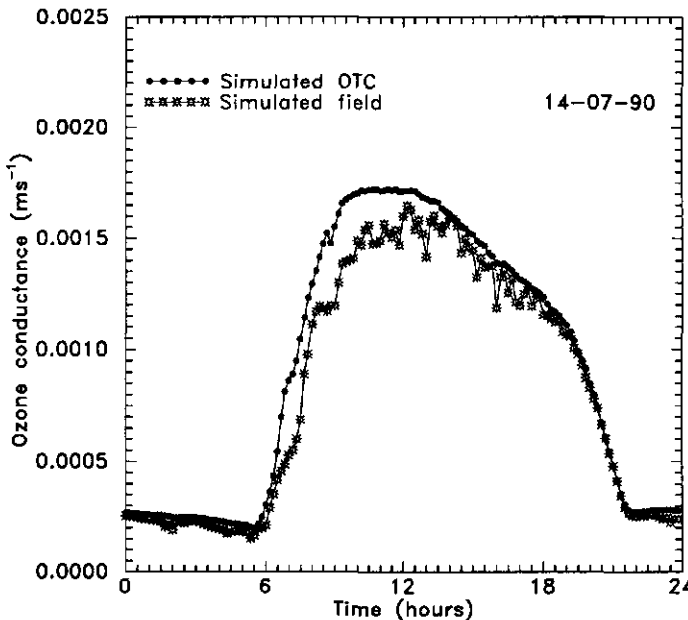


Figure 5.17: Simulated ozone conductance under field and under OTC conditions.

The simulated ratios of cumulative daily ozone flux density for plants grown under non-filtered OTC conditions to plants grown under field conditions for May and July 1990 are given in Figure 5.18 and 5.19. The ozone concentration observed under

field conditions has been used to calculate the ozone exposure under field as well as OTC conditions. The temperature, specific humidity and ozone concentration of the air have been determined using linear interpolation between data which were measured every hour. The mean calculated ratios of ozone uptake inside and outside an OTC for May and July were 1.13 and 1.03, respectively. The ratio difference can be completely explained by weather type differences between these two months. The highest ratio found was 1.29 (18-05-90). This particular day was characterized by an overcast sky and horizontal mean wind velocities at 3 m below 2.5 ms^{-1} . Under cloudy conditions the temperature and vapour pressure deficit increase inside an OTC are relatively small and have a limited effect on fractional conductance while at these wind velocities the bulk aerodynamic resistance is a limiting factor for the ozone transport under field conditions. The lowest ratio found was 0.91 (20-07-90). During this particular day a vapour pressure deficit increase inside the chamber of about 7 mbar was observed. This resulted in a decrease of the fractional conductance representing the effect of vapour pressure deficit. This decrease was large enough to compensate for the bulk aerodynamic resistance term under field conditions.

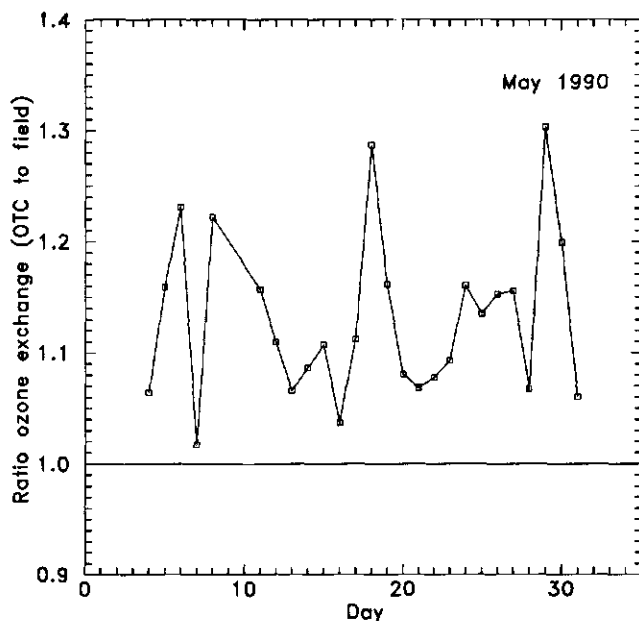


Figure 5.18: Simulated ratio of daily cumulative ozone flux per m^2 floor area under OTC conditions to the flux under field conditions.

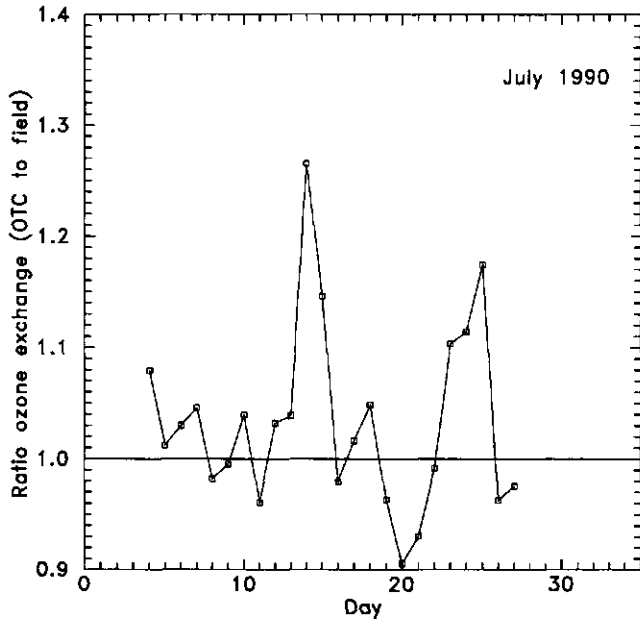


Figure 5.19: Simulated ratio of daily cumulative ozone flux per m^2 floor area under OTC conditions to the flux under field conditions.

CHAPTER 6 FINAL REMARKS AND CONCLUSIONS

6.1 Introduction

The main aim of the OTC design was to create an environment better resembling field conditions than the environment found in closed systems while at the same time controlling air quality. It is obvious - as was pointed out in the Chapter 2 - that the use of OTC's introduces a degree of artificiality which makes it impossible to duplicate field conditions exactly. In this study a physical description of the exchange processes of mass, momentum and energy inside the chamber in relation to field conditions has been given using experimental observations and two models, the FLUENT model and the OTC-resistance model. Both models can easily be applied to other Heagle-type OTC systems but the various model parameters have to be determined experimentally. The literature, experiments and model calculations have been used to determine to what extent the OTC microclimate differs from field conditions. The models have been used as a tool to study the effect of OTC conditions on ozone uptake by plants. Furthermore, they give better insight into the way the OTC configuration has to be changed in order to achieve a microclimate inside the chamber that more closely resembles field conditions. We do not expect that the use of other models or more detailed models will change the results drastically but it can lead to small quantitative improvements.

6.2 Model computations

The FLUENT model has been used to simulate the turbulent exchange processes inside a KEMA-type OTC for thermally neutral conditions. We showed that for a qualitative analysis of the flow regime inside a KEMA-type OTC the regular $k-\epsilon$ model can be used. The flow in the lower part of the ventilated OTC and in the open top region shows many flow phenomena with a length scale of a few centimetres. The spatial resolution of the model, however, is not sufficient to reveal flow features of the order of a few centimetres. In addition, the flow inside a

ventilated chamber has been computed for a circular symmetric flow. In reality this symmetric flow regime will be disturbed since:

- the air-inlet holes are not divided exactly circular symmetric over the chamber walls,
- there is some influence from the chamber door and netting,
- the mean inlet velocities are not exactly perpendicular to the chamber wall,
- the effect of the flow field outside the chamber on the flow field inside the chamber has not been taken into account.

Since incursion of environmental air into the chamber is limited the last effect is considered to be of minor importance. To take all these features into account one has to extend the size of the grid configuration to the whole of the flow field inside and around an OTC without increasing the size of the various grid cells. Testing the effect of the use of a grid with a higher spatial resolution or a larger computational domain, however, is limited by computer memory.

The OTC-resistance model has been used as a qualitative tool to study the exchange processes inside the OTC system. Since a detailed analysis of the whole OTC system is not feasible, the model only computes bulk exchange processes and a quantitative verification is restricted to spatial mean values measured within the OTC system. The model does not take into account the individual plants and plant layers and the parameterization of fractional conductances is rather simple. Use of more detailed multi-layer models (i.e. Goudriaan, 1977) will yield more information about differences between vertical plants layers assuming horizontal homogeneity. However, due to the complicated flow regime within a ventilated chamber, global radiation differences at canopy height and a not-completely-closed canopy a detailed analysis is difficult or even unfeasible. Therefore, we conclude that improvement of the parameterization schemes used is the most logical way of improving the OTC-resistance model. Special attention should be paid to the exchange processes inside the air-supply system and the exchange processes between the chamber floor and the air inside the chamber which are modelled rather crudely. The parameters which determine these exchange processes are largely unknown and have to be computed via empirical methods. Detailed experiments are needed to see if the exchange processes have been modelled in

the right way and how the parameterization schemes can be improved.

6.3 The KEMA-type OTC system

Soil conditions and agronomic procedures

One of the main objectives of the OTC use is to keep OTC conditions as close as possible to field conditions. The use of OTC's under real field soil conditions including standard agronomic procedures for planting dates, plant densities, fertilizer rates and use of herbicides and pesticides is certainly the most realistic one, but it provides practical difficulties since natural variation in soil structure or soil chemistry can modify plant responses to air pollution, thus making more chamber duplicates necessary.

The KEMA-type OTC was not situated in a real field situation but in an experimental area. The use of pots with a known soil and greenhouse sown and grown plants reduces the degrees of freedom and thus the variability in an experimental set-up because a preselection of the plants can be made before the fumigation experiments start. Furthermore, the composition of the soil is known and uniform over the OTC's and between OTC's.

Within the KEMA-type OTC a wooden floor-plate covers the soil between the plants. This plate is primarily used for practical reasons. However, it changes the energy balance near the soil. The latent heat flux above the bottom plate is negligible since the floor-plate itself does not transport water and most of the energy absorbed results in a temperature increase of the air inside the chamber.

In order to keep OTC conditions as close as possible to field conditions, removal of the floor-plate and the use of well-defined real field plot locations is necessary. Here we meet an important limitation of the KEMA-type OTC system. The chamber itself is transportable but the construction of the air-supply system is too rigid to transport it easily.

Flow inside chamber

Plants grown inside the chamber are exposed to an inhomogeneous flow where velocity magnitude and turbulent kinetic energy varies from place to place. Consequently, plants or part of plants will start fluttering. Particularly plants situated

in the outer plant-hole circle are exposed to a flow regime with local velocity differences of the order of 1 ms^{-1} over a few centimetres. It is recommended that biological observations should be restricted to the middle and inner plant-hole circles in order to avoid flow field effects on plant growth and development

The differences in scalar uptake by plants grown under OTC conditions are partly caused by differences of the leaf boundary layer resistance between plants or part of plants. The leaf boundary layer resistance to water vapour exchange has been determined using Eqs. (3.96) and (3.103) and varies, depending on mean wind speed, from 17 (2.0 ms^{-1}) to 53 sm^{-1} (0.2 ms^{-1}). The characteristic length scale is taken as 0.02 m. Turbulent intensity and leaf fluttering can influence the leaf boundary layer resistance but are not taken into account. The minimum stomatal resistance for *Vicia faba* (Aben, 1990) is of the order of $150\text{-}200 \text{ sm}^{-1}$. Therefore, maximum differences of water exchange between leaves and their environment due to differences of leaf boundary layer resistance inside a ventilated chamber are estimated to be of the order of 25%.

The time mean wind speed at a particular location in the lower half of the chamber is rather constant during the day. This situation differs from field conditions where the time mean wind speed changes continuously in time. Furthermore, individual leaves within a plant canopy exist in an unsteady environment where large eddies from above the canopy penetrate into the canopy intermittently. During the renewal of canopy air by these large eddies, turbulent mixing within the canopy occurs on a much larger scale than in the relatively quiet periods between two penetrations. Finnigan and Raupach (1987) showed that approximately half of a flux can be transported in 10 percent of the time. The largest part of the momentum transport to a canopy is not due to the local properties of the flow but is caused by gusts of air with higher wind speed, which originate in the boundary layer above the canopy and penetrate into the canopy. During thermally near-neutral conditions heat and momentum transport within a canopy are closely related to each other. The sweeps that displace the warm air in the canopy are the downward moving air masses that dominate the momentum transport. In thermally unstable conditions this coupling will diminish since heat exchange becomes more ejection dominated.

Plants grown under OTC conditions are exposed to a non-natural flow which does

not show large-scale eddies which penetrate the canopy intermittently. The typical chamber flow pattern cannot be changed without removing the whole OTC-configuration. However, one can increase the homogeneity of the flow regime inside the lower part of the chamber by reducing the effect of the air-inlet jets via

- a decrease of the flow rate,
- an increase of the inlet area without changing the width of an air-inlet hole,
- a decrease of the width of an air-inlet hole without changing the total inlet area.

A reduction of the width of the air-inlet holes without changing the total inlet area seems the most effective way. According to Eq. (3.26) the velocity at a particular distance perpendicular to the air-inlet hole is linearly dependent on the width of the air-inlet hole itself. Consequently, a reduction of the width of an air-inlet hole to 50% of its original value will result in an estimated decrease of 50% of the velocity magnitude perpendicular to the air-inlet holes. A decrease of the flow rate is not feasible since this would result in a temperature increase inside the chamber. An increase of the inlet area would result in a decrease of the mean wind speed but it is not certain whether the mean air-inlet velocity within an air-inlet hole will be constant over an OTC.

The ventilation rate applied for a KEMA-type OTC in combination with the open top nozzle is very effective in preventing incursion. At ambient wind speeds at open top height lower than 5 ms^{-1} no incursion was observed. Consequently, air flow and turbulence inside a chamber are only influenced in a minor way by air flow and turbulence outside the OTC. The use of a nozzle results in a temperature increase inside the chamber due to decreased incursion. Since two of the main objectives of the OTC design are

- excluding and controlling air gaseous pollutant levels completely,
- creating a homogeneous atmosphere inside the chamber (temperature, specific humidity, ozone concentration),

the use of a nozzle is necessary.

Radiation

In the lower part of the chamber a spatial mean reduction of global radiation

intensity of about 20% of field conditions is observed. Reflection of radiation by the chamber walls, shading effects of the frame and the partitioning of global radiation into a direct and a diffuse component cause space differences of radiation intensities over the chamber. Spots of increased radiation intensity of often less than a few centimetres in diameter have been observed due to focusing effects of the chamber walls. This effect can be largely prevented by the use of a more angular chamber wall configuration. The netting stretched against the lower part of the northern wall of the chamber is primarily meant to reduce reflection of light. However, there is still reflection of light by the eastern and western walls, the upper part of the northern wall and the nozzle. A temporary increase of radiation intensity at particular positions inside the chamber during the early morning and late afternoon can play an important role because, at that time, radiation intensity is a limiting factor for plant photosynthesis. Since the KEMA-type OTC is constructed in an experimental field without plants around it global radiation penetrates into the canopy from the side. This is certainly not a real field situation. We conclude that, taking account of reflectance and the side effects, the middle section of the chamber is the best section to execute biological observations. Shading effects of the frame cause reductions of global radiation inside the chamber of 40-80% of ambient levels which can last for more than one hour. Therefore, reducing the shading effects of the frame should have a high priority. Particularly the size and position of the frame elements and special facilities like entrances have to be taken into consideration.

The long-wave radiation emitted and the short-wave radiation absorbed by the chamber walls are the main reasons for the differences between net radiation flux densities observed under OTC and under field conditions. Under clear night conditions the less negative net radiation compared to field conditions and the continuous air flow prevent radiative cooling inside the OTC. Within the chamber it is impossible to obtain radiative cooling without removing the wall and switching off the fan. In air pollutant studies ambient ozone concentrations during the night are usually low. To achieve dew formation and ground frost inside a chamber it is recommended that the wall material will be removed during the night hence exposing plants to real field conditions. This is laborious work and can only be done for a limited amount of OTC's and with a less rigid type of wall material than

Lexan.

Temperature

The temperature increase inside the OTC is caused both by the air-supply system and by the chamber itself.

The temperature increase due to the chamber itself is largely caused by the level of global radiation. It strongly depends on the flow rate and the effective floor area of the chamber and can reach more than 3 K at a flow rate of $1.4 \text{ m}^3\text{s}^{-1}$. There are not many ways to prevent this temperature increase as it is inherent in the use of OTC's. The use of an air cooling device is the only way to reduce the temperature increase inside the chamber to 1 K or less. Doing so will increase the costs of the OTC use and change the configuration more and more into a kind of laboratory chamber.

The air-supply system causes a maximum temperature increase inside the KEMA-type OTC of approximately 2.5 K (flow rate: $1.4 \text{ m}^3\text{s}^{-1}$). The most obvious advantage of the KEMA-type air-supply system is the possibility it gives of allowing the measurement and control of the air flow to the OTC in an accurate way. However, the construction of a valve at the beginning of the air connecting duct interferes with the air flow measurements. Removal of the valve and the use of more honeycomb air straightening sections is necessary in order to improve the quality of the flow rate measurements. If all OTC configurations used are exactly the same the flow rate differences between the OTC's will be small. However, the removal of a charcoal filter can result into a change of flow rate. The resulting microclimate inside an OTC depends on the flow rate. A decrease of the flow rate by 10% at $1 \text{ m}^3\text{s}^{-1}$ can lead to an extra temperature increase within the chamber, due to global radiation, of the order of 0.5 K.

The fan inside the OTC system causes a temperature increase of approximately 1.4 K. The fan needs a power input of a few kW. The major part of the temperature increase caused by the ventilation system is due to internal heat production. The installation of the power unit of the fan outside the air-supply system (inside a separated ventilated compartment) will lower the mean temperature increase.

The filters adsorb air pollutants but at the same time adsorption or desorption of water vapour occurs. Usually the filters during the day will release water that has been adsorbed during the night. A temperature increase or decrease of the passing air of the order of 1 K is related to this. A balance has to be found between extra filter efficiency gained by using more filter material and adsorption or desorption of water by the filters. Consequently, the removal of the filters results in microclimate differences between filtered and non-filtered OTC's.

The temperature increase caused by radiation absorption by the walls of the air-supply system during the day is of the same order as the temperature decrease due to evaporation processes. We expect that the construction of a radiation shield above and beside the air-supply system and the use of white paint will reduce the absorption of radiation by the walls of the air-supply system by at least 50%.

The height of the input of the air-supply system will not cause problems during cloudy and windy conditions. However, during calm periods with radiative cooling, temperature gradients of the order of 5 K can occur between the earth's surface and a height of 1.5 m. Consequently, temperature differences of the same order can be observed between the air just above the earth's surface and the air inside the chamber. These temperature differences can be reduced by a few degrees centigrade by lowering the height of the input.

For use in field conditions we recommend small and flexible air-supply systems as used by Heagle et al. (1988) or Sanders et al. (1991). Compared to these air-supply systems the system used by KEMA is rather large and expensive. It is necessary to extend the connecting duct with some honeycomb air straightening sections in combination with a multipoint pitot tube meter or another multipoint air speed measuring device in order to determine the flow rate exactly.

Vapour pressure deficit

The differences between the mean specific humidities measured at canopy height (0.2-0.4 m) inside a chamber and ambient air (height: 0.5 m) were usually within 1.0 gkg^{-1} . Since the mean temperature increase at canopy height inside the chamber was of the order of 2 K the mean vapour pressure deficit at canopy height inside the KEMA-type OTC was 2-3 mbar higher than the one observed under ambient conditions (0.5 m). In the OTC-resistance model an increase of vapour

pressure deficit affects evapotranspiration directly (increase) and indirectly (decrease via an effect on stomatal aperture). Since a time mean temperature increase inside the chamber of the order of 1 K is inherent in the OTC use, a minimum mean vapour pressure deficit increase of the order of 1 mbar cannot be prevented.

Ozone exchange

The present study deals with the physical exchange processes within an OTC. The ultimate aim of the KEMA subproject is to compare the exchange coefficients under field and OTC conditions. These coefficients can be used to estimate the differences in pollutant uptake by plants inside and outside OTC's. Mean ratios for the daily cumulative ozone flux density under OTC conditions to the one under field conditions for May and July 1990 of 1.13 and 1.03, respectively, have been computed by the OTC-resistance model. The plant configuration (fraction vegetation, LAI, plant heights) under field conditions has been taken as being equal to the configuration under OTC conditions. Furthermore, the ozone concentrations observed under field conditions have been used to compute the ozone exposure under field as well as OTC conditions. The computed ratios for the daily cumulative ozone flux density under OTC conditions to the one under field conditions fluctuate between 0.91 and 1.29. The ozone damage to plants depends on the ozone uptake. Therefore, we conclude that the use of a correction factor within the exposure-response curves is necessary in order to calculate uptake-response curves. The computed ratio differences are largely due to a bulk aerodynamic resistance term and the fractional stomatal conductances set by the PAR-intensity, the temperature and the vapour pressure deficit of the environmental air. The decrease of the global radiation intensity and the increase of the vapour pressure deficit under OTC conditions decrease the ratio OTC ozone uptake to field ozone uptake. The bulk aerodynamic resistance calculated under field conditions, which is set by mean wind speed, thermal stability and canopy configuration, increases this ratio.

6.4 Conclusions

It is remarkable that an extensive study of the physical aspects of an open top chamber has been conducted in this stage of the open top chamber research. It should have been done 20 years ago as the results found within this study change the interpretation of the exposure-response curves found in various studies.

This study describes only one OTC type. Within Europe various types of open top chambers have been used during the last decade. We conclude that:

- *There is a need for coordination of the research projects going on (CO₂ as well as air pollution fumigation experiments) in order to achieve a degree of compatibility between the various research groups. Furthermore, it is important to start a detailed physical characterization of the OTC's which have been used as soon as possible.*

Despite the uncertainties found, OTC's are still widely used, although attention nowadays is focused on damage to forests and the effects of CO₂ enrichment (Drake et al., 1989). A possible alternative to the OTC experiments is the use of open-air fumigation experiments.

Open-air fumigation experiments do use natural environmental and soil conditions. However, the high cost limits the number of duplicates and they do not allow for a control treatment (exposure to less than ambient concentrations). Furthermore, concentration fields within the canopy will be artificial and can deviate from natural field conditions due to atmospheric turbulence. OTC's on the other hand allow treatment duplicates against moderate costs and an adequate control of concentrations of air pollutants or CO₂.

We conclude that:

- *The OTC-configuration clearly influences the physical exchange processes inside the chamber. The flow inside the chamber is a non-natural one where the influence of the free atmosphere is restricted to the setting of the inlet temperature, specific humidity, air pollutant concentrations and radiation levels, but all of them are changed by the OTC system itself.*

- *The KEMA-type OTC-configuration can be changed to some extent in order to achieve a microclimate inside the chamber more closely resembling field conditions. Typical OTC effects on the chamber microclimate such as
 - filter effects,
 - a 10-20% reduction of global and PAR radiation load,
 - an increase of long-wave radiation intensity
 - a mean temperature increase of the order of 1 K,
 - a mean vapour pressure deficit increase of the order of 1 mbar,cannot be prevented without creating a kind of laboratory chamber. Furthermore, the typical chamber flow pattern cannot be changed without removing the whole OTC-configuration.*

- *Microclimate differences over the chamber occur (i.e. in radiation intensity, in wind velocity). It is recommended that biological observations should be executed in the middle section of the chamber since here the differences are restricted.*

In literature the results of pollutant fumigation experiments are often expressed as exposure-response relationships but a rather large variation between experimental results was found. In this thesis it is shown that the ratio ozone exposure to ozone uptake by plants inside an OTC varies depending on the weather. The quality of the experimental results can be increased by employing a correction scheme depending on meteorological conditions and their relations to scalar uptake. Doing so would express the ozone transport to a plant in terms of uptake-response curves while exposure-response curves were used before. In that case relations between uptake of pollutants by stomata and environmental conditions should be known exactly for various plant species. In CO₂ enrichment experiments the situation becomes even more complicated as it is known that CO₂ concentrations affect the stomatal resistance directly (Morison, 1987).

The present study deals with meteorological conditions directly affecting the uptake of a gaseous pollutant within an OTC. The uptake of gaseous pollutants is a complicated process depending on properties of the atmosphere, soil and plants. Within the OTC-resistance model it is assumed that plants grown under OTC

conditions have the same properties as plants grown under field conditions. Consequently, the model does not take into account the effects of a changed microclimate on biochemical processes inside a plant. Furthermore, the environmental conditions within an OTC can indirectly modify the effects of gaseous pollutants on a plant. They can change the pollutant sensitivity of the physiological processes in a plant or affect the detoxification rate.

Sanders et al. (1991) found for field-sown *Vicia faba* (cv. Tirol) chamber effects on growth and development of plants. Plant development progressed more rapidly inside a chamber in response to the faster accumulation of thermal time (degree days). The observed increase of leaf area could partially be explained by an increase in temperature and a reduction of PAR radiation within the chamber. The chamber-grown plants had a higher proportion of their weight allocated to assimilation than the plants grown under field conditions. The stomatal density (number of stomata per m² leaf area) at the same time decreased, probably due to a greater cell expansion as a response to partial shading.

The present study ends at the interface between plants and their environment, the leaf boundary layer and the stomata. We confirm the view of Heagle et al. (1988) and Sanders et al. (1991) that there is a need for detailed experiments specifically designed to determine whether the chamber itself influences the crop responses to pollutants. Finally we conclude that:

- *Experiments with OTC's where plants are exposed to various levels of gaseous air pollutant or CO₂ concentrations in combination with one or more environmental stresses can be used only to determine the effects of these components under OTC conditions. The OTC-experiments do give an impression of the qualitative effects under fluctuating field conditions. Furthermore, they can be used to study the mechanisms by which this effect is caused. However, the exposure-response curves derived under OTC conditions cannot be used directly to estimate a quantitative effect under field conditions.*
- *An extrapolation of the exposure-response curves derived under OTC conditions to field conditions taking into account the differences in microclimate between OTC and field conditions can improve the quality of the experimental results. The*

results are of limited value only if they are used without being combined with a crop growth model which incorporates the effects of the changed microclimate inside an OTC on plant physiological processes.

- *Open-air fumigation experiments are the only way to determine the effect of increased gaseous air pollutants or CO₂ concentrations under real field conditions. However, unrealistic concentration fields within a canopy can occur. When using OTC's a comparison between plant growth and development inside fumigated OTC's and open-air fumigation experiments at various fumigation loads is necessary in order to estimate an effect under field conditions.*

APPENDIX 1 SENSORS USED

name	parameter	method	accuracy	response time/length
thermocouple (Van Asselt et al., 1989)	temperature	manganin-constantan thermocouple	<0.2 K, depending on wind speed	time constant <0.1 s depending on wind-speed
Stigter psychrometer (Stigter et al., 1976)	dry - wet bulb temperature	temperature difference between 2 constantan-manganin thermocouples skewly wounded with a wick	<0.1 K, depending on wind speed	
LUW-psychrometer (Harrison, 1963)	dry - wet bulb temperature	ventilated (> 4 ms ⁻¹) Pt-100 resistance elements	0.02 K per Pt-100	
heat bulb anemometer (Fritschen and Shaw, 1961)	wind speed	temperature difference between 2 copper-constantan thermocouples in 2 Woodsmetal bulbs, 1 bulb is heated by a constant current	<0.1 ms ⁻¹ , depending on wind speed	order of seconds
cup anemometer (Smedman et al., 1973)	horizontal wind speed	cup-rotation measured with photochopper system	3% (within 1-15 ms ⁻¹)	first order response length 0.9 m
sonic anemometer thermometer Kaijo Denki type DAT-310 and PAT-112-1 (Van Boxel, 1986)	velocity, temperature fluctuations	the time needed by a sound pulse to travel the distance between a transmitter and receiver, dependent on path-length, sound speed and wind velocity	1%	10 Hz sample frequency
pyrgeometer Eppley (Fritschen and Gay, 1979)	long-wave radiation (>5 μ m)	temperature difference between black painted plate with a coated silicon hemisphere and house, measured by thermopile, compensation for detector temperature by thermistor-battery resistance circuit	+/- 2% temperature dependency +/- 1% linearity	
pyranometer Kipp CM 5 (Fritschen and Gay, 1979)	short-wave radiation (0.4-4 μ m)	temperature difference between black painted plate with a double glass hemisphere and house, measured by manganin-constantan thermopile	+/- 0.2% K ⁻¹	98% response time 30 s

APPENDIX 1 SENSORS USED (continued)

name	parameter	method	accuracy	response time/length
pyrradiometer Funk, type Middleton (Fritschen and Gay, 1979)	net radiation (0.4-50 μm)	temperature difference between 2 sides of black plate with 2 poly-ethylene hemispheres, ventilated with nitrogen, measured by thermopile		
infrared thermometer Heimann KT15 (Choudhury and Idso, 1985)	surface temperature	infrared radiation 8-14 μm		90% response time 1 s
soil heat flux meter TNO WS-31 Cp (Fritschen and Gay, 1979; Philip, 1961; Overgaard Mogensen, 1970)	soil heat flux density	temperature difference between 2 sides of black plate measured by thermopile, correction has to be done for conductivity and heat capacity of the soil	5%	
trace gases		sampling by heated teflon tube (4 mm diameter) with a 10 μm filter		
ozone monitor Thermoelectron type 49-100 (Thermo Elec- tron, 1980)	ozone concentration	extinction of light with a wave- length of 254 nm in 2 reaction chambers, comparison of environmental air with reference air (no ozone)	2 μgm^{-3}	90% response time 20 s
monitor labs NO _x analyzer model 8840 (Monitor Labs Inc., 1985; Budd, 1974; Stevens et al., 1973)	nitrogen oxides concentration (NO/NO _x)	chemiluminescence detection of activated NO ₂ , produced by a chemical reaction between NO and O ₃ ; a photomultiplier tube measures the chemiluminescent emission intensity, NO _x is first reduced to NO (MOLYCON conversion)	NO ₂ : 10 μgm^{-3} NO: 6 μgm^{-3}	time constant 5 s

APPENDIX 2 CASE STUDIES OTC-RESISTANCE MODEL

Input parameters

The model results of temperature, specific humidity and ozone concentration inside an OTC of four case studies are given in this appendix. The cases were selected for the flow rate applied and the weather type. A characterization of the cases can be found in Table A2.1.

Table A2.1: Characterization cases.

Date	14-07-90	23-05-90	08-07-90	13-05-90
Flow rate [m ³ s ⁻¹]	1.6	00.00: 1.6 09.00: 1.2	1.6	1.2
Sky	cloudless	cloudless	cloudy till 18.00	mainly cloudy
Wind maximum open top [ms ⁻¹]	4.0	3.3	6.9	5.1
Maximum ozone concentration ambient air 2.00 m [10 ⁻⁶ gm ⁻³]	110	100	50	80
LAI	3.6	3.6	3.6	3.6
Height crop [m]	0.38	0.39	0.28	0.27
Fraction shielded	0.38	0.39	0.28	0.27
T ₂ OTC °C	17.0	14.5	18.0	12.5
T ₂ Field °C	15.0	12.5	17.0	11.0

-Boundary layer resistances:

- Leaf boundary layer (hypostomatous leaf)
 - Length scale: width leaf (0.02 m).
 - Characteristic velocity scale: 1 ms⁻¹ (see table 5.2).
 - Floor-plate
 - Length scale: 0.001 times the mean distance between the plant-holes (tuning result: 0.42 10⁻³ m).
 - Characteristic velocity scale: 1 ms⁻¹ (see table 5.2).
 - Constant C₁: 306.
 - Pot soil surface
 - Length scale: diameter pot (0.18 m).
 - Characteristic velocity scale: 1 ms⁻¹ (see table 5.2).
 - Constant C₁: 180.
- The heat transfer coefficient between the wooden floor-plate and the upper layer of the soil (α): 3 Wm²K⁻¹.
- Filter efficiency (ozone): 80%.

Results

The OTC-resistance model simulates the temperature increase inside the OTC system with an accuracy of approximately 1 K. The observed discrepancy between the specific humidity calculated by the OTC-resistance model and experimental values is within 0.5 gkg^{-1} .

Deviations between model results and experimental values of temperature and specific humidity are higher on sunny days than cloudy ones. Since evaporation or condensation of water in the filter unit plays a limited role in cloudy conditions, due to more uniform temperatures and relative humidities during the day, the importance of the use of correct filter constants under these conditions decreases. Furthermore, the importance of the air inside the air-supply system and the chamber being heated due to global radiation decreases in cloudy conditions. Consequently, absolute errors in the calculated temperature decrease. Since the model does not take account of evaporation of free water in the pots or at the floor-plate the specific humidity in a chamber within 1-2 hours after the water has been supplied is underestimated.

The filter efficiency for ozone depends on the ozone concentration of ambient air. No obvious incursion effect is seen in one of the case studies.

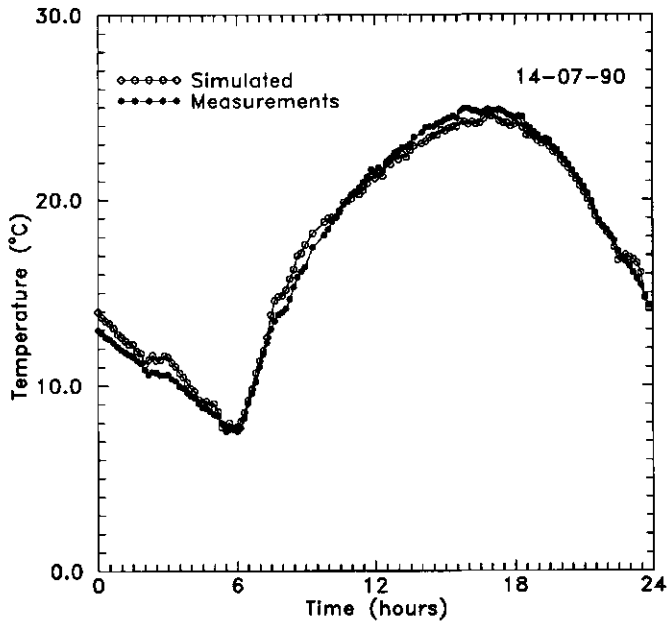


Figure A2.1: Simulated and measured temperatures inside the chamber; date: 14-07-90.

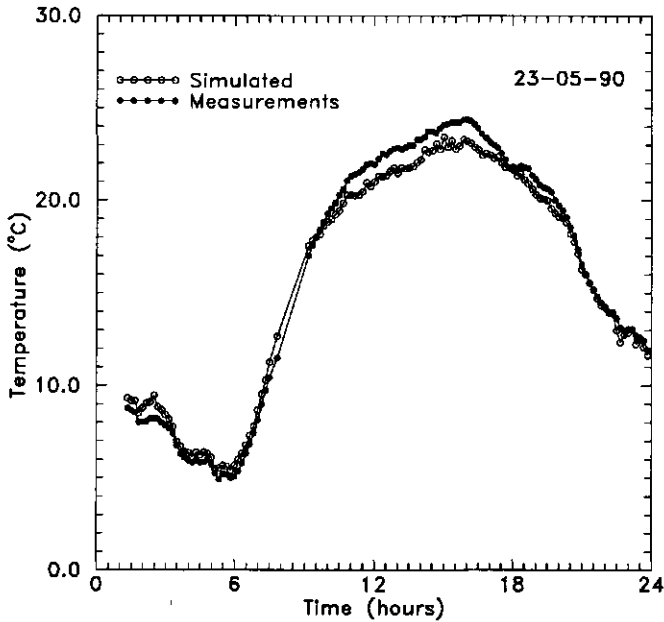


Figure A2.2: Simulated and measured temperatures inside the chamber; date: 23-05-90.

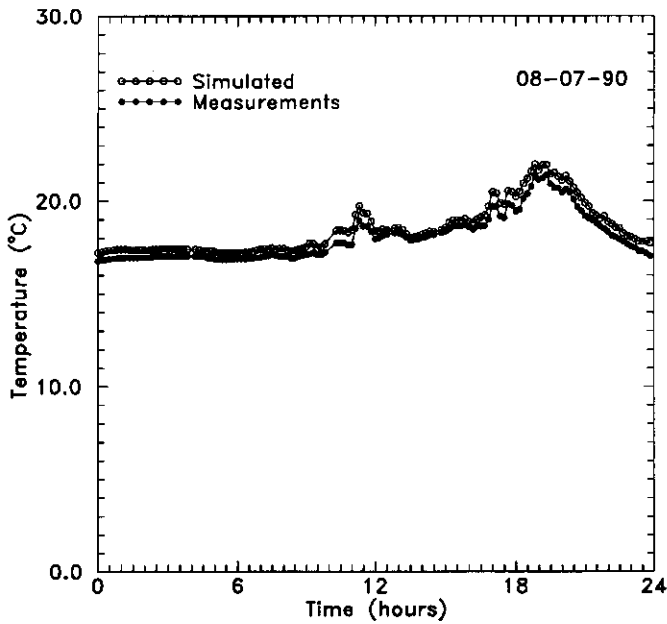


Figure A2.3: Simulated and measured temperatures inside the chamber; date: 08-07-90.

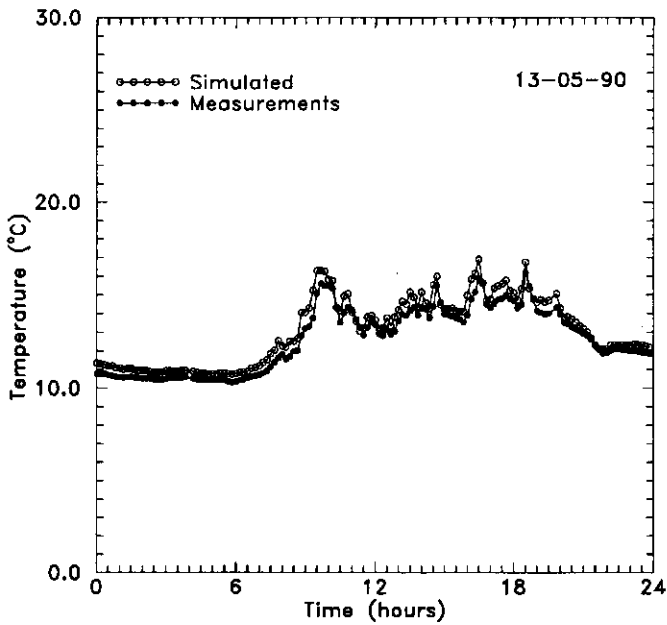


Figure A2.4: Simulated and measured temperatures inside the chamber; date: 13-05-90.

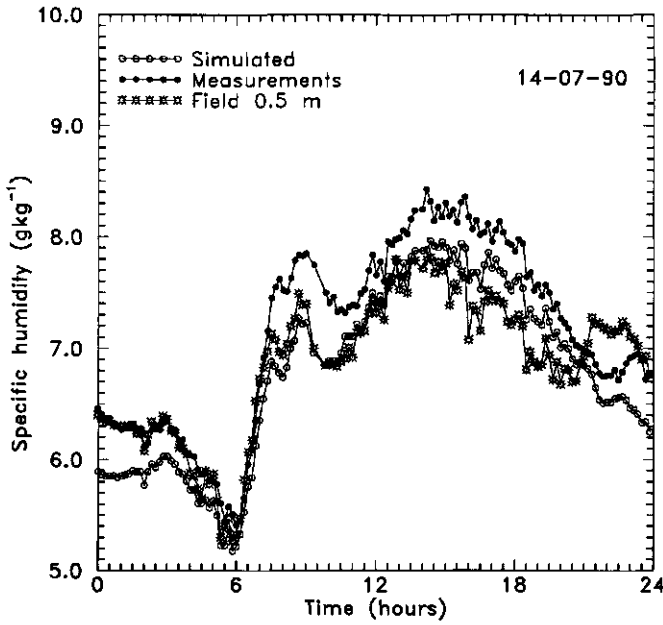


Figure A2.5: Simulated and measured specific humidities inside the chamber; date: 14-07-90.

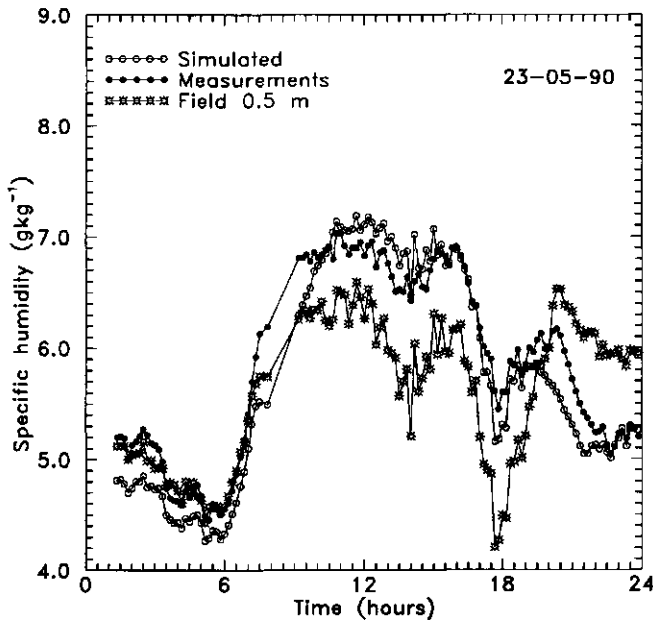


Figure A2.6: Simulated and measured specific humidities inside the chamber; date: 23-05-90.

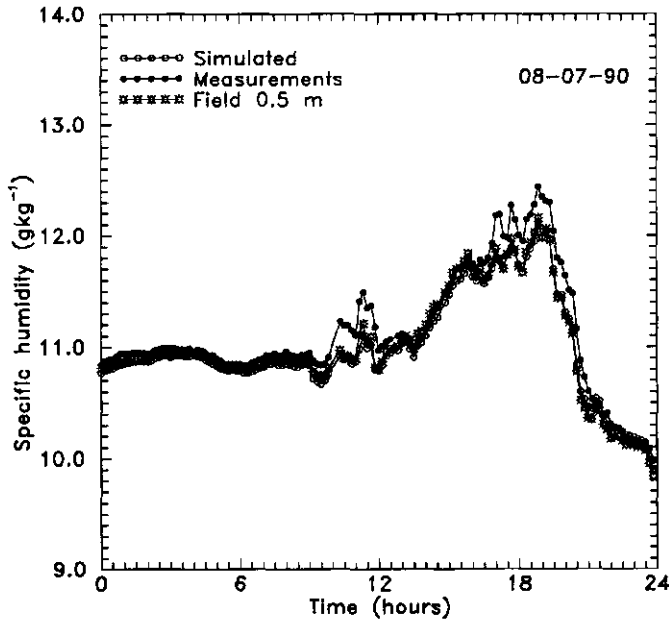


Figure A2.7: Simulated and measured specific humidities inside the chamber; date: 08-07-90.

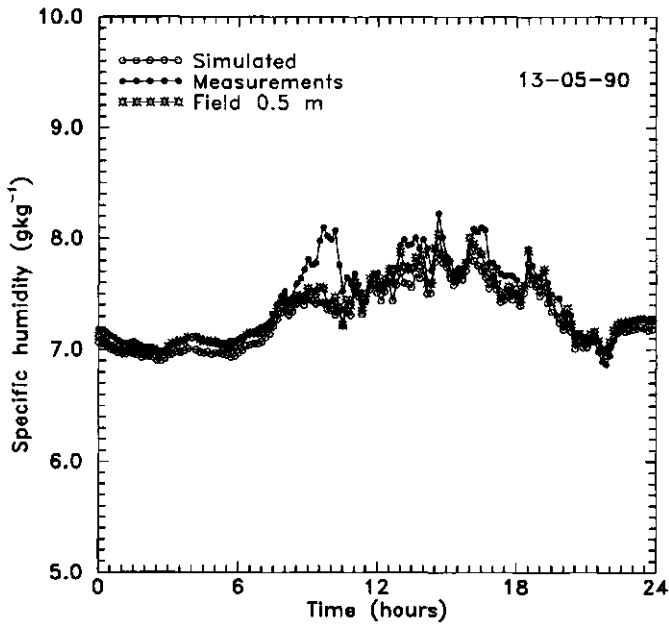


Figure A2.8: Simulated and measured specific humidities inside the chamber; date: 13-05-90.

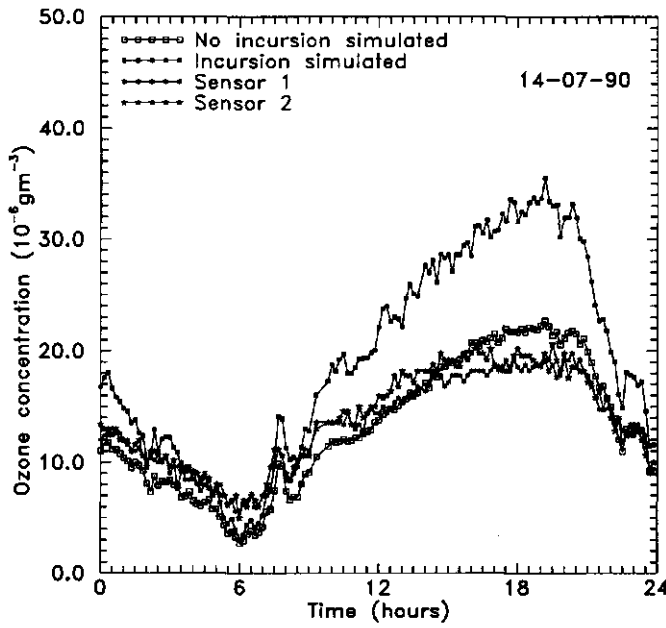


Figure A2.9: Simulated and measured ozone concentrations inside the chamber; date: 14-07-90.

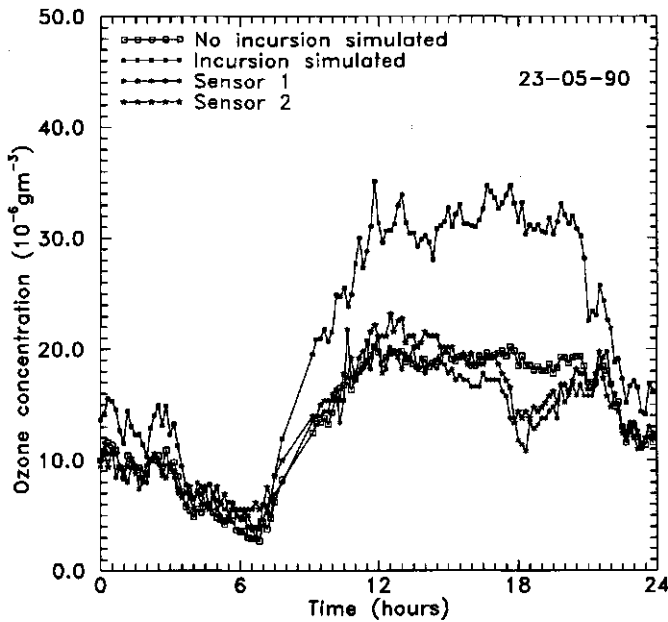
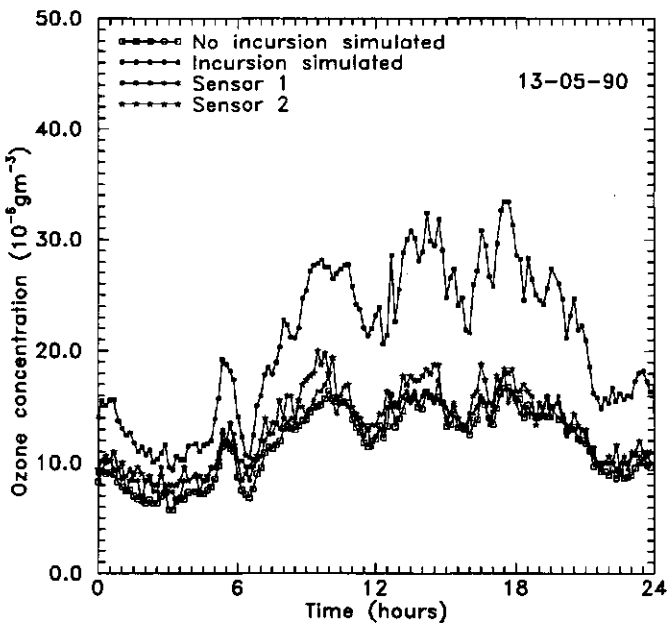
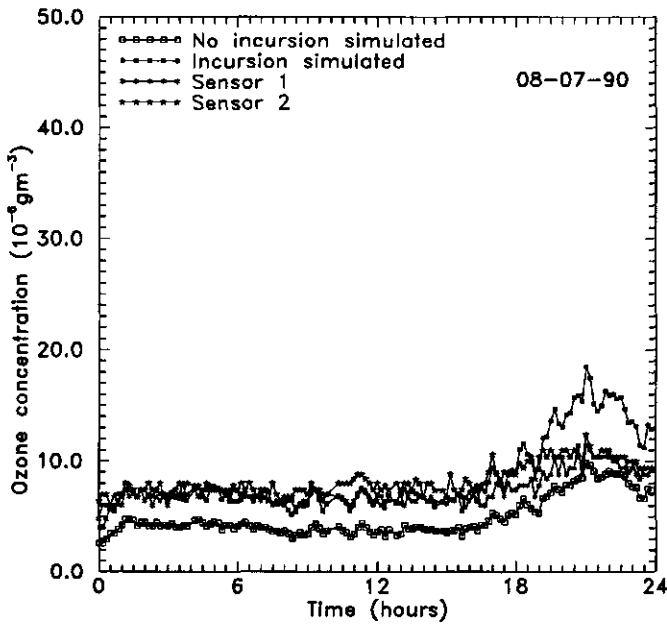


Figure A2.10: Simulated and measured ozone concentrations inside the chamber; date: 23-05-90.



SUMMARY

The impact of ozone, nitrogen oxides and other air pollutants on plants in natural vegetations cannot be described by simple exposure-yield response relationships. Outdoor experiments in which plants are exposed to ambient air pollutant levels yield conflicting results from year to year because the interacting environmental effects are complex and not constant. The best way to study the effects of air pollutants on plants is still one of the issues scientists are dealing with.

The experimental design plays an important role in extrapolating the experimental results to real field conditions. To determine the impact of air pollutants on a crop requires growing conditions which are as natural as possible and the simultaneous control of ambient pollutant levels.

The Open Top Chamber is one of the experimental set-ups to study the effect of air pollutants on plants. The original objective of the OTC design was to create an environment closely resembling field conditions while, at the same time, allowing control of air quality. The U.S. NCLAN programme was the first to use OTC's on a large scale. Nowadays the use of OTC's shifts from air pollutant exposure experiments to carbon dioxide fumigation experiments. OTC's have been used by KEMA to study the effects of air pollution on natural vegetation, in particular on the biomass production of agricultural crops in The Netherlands. The chamber consists of a cylindrical construction (diameter: 3 m; height: 3 m) with an open top through which filtered or non-filtered air is blown by a fan. Gaseous air pollutants can be added simultaneously to the incoming air.

Experimental results have shown differences in plant growth and development between non-filtered OTC's and ambient plots. It is obvious that the use of OTC's introduces a degree of artificiality which makes it impossible to duplicate field conditions exactly.

The major aims of the present study are:

- to give a physical description of the transport processes (mass, momentum and energy) inside a KEMA-type OTC in relation to field conditions,
- to determine the influence of the ventilation rate and the atmospheric boundary layer on the turbulent transport processes inside an OTC.

The study is composed of a theoretical as well as an experimental part. An OTC identical to the KEMA-type OTC was situated at the weather station of the Agricultural University's Meteorological Department. Broad beans were grown in the chamber. Wind velocity, temperature, humidity, radiation and concentrations of gaseous air pollutants were continuously measured at various positions inside and outside the OTC. Turbulence parameters were measured occasionally (wind velocity, temperature fluctuations).

The experimental results have been used to derive the prior conditions needed for the two models used and served as a tool to verify the simulation results. The first model simulates the turbulent exchange processes inside and outside the OTC. The model has been used to determine the influence of the OTC environment, ventilation rate and plants on mean air flow and turbulence inside the chamber. The second model is a resistance model which has been developed primarily to calculate the mass and energy fluxes to or from various parts of the OTC system. The model yields information about the temperature, humidity and ozone concentration inside the chamber in relation to field conditions. A special module calculates the bulk exchange processes between soil-vegetation and atmosphere inside as well as outside an OTC.

We conclude that typical OTC effects on the chamber microclimate such as

- filter effects,
 - a 10-20% reduction of global and PAR radiation load,
 - an increase of long-wave radiation intensity
 - a mean temperature increase of the order of 1 K,
 - a mean vapour pressure deficit increase of the order of 1 mbar,
- cannot be prevented without creating a kind of laboratory chamber. Furthermore,

the typical non-natural flow pattern cannot be changed without removing the whole OTC-configuration. The exposure-response curves derived under OTC conditions cannot be used directly to estimate a quantitative effect under field conditions. An extrapolation of the exposure-response curves derived under OTC conditions to field conditions taking into account the differences in microclimate between OTC and field conditions can improve the quality of the experimental results.

SAMENVATTING

De effecten van ozon, stikstofoxiden en andere luchtverontreinigende stoffen op planten in natuurlijke vegetaties kunnen niet volledig worden beschreven door middel van eenvoudige blootstellings-effect relaties. Veldexperimenten waarbij planten worden blootgesteld aan wisselende concentraties luchtverontreinigende stoffen laten, van jaar tot jaar, sterk wisselende resultaten zien, daar de planten complexe interacties met allerlei omgevingsfactoren vertonen. Op welke wijze men het best de effecten van luchtverontreinigende stoffen op planten kan bepalen is nog steeds een punt van discussie.

De experimentele opzet speelt een belangrijke rol bij de extrapolatie van wetenschappelijke experimenten naar echte veldomstandigheden. Wil men zo betrouwbaar mogelijke resultaten verkrijgen dan dient men de groeiomstandigheden zo natuurlijk mogelijk te houden terwijl men tegelijkertijd concentraties van luchtverontreinigende stoffen kan controleren.

Het gebruik van OTC's is één van de mogelijkheden om de effecten van luchtverontreinigende stoffen op planten te bestuderen. Het oorspronkelijke doel van het gebruik van OTC's was een omgeving te creëren waarin planten zoveel mogelijk onder veldomstandigheden opgroeien terwijl men tegelijkertijd de luchtkwaliteit kan regelen. OTC's werden voor het eerst op grote schaal ingezet in het Amerikaanse NCLAN (National Crop Loss Assessment Network) programma. Tegenwoordig worden OTC's meer en meer toegepast in CO₂-begassings-experimenten met als doel de effecten van toenemende CO₂ concentraties op de groei en ontwikkeling van planten te bepalen. OTC's zijn door de KEMA gebruikt om de effecten van luchtverontreinigende stoffen op de natuurlijke vegetatie in het algemeen en de biomassa productie van Nederlandse land- en tuinbouwgewassen in het bijzonder te bestuderen. De OTC bestaat uit een cilindrische constructie (3 m diameter, 3 m hoog) met een open dak. Een ventilator blaast al dan niet gefilterde lucht, waaraan eventueel luchtverontreinigende componenten kunnen worden toegevoegd, door deze constructie.

Tijdens experimenten uitgevoerd met OTC's zijn er echter verschillen waargenomen in de groei en ontwikkeling van planten in een OTC voorzien van niet gefilterde lucht en de groei en ontwikkeling van planten onder veldomstandigheden. Het gebruik van OTC's blijkt bepaalde beperkingen te introduceren waardoor het onmogelijk is veldomstandigheden ideaal na te bootsen.

De belangrijkste doelstellingen van de hier beschreven studie zijn:

- Het geven van een fysische beschrijving van transportprocessen (impuls, energie en massa) binnen een OTC in vergelijking met veldomstandigheden.
- Het bepalen van de invloed van het ventilatievoud en de atmosferische grenslaag op de turbulente uitwisselingsprocessen in een OTC.

De studie bestaat voor een gedeelte uit experimenteel en voor een gedeelte uit theoretisch werk. Er is een uitgebreide meetcampagne aan een KEMA-type OTC geplaatst op het meteo-waarnemingsveld van de vakgroep meteorologie van de Landbouwniversiteit uitgevoerd. Tijdens deze meetcampagne zijn continu luchtbeweging, temperatuur, vocht, inkomende en uitgaande langgolvlige en kortgolvlige straling en concentraties van luchtverontreinigende stoffen op diverse posities binnen en buiten een OTC gemeten. Bovendien zijn incidentele metingen van windsnelheid- en temperatuurfluctuaties uitgevoerd.

De meetresultaten zijn vergeleken met uitgevoerde computerberekeningen op basis van twee modellen, te weten een model dat het stromingsveld in en om een OTC beschrijft en een integraal-model dat de bulk-uitwisselingsprocessen in een OTC beschrijft in de vorm van over vlakken geïntegreerde fluxen. De meetresultaten leverden de startcondities en randvoorwaarden voor de berekeningen.

Het eerst genoemde model is gebruikt om de invloed van het stromingsveld buiten de OTC, het ventilatievoud en de aanwezige beplanting op het microklimaat in een OTC te bepalen. Met behulp van het integraalmodel kan een schatting gemaakt worden van de gemiddelde temperatuur, vochtigheid en ozonconcentraties binnen een OTC. Een speciale module berekent de bulk-uitwisselings-

processen tussen bodem-gewas en omgeving zowel onder OTC als onder veldomstandigheden.

We komen tot de conclusie dat typische OTC effecten op het microklimaat zoals:

- filter effecten,
- een toename van de langgolvlige stralingsintensiteit,
- een 10-20% reductie van inkomende globale en fotosynthetisch actieve straling,
- een gemiddelde temperatuuroename in de orde van grootte van 1 K,
- een gemiddelde toename van het dampdrukdeficiet in de orde van grootte van 1 mbar,

niet kunnen worden voorkomen zonder een of andere vorm van klimaatkas te creëren. Bovendien kan het onnatuurlijke stromingspatroon binnen een OTC niet worden veranderd zonder daarmee de gehele OTC-constructie te herzien. De blootstellings-effect relaties welke onder OTC omstandigheden zijn afgeleid, kunnen niet rechtstreeks in een kwantitatief effect onder veldomstandigheden worden vertaald. Echter, een extrapolatie van de blootstellings-effect relaties gevonden onder OTC omstandigheden naar veldomstandigheden, waarbij de invloed van het microklimaat in de OTC op de uitwisselingsprocessen wordt meegenomen, kan de kwaliteit van deze extrapolatie verbeteren.

REFERENCES

- Aben, J.M.M. (1987). Estimation of the plant-related resistances determining the ozone flux to broad bean plants (*Vicia faba* var. *Metissa*). In: Air pollution and ecosystems. Proceedings of an International CEC Symposium (Grenoble, 1987): 616-619.
- Aben, J.M.M. (1990). A system to determine whole-plant exchange rates of ozone, carbon dioxide and water vapour. Kema Scientific & Technical Reports 8: 109-120.
- Aben, J.M.M., M. Janssen-Jurkovicová & E.H. Adema (1990). Effects of low-level ozone exposure under ambient conditions on photosynthesis and stomatal control of *Vicia faba* L. *Plant, Cell and Environment* 13: 463-469.
- Bell, J.N.B. & M.R. Ashmore (1986). Design and construction of chambers and methods of filtration (equipment and costs). In: Microclimate and plant growth in open-top chambers. Proceedings of a Workshop (Freiburg, 1986). CEC Air Pollution Research Report 5: 44-56.
- Bhumralkar, C.M. (1975). Numerical experiments on the computation of ground surface temperature in an atmospheric general circulation model. *Journal of Applied Meteorology* 14: 1246-1258.
- Blackadar, A.K. (1976). Modelling the nocturnal boundary layer. In: Proceedings of the Third AMS Symposium on Atmospheric Turbulence, Diffusion and Air Quality (Boston, 1976): 46-49.
- Buckenham, A.H., M.A. Parry, C.P. Whittingham & A.T. Young (1981). An improved open-topped chamber for pollution studies on crop growth. *Environmental Pollution (series B)* 2: 475-482.
- Budd, A.L. (1974). A dual channel approach to chemiluminescent analysis of NO_2 and NO . Proceedings of the 20th National Instrument Society of America Analysis Instrumentation Symposium (Pittsburgh, 1974).
- Chamberlain, A.C. (1966). Transport of gases to and from grass and grass-like surfaces. *Proceedings of the Royal Society* 290: 236-265.
- Choudhury, B.J. & S.B. Idso (1985). An empirical model for stomatal resistance of field-grown wheat. *Journal of Agricultural and Forest Meteorology* 36: 65-82.
- Colls, J.J. & C.K. Baker (1988). The methodology of open field fumigation. In: Air pollution and ecosystems. Proceedings of an International CEC Symposium (Grenoble, 1987): 361-371.
- Coppin, P.A., M.R. Raupach & B.J. Legg (1986). Experiments on scalar dispersion within a model plant canopy. Part II: an elevated plane source. *Boundary Layer Meteorology* 35: 167-191.
- CRC handbook of chemistry and physics (61st edition, 1980). CRC Press Inc. (Boca Raton).
- Creare Inc. (1987). FLUENT manual version 2.9 update. Creare Inc. Report TN-369 revision 3.
- Davis, J.M., A.J. Riordan & R.E. Lawson (1983). A windtunnel study of the flow field within and around open-top chambers used for air pollution studies. *Boundary Layer Meteorology* 25: 193-214.
- Davis, J.M. & H.H. Rogers (1980). Wind tunnel testing of open top field chambers for plant effects assessment. *Journal of the Air Pollution Control Association* 30(8): 905-908.

- Deardorff, J.W. (1978). Efficient prediction of ground surface temperature and moisture, with inclusion of a layer of vegetation. *Journal of Geophysical Research* 83(C4): 1889-1903.
- Detering and Elling (1985). Application of the $k-z$ turbulence model to the atmospheric boundary layer. *Boundary Layer Meteorology* 33: 113-133.
- Dickinson (1984). Modelling evapotranspiration for three dimensional global climate models. *Climate processes and climate sensitivity. Geophysical Monographs* 29: 58-72.
- Dorman, J.L. & P.J. Sellers (1989). A global climatology of albedo, roughness length and stomatal resistance for atmospheric general circulation models as represented by the simple biosphere model (SiB). *Journal of Applied Meteorology* 28: 833-
- Drake, B.G., P.W. Leadly, W.J. Arp, D. Nassiry & P.S. Curtis (1989). An open top chamber for field studies of elevated atmospheric CO₂ concentration on saltmarsh vegetation; Technical Report. *Functional Ecology* 3: 363-371.
- Finnigan, J.J. & M.R. Raupach (1987). Transfer processes in relation to stomatal characteristics. In: *Stomatal function*. Stanford University Press (Stanford): 385-429.
- Fritschen, L.J. & L.W. Gay (1979). *Environmental instrumentation*. Springer Verlag (New York).
- Fritschen, L.J. & R.H. Shaw (1961). A thermocouple anemometer and its use. *Bulletin of the American Meteorological Society* 24(1): 42-46.
- Fuhrer, J., A. Grandjean, B. Lehnerr, A. Egger & W. Tschannen (1987). Effects of ozone in ambient air on growth yield and physiological parameters of spring wheat. In: *Air pollution and ecosystems. Proceedings of an International CEC Symposium (Grenoble, 1987)*: 142-147.
- Garrat, J.R., (1978). Transfer characteristics for a heterogenous surface of large aerodynamic roughness. *Quarterly Journal of the Royal Meteorological Society* 104: 491-502.
- Garrat, J.R. and B.B. Hicks (1973). Momentum, heat and water vapour transfer to and from natural and artificial surfaces. *Quarterly Journal of the Royal Meteorological Society* 99: 680-687.
- Gates, D.M. (1980). *Biophysical ecology*. Springer Verlag (New York).
- General Electric Plastics (1989). *Technisch handboek Lexan Exell en Lexan Margard*. General Electric Plastics B.V. Structure Products Europe (Bergen op Zoom) Netherlands.
- Goudriaan, J. (1977). *Crop micrometeorology: a simulation study*, Ph.D. Thesis. Pudoc (Wageningen).
- Harrison, L.P. (1963). Some fundamental considerations regarding psychrometry. In: *Humidity and moisture vol. 1*, Reinhold (New York): 165-174.
- Heagle, A.S. (1989). Ozone and crop yield. *Annual Review Phytopathology* 27: 397-423.
- Heagle, S., D.E. Body & W.W. Heck (1973). An open-top field chamber to assess the impact of air pollution on plants. *Journal of Environmental Quality* 2(3): 365-368.
- Heagle, A.S., L.W. Kress, P.J. Temple, R.J. Kohut, J.E. Miller & H.E. Heggstad (1988). Factors influencing ozone dose-yield response relationships in open-top field studies. In: *Assessment of crop loss from air pollutants. Proceedings of an International Conference (Raleigh, 1987)*: 141-179.
- Heagle, A.S, M.B. Letchworth & C.A. Mitchell (1983). Effects of growth medium and fertilizer rate on

- the yield response of soybeans exposed to chronic doses of ozone. *Phytopathology* 73: 134-139.
- Heagle, A.S., R.B. Philbeck, H.H. Rogers & M.B. Letchworth (1979). Dispensing and monitoring ozone in open top field chambers for plant-effects studies. *Phytopathology* 69(1): 15-20.
- Hewlett Packard Company (1988). HP 3852S data acquisition and control system data book. Technical data, januari 1988. Hewlett Packard Company.
- Hinze, J.O. (1959). *Turbulence*. McGraw-Hill (New York).
- Holtslag, A.A.M. and A.C.M. Beljaars (1988). Surface flux parameterization schemes: developments and experiences at KNMI. KNMI Scientific Reports WR-nr 88-06.
- Hov, O., I. Allegrini, S. Beilke, R.A. Cox, A. Eliassen, A.J. Elshout, G. Gravenhorst, S.A. Penkett & R. Stern (1987). Evaluation of atmospheric processes leading to acid deposition in Europe. CEC Air Pollution Research Report 10.
- Hov, O., K.H. Becker, P. Builtjes, R.A. Cox & D. Kley (1986). Evaluation of the photooxidants-precursor relation-ship in Europe. In: CEC Air Pollution Research Report 1.
- Iqbal, M. (1983). *An introduction to solar radiation*. Academic Press (London).
- Jacquemin, B. & J. Noilhan (1990). Sensitivity study and validation of a land surface parameterization using the Hapex-Mobilhy data set. *Boundary layer meteorology* 52: 93-134.
- Jäger, H.-J., H.J. Weigel, R. Guderian, U. Arndt & G. Seufert (1987). Methodological approaches: part I: Experiments with open-top chambers: results, advantages and limitations. In: *Air pollution and ecosystems. Proceedings of an International CEC Symposium (Grenoble, 1987): 327-337.*
- Jarvis, P.G. (1976). The interpretation of the variations in leaf water potential and stomatal conductance found in canopies in the field. *Philosophical Transactions Royal Society London (series B)* 273: 593-610.
- Jetten, T.H. (1991). Evaluation of the microclimate impact on the uptake of trace gases by plants growing up in open top chambers in relation to field conditions. Preprints tenth AMS Conference on Biometeorology and Aerobiology (Salt Lake City, 1991): 46-53.
- Jetten, T.H. and B.J.M. Stortelder (1990). Physical description of transport processes inside a KEMA open-top chamber in relation to field conditions: a study of the microclimate in an open-top chamber. *KEMA Scientific & Technical Reports* 8(6): 383-399.
- Johnston, J.W., D.S. Shriner & C.H. Abner (1986). Design and performance of an exposure system for measuring the response of crops to acid rain and gaseous pollutants in the field. *Journal of the Air Pollution Control Association* 36(8): 894-899.
- Last, F.T. (1986). Perspective of open-top chambers in pollution research. In: *Microclimate and plant growth in open-top chambers. Proceedings of a Workshop (Freiburg, 1986). CEC Air Pollution Research Report* 5: 5-9.
- Lauder, B.E. (1984). Second-moment closure: methodology and practice. In: *Turbulence models and their applications Volume 2. Collection de la Direction des Etudes et Recherches d'Electricité de France.*
- Lauder, B.E. & D.B. Spalding (1974). The numerical computation of turbulent flow. *Computer Methods in Applied Mechanics and Engineering* 3: 269-289.
- Louis, J.F. (1979). A parametric model of vertical eddy fluxes in the atmosphere. *Boundary Layer*

Meteorology 17: 187-202.

- Louis, J.F., M. Tiedtke & J.F. Geleyn (1982). A short history of the PBL parameterization at ECMWF. In: ECMWF Workshop on Boundary Layer Parameterization (Reading, 1981): 59-79.
- Mandl, R.H., L.H. Weinstein, D.C. McCune & M. Keveny (1973). A cylindrical open-top chamber for the exposure of plants to air pollutants in the field. *Journal of Environmental Quality* 2(3): 371-376.
- Mathy, P. (1988). The European open-top chambers: objectives and implementation. In: Assessment of crop loss from air pollutants. Proceedings of an International Conference (Raleigh, 1987): 505-513.
- McLeod, A.R., J.E. Fackrell & K. Alexander (1985). Open-air fumigation of field crops: criteria and design for a new experimental system. *Atmospheric Environment* 19(10): 1639-1649.
- Monin, A.S. & A.M. Yaglom (1965). *Statistical fluid mechanics: mechanics of turbulence*. Volume 1. MIT Press (Cambridge).
- Monteith, J.L. (1973). *Principles of environmental physics*. Edward Arnold (London).
- Monteith, J.L. & M.H. Unsworth (1990). *Principles of environmental physics*. Edward Arnold (London).
- Monitor labs, Inc. (1985). *Instruction manual nitrogen oxides analyzer, model 8840*. Monitor Labs, Inc.
- Morison, J.I.L. (1987). Intercellular CO₂ concentration and stomatal response to CO₂. In: *Stomatal function* (Stanford University Press, Stanford): 229-251.
- Noilhan, J. & S. Planton (1989). A simple parameterization of land surface processes for meteorological models. *Monthly Weather Review* 117: 536-549.
- Olszyk, D.M., T.W. Tibbits & W.M. Hertzberg (1980). Environment in open-top field chambers utilized for air pollution studies. *Journal of Environmental Quality* 9(4): 610-615.
- Ormrod, D.P., B.A. Marie & O.B. Allen (1988). Research approaches to pollutant crop loss functions. In: Assessment of crop loss from air pollutants. Proceedings of an International Conference (Raleigh, 1987): 27-44.
- Overgaard Mogensen, V. (1970). The calibration factor of heat flux meters in relation to the thermal conductivity of the surrounding medium. *Agricultural Meteorology* 7: 401-410.
- Owen, P.R. & W.R. Thomson (1963). Heat transfer across rough surfaces. *Journal of Fluid Mechanics* 15: 321-334.
- Parlange, J., P.E. Waggoner & G.H. Heichel (1971). Boundary layer resistance and temperature distribution on still and flapping leaves. I. Theory and laboratory experiments. *Plant Physiology* 48: 437-442.
- Patankar, S.V. (1980). *Numerical heat transfer and fluid flow*. Hemisphere Publishing Corporation (New York).
- Pearman, G.I., H.L. Weaver & C.B. Tanner (1972). Boundary layer heat transfer coefficients under field conditions. *Agricultural Meteorology* 10: 83-92.
- Philip, J.R. (1961). The theory of the heat flux meters. *Journal of Geophysical Research* 66: 571-579.

- Roberts, T.M., R.M. Bell, D.C. Horsman & K.E. Colvill (1983). The use of open-top chambers to study the effects of air pollution, in particular sulphur dioxide, on the growth of ryegrass *Lolium perenne* L. Part I-Characteristics of modified open-top chambers used for both air-filtration and SO₂-fumigation experiments. *Environmental Pollution (Series A)* 31: 9-33.
- Rodi, W. (1976). A new algebraic relation for calculating the Reynolds stresses. *ZAMM* 56: T219-T221.
- Rodi, W. (1980). Turbulence models for environmental problems. In: *Prediction methods for turbulent flows*. Hemisphere Publishing Corporation (Washington): 259-350.
- Rodi, W. (1981). Examples of turbulence models for incompressible flows. *AIAA Journal* 20(7): 872-879.
- Rodi, W. (1984). Turbulence models and their applications in hydraulics - A state of the art review. Book Publication of the International Association for Hydraulic Research (Delft).
- Sanders, G.E., A.G. Clark & J.J. Colls (1991). The influence of open-top chambers on the growth and development of field bean. *The New Phytologist* 117: 439-447.
- Schmitt, F. & B. Ruck (1987). Flow visualisation studies of the aerodynamic characteristics of an open top chamber. *Environmental Pollution* 48: 223-233.
- Sellers, P.J., Y. Mintz, Y.C. Sud & A. Dalcher (1986). A simple biosphere model (SiB) for use within general circulation models. *Journal of the Atmospheric Sciences* 43(6): 505-531.
- Smedman, A. & U. Hogstrom (1973). The mastra micro-meteorological project. *Boundary Layer Meteorology* 5: 529-573.
- Spitters, C.J.T., H.A.J.M. Toussaint & J. Goudriaan (1986). Separating the diffuse and direct component of global radiation and its implications for modelling canopy photosynthesis. Part I: Components of incoming radiation. *Agricultural and Forest Meteorology* 38: 217-229.
- Stevens, R.K. (1973). Instrumentation for the measurement of nitrogen dioxide. *Proceedings of a Symposium on Instrumentation for Monitoring Air Quality (Boulder, 1973)*. American Society for Testing and Materials (ASTM, Philadelphia).
- Stigter, C.J. & A.D. Welgraven (1976). An improved radiation protected differential thermocouple psychrometer for crop environment. *Archiv Meteorologie und Bioklimatologie (Series B)* 24: 177-187.
- Stull, R.B. (1988). *An introduction to boundary layer meteorology*. Kluwer Academic Publishers (Amsterdam).
- Tennekes, H. & J.L. Lumley (1972). *A first course in turbulence*. MIT press (Cambridge).
- Thermo Electron Corporation (1980). *Instruction manual series 49*. Thermo Electron Corporation, Environmental Instruments Division.
- Thom, A.S. (1968). The exchange of momentum, mass and heat between an artificial leaf and the airflow in a wind-tunnel. *Quarterly Journal of the Royal Meteorological Society* 94: 44-55.
- Thom, A.S. (1971). Momentum absorption by vegetation. *Quarterly Journal of the Royal Meteorological Society* 97: 414-428.
- Thom, A.S. (1972). Momentum, mass and heat exchange of vegetation. *Quarterly Journal of the Royal Meteorological Society* 98: 124-134.

- Thom, A.S. (1975). Momentum, mass and heat exchange of plant communities. In: *Vegetation and the atmosphere. Volume 1: Principles*. Academic Press (London): 57-109.
- Thompson, N., Barrie & M. Ayles (1981). The meteorological office rainfall and evaporation calculation system: MORECS. Hydrological Memorandum 45.
- Unsworth, M.H. (1982). Exposure to gaseous pollutants and uptake by plants. In: *Effects of gaseous air pollution in agriculture and horticulture*. Butterworths (London): 43-63.
- Unsworth, M.H. (1986). Principles of microclimate and plant growth in open-top chambers. In: *Microclimate and plant growth in open-top chambers. Proceedings of a Workshop (Freiburg, 1986)*. CEC Air Pollution Research Report 5: 16-29.
- Unsworth, M.H., A.S. Heagle & W.W. Heck (1984). Gas exchange in open-top field chambers-I. Measurement and analysis of atmospheric resistances to gas exchange. *Atmospheric Environment* 18(2): 373-380.
- Van Asselt, C.J., A.F.G. Jacobs, J.H. van Boxel & A.E. Jansen (1989). A simple fast-response thermometer for outdoor use. In: *Report of fourth WMO technical conference on instruments and methods of observation (TECIMO-IV)*. Instruments and Observing Methods Report 35: 129-134.
- Van Boxel, J.H. (1986). Heat balance investigations in tidal areas. Ph.D. thesis Free University of Amsterdam.
- Van der Eerden, L.J., A.E.G. Tonneijck & J.H.M. Wijnands (1988). Crop loss due to air pollutants in The Netherlands. *Environmental Pollution* 53: 365-376.
- Van Pul (1992). The flux of ozone to a maize crop and the underlying soil during a growing season. Ph.D. thesis Agricultural University, Wageningen.
- Weinstock, L., W.J. Kender & R.C. Musselman (1982). Microclimate within open-top air pollution chambers and its relation to grapevine physiology. *Journal of the American Society of Horticultural Sciences* 107(5): 923-929.
- Wieringa, J. (1986). De atmosferische grenslaag. KNMI Technisch Rapport 89 (De Bilt, 1986).
- Wigley, G. and J.A. Clark (1974). Heat transport coefficients for constant energy flux models of broad leaves. *Boundary Layer Meteorology* 7: 139-150.

LIST OF SYMBOLS

Upper cases

- A : Characteristic surface area [m^2].
 A_{\odot} : Area (b : base area of the chamber; x : shaded area by a wall of the air-supply system; y : wall surface area of the air-supply system) [m^2].
 Abs_{\odot} : Percentage of global radiation absorbed (l : Lexan; w : wall and net) [-].
 C : Concentration of a scalar quantity [Jm^{-3}/kgm^{-3}].
 Alb : Albedo [-].
 C_D : Inertial resistance coefficient [m^{-1}].
 C_{II} : Characteristic scale for scalar quantity concentration fluctuations [kgm^{-3}].
 C_{I1} : Filter constant [s^{-1}].
 C_{I2} : Filter constant [-].
 C_p : Specific heat capacity at constant pressure [$Jkg^{-1}K^{-1}$].
 C_{pd} : Specific heat capacity for dry air at constant pressure [$Jkg^{-1}K^{-1}$].
 C_r : Ratio [-].
 C_T : Coefficient [Km^2J^{-1}].
 $C_{W,P}$: Heat capacity floor-plate [$Jkg^{-1}K^{-1}$].
 C_x : Concentration at location x [kgm^{-3}].
 C_1 : Coefficient [$s^{0.5}m^{-1}$].
 $C_{1,asp}$: Percentage of the incoming global radiation transported to the air within the air-supply system [-].
 C_{\odot} : Scalar quantity concentration (c : inside chamber; i : end of the air-supply system; o : outside the OTC at open top height) [kgm^{-3}].
 Cd_m : Bulk exchange coefficient for momentum during thermal-neutral conditions [-].
 ΔC : Characteristic scale for scalar quantity concentration [kgm^{-3}].
 D_t : Turbulent diffusivity for heat or mass [m^2s^{-1}].
 D_{sc} : Molecular diffusivity (O_3 : ozone, sc : scalar quantity; v : water vapour) [m^2s^{-1}].
 E : Roughness parameter [-].
 E_v : Evapotranspiration of the vegetation [$kgm^{-2}s^{-1}$].
 F_i : Body force per unit mass in i -direction [Nkg^{-1}].
 F_{\odot} : Fractional conductance describing the influence on stomatal resistance of solar radiation (F_1), soil moisture (F_2), water vapour pressure deficit (F_3) and air temperature (F_4), respectively.
 F_{\odot} : Scalar flux (p : plants; r : chemical reactions; s : soil; w : wall) [$kg s^{-1}$].
 G : Production of turbulent kinetic energy by buoyancy [m^2s^{-3}].
 G_{ij} : Production of turbulent momentum flux by buoyancy [m^2s^{-3}].
 H : Sensible heat flux density to soil-vegetation medium [Wm^{-2}].
 H_p : Height of the plants [m].
 $Hc_{t-\Delta t}$: Water content of the filter 1 time step earlier [kg].
 Hc_t : Equilibrium water content of the filter [kg].
 I : Turbulent intensity [-].

- L : Characteristic length scale [m].
 L : Latent heat [Jkg^{-1}].
 L_a : Characteristic length scale in a -direction [ms^{-1}].
 L_p : Thickness of the floor-plate [m].
 LA : Total leaf area (double-sided) [m^2].
 LA_l : Leaf Area Index (one-sided) [-].
 LE : Latent heat flux density to soil-vegetation medium [Wm^{-2}].
 Lw_i : Incoming longwave radiation [Wm^{-2}].
 N_i : The rate of air change due to incursion [s^{-1}].
 P : Hydrostatic pressure [Nm^{-2}].
 P : Production of turbulent kinetic energy by mean wind shear [m^2s^{-3}].
 P_y : Production of turbulent momentum flux by mean wind shear [m^2s^{-3}].
 ΔP : Characteristic pressure scale [Nm^{-2}].
 Q : Energy exchanged [Js^{-1}].
 Q_{\odot} : Energy flux (p : plants; r : chemical reactions; s : soil; w : wall) [Js^{-1}].
 R : Resistance [sm^{-1}].
 $R_{a,\odot}$: Bulk aerodynamic resistance (h : heat transport; v : water vapour transport) [sm^{-1}].
 $R_{b,\odot}$: Boundary layer resistance (h : heat transport; sc : scalar transport) [sm^{-1}].
 R_i : Absorbed longwave radiation from the sky [Wm^{-2}].
 R_n : Net radiation from sky [Wm^{-2}].
 $R_{s,\text{max}}$: Maximum stomatal resistance observed [sm^{-1}].
 $R_{s,\text{min}}$: Stomatal resistance observed at high solar intensities, well irrigated soil, saturated air and optimal ambient temperature [sm^{-1}].
 $R_{s,\odot}$: Bulk surface resistance (O_3 : ozone transport; v : water vapour transport) [sm^{-1}].
 R^* : Universal gas constant [$\text{Jmol}^{-1}\text{K}^{-1}$].
 R_{\odot} : Resistance per unit base area (i : incursion; v : ventilation) [sm^{-1}].
 S : Flux density into the soil and heat storage in the vegetation medium [Wm^{-2}].
 S_B : Heat transport to the soil medium under the wooden floor-plate [Wm^{-2}].
 S_g : Global radiation on a horizontal plane [Wm^{-2}].
 S_g^i : Species-dependent limit value [Wm^{-2}].
 S_g^w : Total global radiation absorbed by a wall [W].
 S_p : The energy absorbed by the wooden floor-plate [Wm^{-2}].
 S_{sc} : Production or loss of a scalar quantity [$\text{kgm}^{-3}\text{s}^{-1}$].
 T : Temperature of the gas [K].
 T_{fl} : Characteristic scale for the temperature fluctuations [K].
 T_{ov} : Virtual temperature at a reference height [K].
 T_s : Surface temperature of the soil/soil-vegetation medium [K].
 $T_{s,B}$: The temperature of a thin upper layer of the soil just below the floor-plate [K].
 T_v : Virtual temperature [K].
 $T_{z,r}$: Temperature of the air at a reference height [K].
 T_1 : Virtual temperature difference with virtual temperature at a reference height [K].

- T_2 : Time averaged mean surface temperature [K].
 T_o : Temperature (*a*: ambient air; *c*: inside chamber; *i*: end of the air-supply system; *o*: outside the OTC at open top height; *P*: soil; *w*: wall) [K].
 ΔT : Characteristic temperature scale [K].
 ΔT : Temperature change [K].
 U : Characteristic mean velocity scale [ms^{-1}].
 U_a : Characteristic mean velocity scale in *a*-direction [ms^{-1}].
 U_i : Component of velocity vector in *i*-direction [ms^{-1}].
 U_j : Initial velocity jet in the direction of the mean flow [ms^{-1}].
 U_s : Mean centre line velocity component of a jet in the direction of the mean flow [ms^{-1}].
 $U_{z,r}$: Mean wind speed at a reference height [ms^{-1}].
 U_* : Friction velocity [ms^{-1}].
 V : Volume [m^3].
 W_h : Height of a wall [m].
 W_2 : The mean volumetric water content of a bulk soil column [m^3m^{-3}].
 W_o : Volumetric moisture content (*fc*: field capacity; *wilt*: wilting point) [m^3m^{-3}].
 X_i : Distance in *i*-direction [m].
 Z^* : Dimensionless distance perpendicular to a wall.
- a : Molecular thermal diffusivity [m^2s^{-1}].
 c : The speed of sound [ms^{-1}].
 c_d : Drag coefficient [-].
 $c_{\varepsilon,1}$: Empirical constant *k- ε* model [-].
 $c_{\varepsilon,2}$: Empirical constant *k- ε* model [-].
 c_{μ} : Empirical constant *k- ε* model [-].
 c_1 : Constant algebraic stress model [-].
 c_3 : Constant algebraic stress model [-].
 d : Characteristic length scale [m].
 d : Orifice height [m].
 d : Displacement length [m].
 d_o : Length of shaded area (*s*: wall; 1: front wall with or without net; 2: front and back wall with or without net; 3: back wall with or without net) [m].
 f : Dimensionless term representing the incoming photosynthetically active radiation on a foliage, standardized by a species-dependent limit value [-].
 f_{in} : Flow rate as a result of ventilation [m^3s^{-1}].
 f_m : Flux density [$\text{Jm}^{-2}\text{s}^{-1}/\text{kgm}^{-2}\text{s}^{-1}$].
 g : Acceleration due to gravity [ms^{-2}].
 k : Turbulent kinetic energy [m^2s^{-2}].
 k_w : Extinction coefficient of Lexan [m^{-1}].
 k_p : Permeability [m^2].
 l : Distance from the centre line of a jet to the point where the velocity in the direction of the mean flow equals $0.5 U_s$ [m].
 n : Amount of gas [mol].

q_{sat}	: Saturated specific humidity [kgkg^{-1}].
$q_{z,r}$: Specific humidity of the air at a reference height [kgkg^{-1}].
q_{O}	: Specific humidity (a : ambient air; i : end of the air-supply system; inl : air inlet of the air-supply system) [kgkg^{-1}].
t	: Time [s].
Δt	: Time step [s].
u_a	: Characteristic turbulent velocity scale in a -direction [ms^{-1}].
x	: Distance to orifice in the direction of the mean flow [m].
x	: Path length of a light beam through the Lexan wall [m].
x_{hor}	: Total horizontal path length light beam through the Lexan wall [m].
x_{lex}	: Width of the Lexan wall [m].
x_{ver}	: Total vertical path length light beam through the Lexan wall [m].
z	: Distance perpendicular to a wall [m].
z_r	: Reference height [m].
$z_{\text{O},\text{O}}$: Roughness height (h : heat; m : momentum) [m].

Greek

α	: Azimuth (angle with south) [rad].
α_p	: Heat transfer coefficient describing the energy transport between the floor-plate and the upper layer of the soil [$\text{Wm}^{-2}\text{K}^{-1}$].
α_a	: Radius angle [rad].
α_h	: Convective heat exchange coefficient [$\text{Wm}^{-2}\text{K}^{-1}$].
α_1	: Species-dependent empirical parameter [-].
β	: Thermal expansion coefficient for a perfect gas [K^{-1}].
β	: Solar height [rad].
γ	: Constant algebraic stress model [-].
ϵ	: Viscous dissipation rate of turbulent kinetic energy [m^2s^{-3}].
ϵ_l	: Emissivity of Lexan [-].
ϵ_s	: Emissivity of the soil/soil-vegetation medium [-].
ϵ_w	: Effective emissivity chamber wall [-].
δ	: Fraction of the foliage covered by intercepted water [-].
κ	: Von Karman's constant [-].
λ	: Molecular thermal conductivity [$\text{Wm}^{-1}\text{K}^{-1}$].
μ	: Dynamic viscosity [$\text{kgs}^{-1}\text{m}^{-1}$].
ν	: Kinematic viscosity [m^2s^{-1}].
ν_t	: Turbulent viscosity [m^2s^{-1}].
ρ	: Density [kgm^{-3}].
ρ_{O}	: Density (a : air; P : floor-plate) [kgm^{-3}].
ρ_0	: Density of air at a reference height [kgm^{-3}].
σ	: Stefan-Boltzmann constant [$\text{Wm}^{-2}\text{K}^{-4}$].
σ_c	: Cloud fraction [-].
σ_t	: Turbulent Prandtl or Schmidt number [-].
σ_v	: Fraction of the soil shielded by the vegetation [-].
σ_τ	: Ratio of turbulent diffusivity for momentum to dissipation rate in k - ϵ model [-].
τ	: Characteristic time scale [ms^{-1}].
τ	: Force per unit of total leaf surface area in the direction of the flow [Nm^{-2}].
τ_d	: Daily period [s].

- τ_{ij} : Force per unit area in the X_i -direction acting on the face that is normal to the X_j -direction [Nm^{-2}].
- ϕ : General variable.
- ϕ_c : Energy production of chemical reactions [$\text{Jm}^{-3}\text{s}^{-1}$].
- ϕ_s : Energy production through absorption of radiation [$\text{Jm}^{-3}\text{s}^{-1}$].
- Ω_j : Component of angular velocity vector of the rotation of the earth [s^{-1}].

Lower cases

- A* : Subscript denoting the behaviour of the vegetation-shielded part of the chamber floor.
- B* : Subscript denoting the behaviour of the non-shielded part of the chamber floor.
- a,b,c* : Subscript denoting the direction of a characteristic scale (1,2,3).
- i,j,k* : Subscript denoting the direction (1,2,3).
- \odot : General subscript.

Special

- (\dots) : Time averaging operator.
- $(\dots)'$: Deviation from time mean value.
- (\dots) : Dimensionless variable.
- ϵ_{ijk} : Alternating unit tensor.
- δ_{ij} : Kronecker delta.
- Δ : Difference.
- ∇ : Divergence.
- ∇^2 : Laplacian operator.

In all the equations given in this thesis the Einstein's summation convention is used. This convention says that whenever an index occurs twice in a single term, a summation is carried out over the possible values of the index.

- Ar* : Archimedes number $\frac{U^2}{g\beta\Delta TL}$
- Eu* : Euler number $\frac{\rho U^2}{\Delta P}$
- Gr* : Grashof number $\frac{g\beta(T_s - T_a)L^3}{\nu^2}$
- Nu* : Nusselt number $\frac{Q L}{\lambda \Delta T A}$
- Pe* : Péclet number $\frac{UL}{a}$
- Pr* : Prandtl number $\frac{\nu}{a}$
- Re* : Reynolds number $\frac{UL}{\nu}$

$$\begin{aligned}
 Ri_B & : \text{Bulk Richardson number } \frac{g(z_r - d - z_{0,m}) \Delta T}{\overline{T} U_{z,r}^2} \\
 Ro & : \text{Rossby number } \frac{U}{2\Omega_p L} \\
 Sh & : \text{Sherwood number } \frac{UL}{D_{sc}} \\
 Sr & : \text{Strouhal number } \frac{L}{U\tau}
 \end{aligned}$$

Default values used

Air parameters

$$\begin{aligned}
 C_{pd} & : 1005 \text{ [Jkg}^{-1}\text{K}^{-1}\text{]}. \\
 D_{H_2O} & : 23.4 \cdot 10^{-6} \text{ [m}^2\text{s}^{-1}\text{]}. \\
 D_{O_3} & : 13.6 \cdot 10^{-6} \text{ [m}^2\text{s}^{-1}\text{]}. \\
 P & : 101.3 \text{ [kPa]}.
 \end{aligned}$$

$$a : 20.6 \cdot 10^{-6} \text{ [m}^2\text{s}^{-1}\text{]}.$$

$$\begin{aligned}
 \kappa & : 0.41 \text{ [-]}. \\
 \lambda & : 2.53 \cdot 10^{-2} \text{ [Wm}^{-1}\text{K}^{-1}\text{]}. \\
 \mu & : 17.9 \cdot 10^{-6} \text{ [kgm}^{-1}\text{s}^{-1}\text{]}. \\
 \nu & : 14.6 \cdot 10^{-6} \text{ [m}^2\text{s}^{-1}\text{]}. \\
 \rho_a & : 1.225 \text{ [kgm}^{-3}\text{]}.
 \end{aligned}$$

Other constants

$$\begin{aligned}
 L & : 2.45 \cdot 10^6 \text{ [Jkg}^{-1}\text{]}. \\
 R^* & : 8.3144 \text{ [Jmol}^{-1}\text{K}^{-1}\text{]}. \\
 g & : 9.8 \text{ [ms}^{-2}\text{]}. \\
 \sigma & : 5.67 \cdot 10^{-8} \text{ [Wm}^{-2}\text{K}^{-4}\text{]}.
 \end{aligned}$$

CURRICULUM VITAE

Theodorus Hubertus Jetten werd op 10 maart 1963 in 's-Hertogenbosch geboren. Na het doorlopen van de lagere school in Boxtel, volgde hij de VWO-opleiding aan het "Jacob-Roelandslyceum" aldaar. Op veertienjarige leeftijd verhuisde hij naar Lithoyen waarna hij in 1981 zijn Atheneum B-diploma behaalde aan het "Maasland-college" te Oss.

Aansluitend begon hij zijn studie Planteziektenkunde aan de Landbouwniversiteit te Wageningen. Tijdens deze studie heeft de nadruk gelegen op de wisselwerking planteziekten en meteorologie. De doctoraalfase bestond uit twee hoofdvakken: Meteorologie en Entomologie. Zijn belangstelling voor de toepassing van simulatiemodellen in de planteziektenkunde kwam tot uiting in een bijvak Theoretische Teeltkunde (thans Theoretische Productie Ecologie). November 1987 behaalde hij het doctoraaldiploma.

In december 1987 trad hij als toegevoegd onderzoeker in dienst bij de sectie Meteorologie van de toenmalige vakgroep Natuur en Weerkunde (thans vakgroep Meteorologie). Tot en met maart 1992 voerde hij het promotieonderzoek uit waarvan hier verslag is gedaan.

Vanaf april 1992 is hij werkzaam als toegevoegd onderzoeker bij de vakgroep Entomologie van de Landbouwniversiteit.